Universidade Federal do Espírito Santo

MODELLING THE FATE AND TRANSPORT OF OIL SPILLS

Fernando Túlio Camilo Barreto

Tese de Doutorado do Curso de Pós-Graduação em Engenharia Ambiental.
Orientador: Dr. Julio Tomás Aquije Chacaltana
Coorientador: Dr. Valdir Innocentini

Vitória
2019

Universidade Federal do Espírito Santo

MODELLING THE FATE AND TRANSPORT OF OIL SPILLS

Fernando Túlio Camilo Barreto

Tese de Doutorado do Curso de Pós-Graduação em Engenharia Ambiental.
Orientador: Dr. Julio Tomás Aquije Chacaltana
Coorientador: Dr. Valdir Innocentini

Vitória
2019

Ficha catalográfica disponibilizada pelo Sistema Integrado de Bibliotecas - SIBI/UFES e elaborada pelo autor

---

Camilo Barreto, Fernando Túlio, 1990-
C183m Modelling the fate and transport of oil spills / Fernando Túlio Camilo Barreto. - 2019.
129 f. : il.

Orientador: Julio Tomás Aquije Chacaltana.
Coorientador: Valdir Innocentini.
Tese (Doutorado em Engenharia Ambiental) - Universidade Federal do Espírito Santo, Centro Tecnológico.

1. Oceanografia. 2. Derramamento de óleo. 3. Engenharia ambiental. 4. Equações - Soluções numéricas. 5. Água - Poluição por petróleo. I. Aquije Chacaltana, Julio Tomás. II. Innocentini, Valdir. III. Universidade Federal do Espírito Santo. Centro Tecnológico. IV. Título.

CDU: 628

ACKNOWLEDGEMENTS

Agradeço primeiramente a minha família, pelo apoio e confiança. Em especial ao meu pai, por sempre acreditar em mim, principalmente nos momentos em que eu mesmo não acredito.

A Deus, pelas conversas diárias antes de dormir, e por organizar as coisas da maneira mais incrível possível.

Ao professor Júlio, por ter me aceitado no laboratório a muitos anos atrás, dando início na caminhada da pesquisa, e por ter me ensinado o valor de se fazer algo bem feito, mesmo que isso demande muito mais trabalho.

A todos meus colegas do Labesul, Fabio, Leo, Gregorio, Fran, Kaio, Andre, Thiago, Danilo, Carlos, Larissa, Bj, Mirela, Thais, Mateus (e muitos outros que passaram por lá), pelo companheirismo e ajuda ao longo de tantos anos. Neste trabalho em especial ao Kaio e Fran, pela disponilização da base hidrodinâmica.

Ao professor Ilson, por ter me acolhido em seu laboratório e ter me ajudado em um momentos mais dificies da minha vida. Sem ele talvez eu não estivesse aqui hoje escrevendo esses agradecimentos.

A todos os colegas do LADO, por terem me recebido da melhor maneira possível, mesmo em um período em que eu estava mais estranho que o normal.

Ao professor Valdir, por ter oferecido a oportunidade que mudaria em grande parte minha vida, me permitindo recomeçar e reconquistar a confiança que havia perdido.

A Luciana, por ter me integrado em seu projeto, disponibilizando todos os meios possíveis para que eu pudesse alcançar meu objetivo final.

A todos que conheci morando em SP/SJC, Mari, Ana, João, Eduardo, Nayara, Doug, Alex, Bento, Enzo, e muito outros.

Aos membros da banca examinadora: Dr. Roger Matsumoto Moreira, Dr. Fernando Pellon de Miranda, Dr. Diogo Costa Buarque, Dr. Fernando Pellon de Miranda, Dr. Edmilson Costa Teixeira. Obrigado pela avaliação minuciosa do trabalho e pelas valiosas sugestões.

A Coordenação de Aperfeiçoamento de Pessoal de Nível Superior (CAPES) e a

Climatempo pelo auxílio financeiro.

Obrigado.

RESUMO

As consequências associadas a derramamentos de óleo em meios aquosos vão além dos danos ambientais, causando grandes prejuízos econômicos e problemas de saúde para a população. Para minimizar estes efeitos, a aplicação de modelos computacionais para a predição da evolução de manchas de óleo constitui em uma poderosa ferramenta de mitigação de acidentes envolvendo derramamentos de óleos. Nesta tese foi construído um modelo de código aberto 3D para estudar a evolução do transporte e da química de uma mancha de óleo (disponível em `https://github.com/fernandotcbarreto/SYMOS-model`), empregando parametrizações estado-da-arte para os processos físico-químicos, e o método das parcelas lagrangeanas para resolver a advecção e a difusão turbulenta da macha de óleo. Para contornar a natureza não previsível de um derramamento de óleo foi implementado um método probabilístico, em que são simulados um grande número de cenários sob diferentes condições meteo-oceanográficas, a partir dos quais foram calculados parâmetros estatísticos que permitem uma descrição robusta dos impactos de uma mancha de óleo. O transporte e os quatro processos físico-químicos implementados no modelo, evaporação, emulsificação, dissolução, e dispersão vertical (entranhamento), foram validados com dados medidos, com os resultados produzindo bons valores de correlação. Após a validação do modelo, este foi aplicado em um estudo de caso no sistema de baías formado pelas baías do Espírito Santo e de Vitória (SEIV), uma região com intensa atividade portuária, para avaliar a sensibilidade da região a derramamentos de óleo. Para isto, foram realizadas simulações probabilísticas e contínuas para derramamentos hipotéticos em dois locais de intenso tráfico de navios, a entrada da baía de Vitória (derramamento da baía de Vitória) e a adjacência do porto de Tubarão (derramamento do porto de Tubarão). As simulações foram reproduzidas para o período de verão e inverno para incluir a variabilidade sazonal nas análises. Para o derramamento da baía de Vitória, os mapas estatísticos mostraram uma pequena variabilidade entre o verão e o inverno, com as áreas mais afetadas localizadas na entrada da baía de Vitória e região adjacente da baía do Espírito Santo. Este caso foi fortemente controlado pelo regime de maré, com a dinâmica da mancha reproduzindo a dominância das correntes de vazante da região. No derramamento do porto de Tubarão foi observada uma grande variabilidade entre o verão e o inverno. Para o verão ocorreu uma clara tendência da mancha em propagar em direção a praia de Camburi, e para o inverno todas as simulações determinísticas mostraram o transporte da macha para fora do SEIV. Para a simulação contínua o pior cenário analisado foi o do derramamento do porto de Tubarão para o verão, com uma grande área do SEIV e toda extensão da praia de Camburi afetadas pela mancha.

Palavras-chave: Derramamento de óleo. Modelagem computacional. Parcelas lagrangeanas. Simulação probabilística.

ABSTRACT

The consequence associated with oil spills in water bodies goes beyond the dreadful environmental damages, causing a great economical loss and health issues for the population. To minimize its damage, the application of computational models that predict the evolution of oil slicks is a powerful supporting tool in the mitigation of oil spill accidents. In this thesis we constructed an open source three dimensional oil spill fate and transport model (available at `https://github.com/fernandotcbarreto/SYMOS-model`), employing state-of-art parametrizations for the physical-chemical processes undergone by the oil, and the lagrangian parcel method to resolve the advection and turbulent diffusion of the slick. To overcome the unpredictable nature of oil spills we implemented a probabilistic method that simulates a great number of scenarios under different meteoceanographic conditions, from which were calculated statistical parameters that allow a thorough description of the impacts by the oil slick.The transport and the four physical-chemical weathering processes implemented in the model, evaporation, emulsification, dissolution, and vertical dispersion (entrainment), were validated against measured and theoretical data, giving good correlations. After the validation of the model, it was applied to a study case in the Espírito Santo - Vitória bay system (SEIV), a region with intense port activities, to evaluated the sensibility of the study region to oil spills. For this evaluation, were performed probabilistic and continuous simulations for hypothetical spills in two locations of intense traffic of vessels, the entrance of Vitória bay (Vitória bay spill) and near Tubarão port (Tubarão port spill). The simulations were reproduced for a period of summer and winter to account for the seasonal variability in the analysis. For the Vitória bay spill, the statistical maps showed a small variability between summer and winter, with the most affected areas situated in the entrance of the Vitória bay and in the nearby Espírito Santo bay. This case was highly controlled by the tidal regime, with the slick dynamics reproducing the ebb dominance of the local current system. For the Tubarão port spill, on the contrary, there was a great variability between summer and winter. For summer, it was observed a clear tendency for the spill to propagate towards Camburi beach, and for winter all deterministic cases showed a transport outwards of the SEIV. For the continuous case the worst scenario for the study region was the Tubarão port spill in summer, since a great area of the SEIV and all extension of the Camburi beach was affected by the spill.

Keywords: Oil spill. Computational modelling. Lagrangian parcels. Probabilistic simulation.

LIST OF FIGURES

Page

LIST OF TABLES

LIST OF SYMBOLS

A_{go}	–	Surface area of droplet/particle [m^2]
$C_{oj,ds}$	–	Concentration of each pseudo-component j [kg/m^3]
C_p	–	Volumetric concentration of the particle in water column [kg/m^3]
C_s	–	Molar concentration of saline solution [mol/L]
d_{go}	–	Diameter of droplet/oil slick [m]
D	–	Dissipated breaking wave energy per unit surface area [J/m^2]
D_c	–	Critical droplet diameter[m]
$D_{o,a}$	–	Diffusion coefficient (diffusity) of oil in water [cm^2/s]
D_{px}	–	Turbulent diffusion coefficients (eddy diffusivity) of particle in water along x [m^2/s]
D_{py}	–	Turbulent diffusion coefficients (eddy diffusivity) of particle in water along y [m^2/s]
D_{pz}	–	Turbulent diffusion coefficients (eddy diffusivity) of particle in water along z [m^2/s]
F_{Mj}	–	Molar fraction of each pseudo-component
g	–	Acceleration due to gravity [m/s^2]
k_s	–	salting coefficient [kg/mol]
K_{mo}	–	Mass transfer coefficient [kg/s]
m_j	–	Mass of pseudo-component j at droplet/particle [kg]
PM_a	–	Molar mass of the environment [kg/kmol]
PM_o	–	Molar mass of oil [kg/kmol]
PM_{oj}	–	molar mass of each pseudo-component [kg/kmol]
R_e	–	Reynolds number
S_c	–	Schmidt number
S_h	–	Sherwood number
S_{oj}	–	Solubility in water of each pseudo-component [kg/m^3]
$S_{oj,0}$	–	Solubility of a pseudo-component j in pure water [kg/m^3]
S_p	-	Term that represents all weathering processes [kg/m^3·s]
T	–	Temperature of the environment of the plume [K]
T_a	–	Temperature of the environment [K]
u_{PL}	–	Particle velocity along x [m/s]
v_{PL}	–	Particle velocity along y [m/s]
w_{PL}	–	Particle velocity along z [m/s]
u_a	–	Current velocity along x [m/s]
v_a	–	Current velocity along y [m/s]
w_a	–	Current velocity along z [m/s]
u'	–	velocity due to turbulent diffusion along x [m/s]
v'	–	velocity due to turbulent diffusion along y [m/s]
w'	–	velocity due to turbulent diffusion along z [m/s]
V_M	–	Molar volume of solute at its boiling point [cm^3/mol]
w_p	–	Buoyancy velocity. [m/s]
μ_a	–	Dynamic viscosity of the environment [cP]
$\triangle\rho$	–	Relative density difference between water and oil

ρ_p – Density of the droplet [kg/m^3]
k_2 – Empirical coefficient - 1.14 after Fay (1971)
k_1 – Empirical coefficient - 1.15 after Fay (1971)
V_0 – Original volume of spilled oil [m^3]
ν_a – Kinematic viscosity of the environment [m^2/s]
$A(t)$ – Area of the particle as a function of time [m^2]
$\triangle\rho$ – Relative density difference between water and oil
ν_{oil} – Kinematic viscosity of the oil/emulsion [m^2/s]
$\frac{dm_{oj,ds}}{dt}$ – Rate of mass loss for each pseudo-component [kg/s]
$m_{o,go}$ – Total mass of oil at the droplet/slick
u^w – Wind velocity along x [m/s]
v^w – Wind velocity along y [m/s]
u^{wa} – Wave induced stokes drift along x [m/s]
v^{wa} – Wave induced stokes drift along x [m/s]
k_a – Advection factor
k_w – Wind drag coefficient
k_{wa} – Wave coefficient
σ – Interfacial tension [N/m]
k_2 – Mass transfer coefficient (MACKAY; MATSUGU, 1973)
P_j – Vapor pressure [atm]
MW_j – Molecular weight [g mol^{-1}]
f_j – Mass fraction of pseudo-component j
W – Wind magnitude [m/s]
p_r^* – Reduced vapor pressure [p*/p$_c$]
p_c – Critical pressure
w – Acentric factor of hydrocarbon
T_r – Reduced temperature
$\frac{dF_{wc}}{dt}$ – Rate of water incorporation
F_w – Fraction of water in oil [kg/kg]
Y_{max} – Maximum fraction of water [kg/kg]
K_{em} – Emulsion rate constant
X_w – Fraction of wax
X_a – Fraction of asphaltenes
α – Water release rate
C^* – Empirical entrainment constant
S – Fraction of sea surface covered by oil
F – fraction of sea surface hit by breaking waves
Δd – Oil droplet diameter interval [m]
H_b – Breaking wave height [m]
H_{sig} – Significant wave height [m]
U_* – Wind stress factor
U_{th} – Threshold 10 m wind speed for the onset of breaking waves

T_w – Significant wave period
Z_i – Intrusion depth [m]
Z_{mix} – Depth at which the dispersed droplets mix after a wave breaking event
We – Dimensionless Weber number
Oh – Dimensionless Ohnesorge number
σ_{o-w} – Oil-water interfacial tension

CONTENTS

Page

1 INTRODUCTION

1.1 Problem statement

Oil spills are an inevitable and undesirable consequence of producing and transporting petroleum and associated refined products (BERRY et al., 2012). More than two thirds of all large (> 700 ton) oil spills in the past forty years have occurred whilst vessels were underway in open or inland waters and although the incidence of large and medium oil spills ($7 - 700$ ton) from vessels has significantly reduced in the past forty years, the trade in seaborne oil transportation has increased steadily since the mid 1980s (ITOPF, 2011).

In Brazil, the greatest volumes of spilled oil are related to vessels, being the accident with the Sinclair Petrolore ship off Trindade Island (ES) in 1960 the first recorded in Brazil´s territorial waters, with $66.530\,m^3$ of oil spilled (CETESB, 2017). The most recent record is the surfacing of oil at Campo de Frade, in Campos Basis, in a region explored by Chevron, in november/2011 (CABRAL; TEIXEIRA, 2012).

The three questions of most importance at the time of any oil spill incident are: where will it go, when will it get there, and what will it be like when it arrives? (BERRY et al., 2012). The first two questions, related to the transport of oil, are critical in relation to the response operations for combating the spill (Al Rabeh et al., 2000), and the third question, related to the fate of oil, is important for potential removal operations (GOODSON, 2009).

The only tool able to answer these questions is computational modelling, since we need to simulate a great number of scenarios by solving a complex system of coupled equations forced by a great range of environmental data. If in the past the modelling of the dynamics of spilled oil was focused in the application of analytical equations to study each isolated physical-chemical process, with the development of complex oceanographic models, such as Delft3D, HYCOM, and ROMS, hydrodynamical and termohaline data can be generated for any location, allowing the simulation of the fate and transport of the spilled oil.

There are some oil spill models widely used by private companies, research institutions, and governments, such as GNOME/ADIOS (LEHR et al., 2002; BEEGLE-KRAUSE, 2001), SIMAP/OILMAP (FRENCH-MCCAY et al., 2015; SPAULDING et al., 1992), and OSCAR (REED et al., 2000). SIMAP/OILMAP and OSCAR

are commercial black box models, with source codes unavailable to users for modification and improvement. Moreover, some of the algorithms and techniques used in the model are not well described in open literature, hampering the use of the models for research purposes. GNOME and ADIOS are open source models developed by NOAA. Adios can only simulate evaporation, dispersion, emulsification and spreading, and cannot simulate trajectory. GNOME is a 2-dimensional trajectory model, with very limited evaporation and oil-shoreline interaction processes.

Regarding the open source models, they also lack a probabilistic method, which allows the simulation of numerous oil spills under varying environmental conditions. This method was created to address the random nature of oil spill events, by means of repeatedly running abundant times of independent oil spills events to obtain a steady probability distribution over a period of time. From this technique we can calculate statistical parameters, crucial in the evaluation of environmental impacts associated with oil spills.

Most oil spill models, including the four cited above, employs the lagrangian parcel approach to resolve the transport of the spilled oil, solving weathering algorithms to compute the physical-chemical changes undergone by each parcel.

In models based on the lagrangian parcel method the oil slick and the entrained oil mass are represented by parcels, each of which represents in turn a group of oil droplets of like size and composition. Due to the small diameter of droplets in the water column, with values ranging from 1 and $1000\ \mu$, it would require a very refined vertical grid to resolve the turbulent dispersion of droplets, dominant in environments with low velocities, demanding a greater computational time in comparison with a lagrangian method.

According to Zafirakou (2018) the oil spill simulation by a large number of passive (not interacting with the existing hydrodynamics) parcels, transported in a lagrangian frame of reference, is the most effective procedure used in most contemporary models as: (a) it can describe oil spill geometries and shapes at subgrid level (as in the vertical, cited above), (b) the model results are not distorted by numerical errors, like numerical diffusion, and (c) the fraction of the initially introduced particles (at the spill source) reaching the coast can be considered as the probability of pollution from a minor spill.

The chemical and physical changes undergone by an oil slick on the ocean

surface are collectively known as weathering, starting immediatelly after the spillage (FINGAS, 2011). Most of these processes, such as evaporation, emulsification, dissolution, and vertical dispersion (entrainment), are primarily controlled by the characteristics of the local dynamics, and of the oil (KOROTENKO et al., 2001). These processes are not isolated, they interact with each other, improving or hindering a specific transformation, changing the physical-chemical properties of both slick and oil. As an example, evaporation consumes low weight components, increasing the fractions of high molecular weight components, which in turn promotes an easier oil emulsification (FINGAS et al., 1997). The increasing of water as a result of emulsification in the oil slick reduces oil evaporation (ROSS; BUIST, 1995), creating a coupled physical-chemical process.

Regarding the transport model, since the parcels are passive, the success in resolving the advection and diffusion of the oil particles and droplets are related to the robustness of the modelled or measured data of currents (current-induced advection), winds (wind-induced advection), waves (wave-induced advection), and diffusity (turbulent diffusion).

In spite of Brazil's prominent position in the field of oceanic oil exploration and production, the area of oil spill modelling is poorly explored in the country, which depends, most of the time, on the commercial black box models. In addition, the country has seen for the past years an increase in the maritime transport, with the expansion of port terminals followed by an increase in the number and size of ships maneuvering along the coast. Therefore, the application of computational modelling to understand the dynamics of oil spilled in brazilian coastal and oceanic waters is a vast field of research in the country, and is important for the development of specific parametrizations for the region, and for the establishment of study cases along the vast shoreline, including the many port regions and the pre-salt area.

In the present thesis, a 3-dimensional lagrangian oil spill model with a coupled probabilistic method was implemented, aiming to provide a basis for comprehensive, quantitative, environmental impact assessments in the marine environment, employing surface spreading, advection, turbulent diffusion, emulsification, stranding, evaporation, vertical dispersion, and dissolution algorithms to determine the transport and fate of spilled oil (Figure 1.1).

After the validation of the oil fate and transport modules, it was coupled to a validated Delft3D implementation and applied to simulate hypothetical spills in

the Vitória and Espírito Santo bay system, a region surrounded by an important portuary complex, with an intense traffic of vessels. With the model established, were performed simulations employing the probabilistic method to assess the vulnerability of the study region to oil spills. The results gained through this thesis are hoped to be useful for many organizations adressing oil spill response operations and contribute to an effective and efficient coordination among the relevant institutions.

Figure 1.1 - Representation of the physical-chemical processes acting on a slick on the ocean surface.

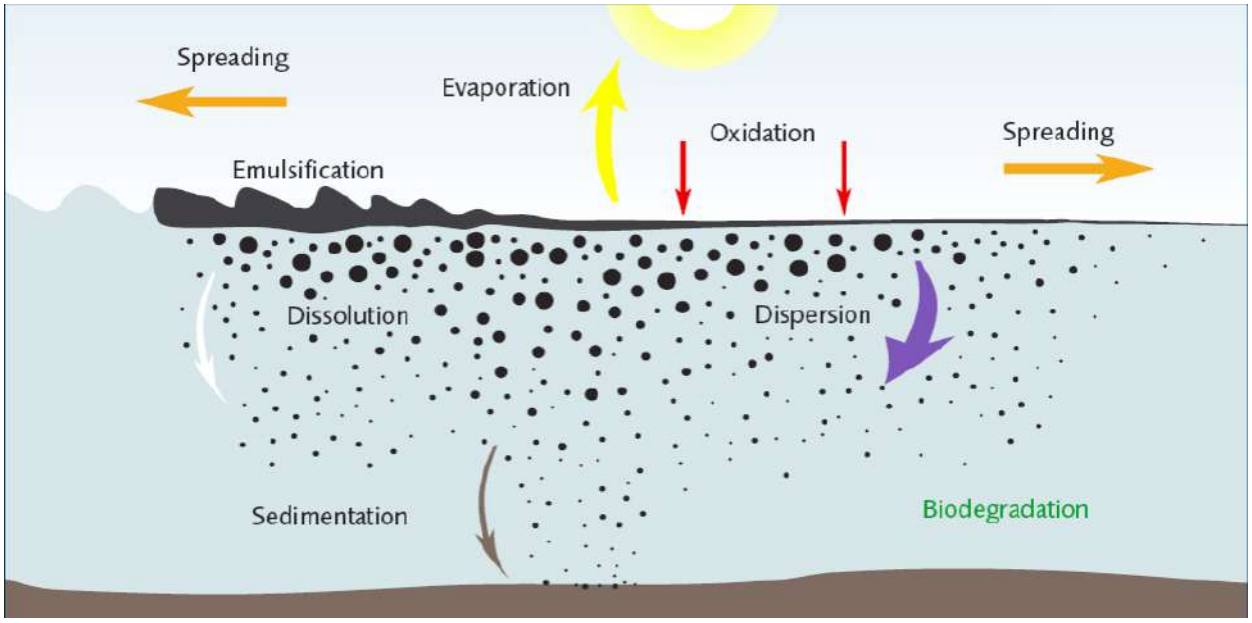

SOURCE: Adaptada de Zheng et al. (2002).

1.2 Hypothesis

The system formed by the Vitória and Espírito Santo bay is hydrodinamically controlled by the tidal regime and variations in the rivers flow rate discharging in the bay, with a wind regime varying among northeast, east and southeast directions. The lack of regional oceanographic processes acting on the system, along with the geomorphologycal configuration of the Espírito Santo bay, with

the main axis directed to the south, narrow down the exchange of momentum between the system and the nearby shelf region to tidal currents. Therefore, oil spilled in regions next to vitória bay and tubarão port, two regions with intense traffic of vessels, are expected to effect meanly the bays system, with a few oil discharged to the nearby shelf region.

1.3 Objectives

The main purpose of this thesis is to study the dynamics of oil spilled on the ocean surface by means of computational modelling. In order to fullfill this purpose, the following specific objectives were established:

- to simulate the oil evaporation of an oil slick;
- to simulate the emulsification undergone by an oil slick;
- to simulate the dissolution of oil slick and droplets;
- to simulate the transference of oil from an oil slick to the water column as a result of vertical dispersion/entrainment;
- to simulate the advection of oil particles;
- to couple the oil model with a validated hydrodynamical model and to atmospheric reanalysis;
- to evaluate the influence of the Tubarão port piers on the slick transport;
- to implement a probabilistic method in order to calculate statistical parameters to be used in the evaluation of the dynamics of the oil spilled in the study region.

2 THEORETICAL REVISION

2.1 Oil spill modelling

Generally, oil spill modelling in the ocean involves two models: a hydrodynamic model and an oil transport and fate model. The dynamics a surface oil slick is controlled by the drift resulting from varying components of winds, currents, waves, the turbulent movement of oil within the upper ocean, and weathering processes.

Accurate modelling of the transport and fate of spilled oil must account for the complex interplay between environmental and oceanic processes resulting from the presence of oil both on the surface and within the water column (three-dimensional modelling), as formulated in mathematical descriptions of physical, chemical, and biological processes (MACKAY; MCAULIFFE, 1988). The complexity of accurate transport modeling was highlighted during the Deepwater Horizon (DWH) oil spill disaster (HUNTLEY et al., 2011), when, e.g., the spilled oil was initially forecasted to be carried into the Atlantic Ocean by the Loop Current but instead was largely maintained within the upper reaches of the Gulf of Mexico. Although the DWH spill resulted in extensive surface slicks and evaporation into the atmosphere, a considerable amount of oil from the DWH blowout never reached the surface but was tracked as an extensive plume at depth that persisted for months before biodegradation (CAMILLI et al., 2010), showing the importance of subsurface oil transport modelling (JONES et al., 2016).

The fate of a spill of crude oil or refined product in the marine environment is determined by spreading, evaporation, dissolution, vertical dispersion/entrainment, emulsification, sedimentation and various degradation processes as discussed by Kuiper e Brink (1987). An ideal model for oil fate and transport simulates the following processes mathematically:

- advection and diffusion (dispersion) - transport;
- mechanical spreading - fate/transport;
- evaporation of oil components - fate;
- dissolution of oil components in water - fate;
- dispersion of oil droplets in water (entrainment) - fate/transport;

- emulsification - fate;
- oxidation of oil components (particularly photooxidation) - fate;
- sedimentation - fate;
- biodegradation - fate.

All of these processes are time-dependent and must be described by dynamic models. State-of-the-art models include some, but not all of these processes at varying degrees of sophistication, but field or laboratory experiments designed to calibrate or test models usually focus on only one process (RIAZI; AL-ENEZI, 1999).

The most used models for pratical purposes are Oil Spill Contingency and Response Model or OSCAR (REED et al., 2000), Spill Impact Model Application Package/Oil Modeling Application Package or SIMAP/OILMAP (FRENCH-MCCAY et al., 2015; SPAULDING et al., 1992), and the GNOME/ADIOS (LEHR et al., 2002; BEEGLE-KRAUSE, 2001).

ADIOS and GNOME are two open source models developed by NOAA. ADIOS2 was released in 2000 (LEHR et al., 2002). The model is widely used as a test of expected oil behaviour and includes an oil library (FERNENDES, 2013). However, ADIOS and ADIOS2 can only simulate evaporation, dispersion, emulsification and spreading (LEHR et al., 2002), and cannot simulate trajectory. GNOME is a 2-dimensional trajectory model with very limited evaporation and oil-shoreline interaction processes (BEEGLE-KRAUSE, 2001). A new version of GNOME combining ADIOS2 and GNOME is still under development.

SIMAP/OILMAP are commercial, 3-dimensional models, which can simulate oil trajectory and most of the weathering processes. SIMAP can simulate oil sedimentation and biodegradation. OSCAR is a 3-dimensional state-of-the-art model developed by SINTEF with comprehensive weathering processes including evaporation, dissolution, biodegradation, sedimention and dispersion. The model has been validated with several full-scale, open ocean, oil release experiments. Being commercial softwares, the source codes of both SIMAP/OILMAP and OSCAR are unavailable to users for modification and improvement.

The great majority of oil models share in commom the use of Lagrangian based methods and the random walk for the transport processes (advection/diffusion). The wind, wave and currents necessary as input are provided by supporting

environmental (hydrodynamic, wind, and wave) models. The hydrodynamic models may be either 2- or 3- dimensional, while the wind and wave models are typically two-dimensional, focusing on surface transport processes. As an alternative, information for ocean currents may come from broad scale measurement systems, such as high frequency radar (HFR) or data-based methods, and winds from offshore buoys (SPAULDING, 2017).

The algorithms that describe the fate processes are typically based on underlying fundamental principles and informed/calibrated/validated by laboratory and field observations. The fate processes are modeled either by transferring oil mass between the environmental compartments (sea surface, atmosphere, water column, sea bed, and shoreline) or changing the oil's composition or physical characteristics (e.g. density, viscosity, and interfacial tension) (SPAULDING, 2017).

The oil in spill models is either characterized as a bulk oil of a given type (e.g. medium crude, No 2 fuel oil, etc.), or described in terms of the various components, typically related to its distillation, that comprise the oil (SPAULDING, 2017).

The most complete validation of an oil model to date has been performed for the Deepwater Horizon (DWH) spill by Spaulding et al. (2015) for the blowout model OILMAP DEEP (nearfield subsurface oil model), and by French-McCay et al. (2016) for the far field fate and transport model (including surface model).

French-McCay et al. (2016) compared the model results to observations for the balance of oil mass, sediment-oil interaction, surface (floating) and subsurface oil, and shoreline stranding. The model was fully three-dimensional and included subsurface and surface oil transport, oil droplet surfacing, evaporation of volatiles from surface oil to the atmosphere, stranding of oil on shorelines (also known as beaching), emulsification of oil, entrainment of oil as droplets into the water column, resurfacing of oil, dissolution of soluble components into the water column, volatilization from the water column to the atmosphere, partitioning of oil between water and sediment, sedimentation of oil droplets, and degradation.

The oil was characterized in terms of both soluble and insoluble pseudo-components. Output of the fate model included the location and dimensions of floating oil, mass and concentrations of hydrocarbon constituents in water, and fluxes of hydrocarbons to the atmosphere and sediment over time. The input data used to initialize the model came from the blowout model

(OILMAP DEEP).

Model simulations were driven by a variety of different wind (four) and hydrodynamic (six) models that covered the study area and duration of the spill.

The results from French-McCay et al. (2016) showed that the oil mass balance, and observations of the surface and shoreline oiling pattern were consistent with the extensive remote sensing data which provided information on the spatial extent and thickness (volume per unit surface area) of the oil (MCDONALD et al., 2015; SUN et al., 2016). The subsurface oil concentrations were consistent with the limited observations with both model predictions and observations showing substantial patchiness in space and time. Model predictions, in agreement with observations, showed very limited sediment-oil interaction. Spill model predictions showed considerable sensitivity to predicted model currents at depth and to winds and currents at the surface as evidenced by tests performed using the varying meteorological and ocean current model predictions as input.

For Brazil's oceanic region, Lemos et al. (2009) performed theoretical oil spill simulations with the OSCAR model in the probababilistic mode to evaluate the effect of astronomical tide on the oil transport on the continental shelf associated with the Abrolhos reefs, in eastern Brazil.

The probabilistic oil simulations were conducted as randomly chosen 30-days simulations within a 90-days data period. Since the domain experiences significant seasonal hydrodynamic variations, due to variations in wind stress and in the Brazil Current volume transport, the study was conducted in two distinct three-month-long periods, one spanning the austral summer and another spanning the austral winter of 1989. The 1989 year was chosen because the hydrodynamic model was already run and validated for this period. Regarding the hydrodynamical simulations, they were conducted with the Princeton Ocean Model (POM) (BLUMBERG; MELLOR, 1987).

To evaluate the influence of tide, simulations were carried out with and wihout tidal-induced currents. The authors concluded that, in overall, the presence of astronomical tide strongly influenced the transport of oil in the study region. The tidal currents were more effective in the Abrolhos Bank, where the cross-shelf transport provided by the tidal currents resulted in higher probabilities of oil contamination of the protection areas.

In following sections will be presented the physical-mathematical description of the main weathering processes.

2.2 Mechanical spreading

Oil will spread on the surface of a water body even without external forces such as tidal currents or wind stresses. The spreading of the oil on calm waters is due to the force of gravity and the interfacial tension between oil and water, with the oil viscosity and inertia retarding the spreading forces (FAY, 1969). The most widely used model is the one of Fay (1971), which divided spreading into three phases: the gravity-inertial phase, the gravity-viscous phase, and the surface-tension phase. The spreading ceases when all the volatile fractions of the oil have been lost or when the spill reaches the minimum thickness defined in the oil database.

The gravity-inertial phase generally lasts for less than an hour, except for the largest spill (BERRY et al., 2012). As the time for the first phase is so short, the model begins the oil weathering processes once the end time, t_0, of this phase has been reached, which is determined by Fay (1971) as:

$$t_0 = \left(\frac{k_2}{k_1}\right)^4 \left(\frac{V_0}{\nu_a g \triangle \rho}\right)^{1/3}, \tag{2.1}$$

where k_2 and k_1 are empirical coefficients (1.14 and 1.15 respectively after Fay (1971)), V_0 is the original volume of spilled oil (m^3), ν_a is the kinematic viscosity of the environment (m^2/s), g is the acceleration due to gravity, and $\triangle\rho$ is the relative density difference between water and oil.

The area (m^2) over which the oil slick has spread at the end of this first spreading phase is determined as (FAY, 1971):

$$A_0 = \pi \frac{k_2^4}{k_1^2} \left(\frac{V_0^5 g \triangle \rho}{\nu_a^2}\right)^{1/6}, \tag{2.2}$$

The second stage of slick spreading known as gravity-viscous phase is governed by the balance between the viscosity of the oil and the oil-water interfacial tension. The viscous spreading phase continues to such a time that the slick gets so thin that surface tension forces alone play a role in spreading the slick, leading to the third, surface-tension phase (BERRY et al., 2012).

The area growth during the gravity-viscous phase spreading is described as:

$$A(t) = \pi^3 \frac{k_2^4}{k_1^2} \sqrt{\frac{V_0^2 g \triangle \rho \, t^{3/2}}{\nu_{oil}^{1/2}}}, \tag{2.3}$$

where $A(t)$ is the area of the particle as a function of time (m^2), and ν_{oil} is the kinematic viscosity of the emulsion (m^2/s).

The Fay formulations only deal with an idealised spreading of a slick in a radial manner on calm seas. They take no account of wind conditions, which play an important role in determining the shape and area of actual spills (BERRY et al., 2012).

Spreading due to surface tension (wind shear) and/or currents is entirely handled by the Lagrangian parcel model.

2.3 Dissolution

Dissolution is the process by which soluble hydrocarbons (most of which are aromatics) enter the water from a surface slick or from subsurface oil droplets. The lower molecular weight hydrocarbons tend to be both more volatile and more soluble than those of higher molecular weight (SPAULDING, 2017).

Regardless of the small amount of oil typically lost in dissolution, usually less than 1% of the slick volume, this is a very important process from an environmental point of view, since many of the soluble components, specially the aromatics, are very toxic to aquatic species (FINGAS, 2011).

Dissolution rates depends on the dissolution of each component on water (RYE, 1994), and Johansen (2003) defined the mass loss rate by dissolution for each pseudo-component j ($dm_{oj,ds}/dt$) as

$$\frac{dM_j}{dt} = K_{mo} \, A_{go} \left(F_{Moj} \, S_{oj} \, - \, C_{oj,ds} \right) , \tag{2.4}$$

where $\frac{dM_j}{dt}$ is the rate of mass loss for each pseudo-component j [kg/s], K_{mo} is the mass transfer coefficient [kg/s], A_{go} is the surface area of droplet/particle [m^2], F_{Moj} is the molar fraction of each pseudo-component j, S_{oj} is the solubility in water of each pseudo-component j [kg/m^3], $C_{oj,ds}$ is the concentration of each

pseudo-component j [kg/m^3].

The mass transfer coefficient K_{mo} can be computed as following:

$$K_{mo} = \frac{S_h \, D_{o,a}}{d_{go}} \ , \tag{2.5}$$

where $D_{o,a}$ is the diffusion coefficient (diffusity) of oil in water [m^2/s], d_{go} is the diameter of droplet/particle, S_h is the Sherwood number.

Following Wilke e Chang (1955) and Reid et al. (1987) the diffusity of a solute (oil, gas) in a solvent (like seawater) was defined as

$$D_{o,a} = \frac{7,4 \times 10^{-8} \, T_a \, (\varphi \, PM_a)^{1/2}}{\mu_a \, {V_M}^{0,6}} \ , \tag{2.6}$$

where $\varphi = 2,6$ is the parameter for effective molar mass of solvent in diffusion, μ_a is the dynamic viscosity of the environment [cP], V_M is the molar volume of solute at its boiling point [cm^3/mol], PM_a is the molar mass of the environment [kg/kmol], T_a is the temperature of the environment (K).

Molar fraction F_{Moj} is defined as

$$F_{Mj} = \frac{M_j \, PM_o}{PM_{oj} \, m_{o,go}} \ , \tag{2.7}$$

where M_j is the mass of pseudo-component j at droplet/particle [kg], PM_o is the molar mass of oil [kg/kmol], PM_{oj} is the molar mass of each pseudo-component j [kg/kmol], $m_{o,go}$ is the total mass of oil at the droplet/slick.

According to Pierotti (1976), the solubility of nonelectrolytes [1] in a solvent depends on the necessary energy to create a cavity with a size enough to accommodate the molecule of solute and of the energy involved in the interaction between the molecules of solvent and solute. The presence of salt in water affects the relation between pseudo-components on oil and environment, demanding the adjusment of S_{oj}. Xie et al. (1997) found that organic compounds are in general less soluble in saline solutions, with this modification calculated through

[1] nonelectrolytes are compounds that do not dissociate into ions in a solution

Setschenow equation

$$ln\left(\frac{S_{oj,0}}{S_{oj}}\right) = k_s\, C_s\ , \tag{2.8}$$

where $S_{oj,0}$ is the solubility of a pseudo-component j in pure water [mol/m^3], k_s is the salting coefficient [Kg/mol], C_s is the molar concentration of saline solution [mol/L].

Gold e Rodriguez (1989) revised some theories developed to calculate the salting coefficient and noted that, to solutes with large molecules, such as the pseudo-components of oil, the method of Aveyard (1982) gives the best results for k_s when comparing to observations.

2.4 Advection-diffusion of oil particles-droplets

The Advection-diffusion model is designed to simulate the surface and subsurface transport of oil particles and droplets, respectivelly. These parcels move under the influence of advective and diffusive processes, being the spatial coordinates in the flow of each parcel calculated from the advection with the surrounding water body (current, wind, wave), and the diffusion due to turbulence.

The advection-diffusion equation modified to include buoyancy and weathering processes is

$$\frac{\partial C_p}{\partial t} + \frac{\partial (u_a C_p)}{\partial x} + \frac{\partial (v_a C_p)}{\partial y} + \frac{\partial (w_a C_p)}{\partial z} = \\ \frac{\partial}{\partial x}\left(D_{px}\frac{\partial C_p}{\partial x}\right) + \frac{\partial}{\partial y}\left(D_{py}\frac{\partial C_p}{\partial y}\right) + \frac{\partial}{\partial z}\left(D_{pz}\frac{\partial C_p}{\partial z}\right) + \frac{\partial (w_p C_p)}{\partial z} - S_p\ , \tag{2.9}$$

where C_p is the volumetric concentration of the particle in water column [kg/m^3], D_{px}, D_{py}, D_{pz} are the x, y, z turbulent diffusion coefficients (eddy diffusivity) of particle in water [m^2/s], respectivelly; S_p is the term that represents all weathering processes, and w_p is the buoyancy velocity.

The insertion of S_p greatly increases the complexity of the equation, since weathering processes modify the physical-chemical characteristics of particles/droplets.

The lagrangian parcel method is the most widely used in oil spill models to numerically resolve the advection/diffusion equation, representating the plume as a number of passive particles. According to Spaulding (2017), this method allows the model to account for the temporally and spatially varying release, transport, and fate of the oil. This strategy is also amenable to sensitivity testing of results to the number of particles/droplets in the simulation. Care needs to be exercised in the particle/droplet tracking and aggregation/disaggregation routines, to ensure that the total oil mass and the mass by each component is preserved.

In the Lagrangian parcel method each particle and a group of droplets are adressed as lagrangian parcels (Lps), which represents a group oil droplets of like size and composition. When a parcel is on surface, it behaves as a slick; when in the water column, a parcel behaves as a droplet (SPAULDING, 2017). For convencience, for now on, a parcel at the surface will be called particle, and in the water column, droplet.

At each time step the advection-diffusion equation is resolved for each particle/droplet, which creates a direct relationship between slick resolution and computation time. With more particles, better the resolution of the slick and greater the computation time, since more calculations are resolved at each time step.

In each time k, the location x_{LP}, y_{LP}, z_{LP} of each particle is resolved as (REED et al., 1995; ABASCAL et al., 2009)

$$x_{LP,k+1} = x_{LP,k} + k_a u_{PL,k}\,\Delta t + k_w u^w_{PL,k}\,\Delta t + k_{wa} u^{wa}_{PL,k}\,\Delta t\,, \tag{2.10}$$

$$y_{LP,k+1} = y_{LP,k} + k_a v_{PL,k}\,\Delta t + k_w v^w_{PL,k}\,\Delta t + k_{wa} v^{wa}_{PL,k}\,\Delta t\,, \tag{2.11}$$

$$z_{PL,k+1} = z_{PL,k} + w_{PL,k}\,\Delta t\,; \tag{2.12}$$

where u_{PL} is the x direction particle velocity [m/s], v_{PL} is the y direction particle velocity [m/s], w_{PL} is the z direction particle velocity [m/s], u^w is the x direction wind velocity [m/s], v^w is the y direction wind velocity [m/s], u^{wa} is the x direction wave induced stokes drift [m/s], v^{wa} is the y direction wave induced stokes drift [m/s], k_a is the advection factor, k_w is the wind drag coefficient, k_{wa} is the wave coefficient. For droplets the equations above are applied lacking wind and wave components.

The particle velocity is defined as the sum of the current velocity interpolated to particle location (u_a, v_a, w_a), the velocity due to turbulent dispersion (u',v',w'), and the velocity due to buoyancy (w_p):

$$u_{PL} = u_a + u' \,, \tag{2.13}$$

$$v_{PL} = v_a + v' \,, \tag{2.14}$$

$$w_{PL} = w_a + w' + w_p \,; \tag{2.15}$$

In lagrangian models the velocity due to turbulent diffusion/dispersion is usually parameterized through a random walk model, also know as Monte Carlo method, as described in Lonin (1999) and Yapa (2013):

$$u' = \varepsilon_1 \sqrt{\frac{2\,D_{px}}{\Delta t}}\, sen(2\,\pi\,\varepsilon_2) \,, \tag{2.16}$$

$$v' = \varepsilon_1 \sqrt{\frac{2\,D_{py}}{\Delta t}}\, cos(2\,\pi\,\varepsilon_2) \,, \tag{2.17}$$

$$w' = \varepsilon_3 \sqrt{\frac{2\,D_{pz}}{\Delta t}} \,; \tag{2.18}$$

where ε_1 and ε_2 are the random numbers between 0 and 1, and ε_3 is the random number between -1 and 1.

Models based on the random walk concept are significantly more effective than the finite-difference models mainly because they describe exactly the diffusion (HUNTER, 1987). Most oil spill models uses a random walk strategy, as GNOME, OSCAR, OILMAP, and LTRANS (Larval TRANSport model system, see North et al. (2008))

2.4.1 Bouyancy Velocity

Most petroleum products have a density lighter than sea water. The submerged oil droplets rise due to their buoyancy, which is controlled by their droplet size and the density difference between the oil and water.

Clift et al. (1978) formulated equations for the bouyancy velocity based on the size of droplets:

- To spherical droplets (diameter less than 1 mm),

$$w_p = \frac{R_e\,\nu_a}{d_p}\ , \tag{2.19}$$

where d_p is the diameter of the droplet [m], R_e is the Reynolds number for the droplet, as defined in table 2.1.

Table 2.1 - Correlation for R_e as function of N_D^a and W^b

Range	Correlation
$N_D \leq 73$; $R_e \leq 2,37$	$R_e = \frac{N_D}{24} - 1,7569 \times 10^{-4} N_D^2 + 6,9252 \times 10^{-7} N_D^3 - 2,3027 \times 10^{-10} N_D^4$
$73 < N_D \leq 580$; $2,37 < R_e \leq 12,2$	$\log_{10} R_e = -1,7095 + 1,33438W - 0,11591W^2$
$580 < N_D \leq 1,55 \times 10^7$; $12,2 < R_e \leq 6,35 \times 10^3$	$\log_{10} R_e = -1,81391 + 1,34671W - 0,12427W^2 + 0,006344W^3$
$1,55 \times 10^7 < N_D \leq 5 \times 10^{10}$; $6,35 \times 10^3 < R_e \leq 3 \times 10^5$	$\log_{10} R_e = 5,33283 - 1,21728W + 0,19007W^2 - 0,007005W^3$

[a] $N_D = \frac{4\rho_a g d_p (\rho_p - \rho_a)}{3\mu_a^2}$

[b] $W = \log_{10} N_D$

Fonte: Adaptada de Clift et al. (1978).

- To droplets with ellipsoidal shape (diamater between 1 mm and D_c),

$$w_p = \frac{\mu_a}{\rho_a\, d_p}\, M_{or}^{-0,149}\, (J\, -\, 0,857)\ , \tag{2.20}$$

with

$$J = \begin{cases} 0,94\, H^{0,757} & \text{to} \quad 2 < H \leq 59,3\ , \\ 3,42\, H^{0,441} & \text{to} \quad H > 59,3\ , \end{cases} \tag{2.21}$$

$$H = \frac{4}{3}\, E_o\, M_{or}^{-0,149} \left(\frac{\mu_a}{\mu_{a,0}}\right)^{-0,14}\ ; \tag{2.22}$$

$$E_o = \frac{g\, d_p^2}{\sigma} \left(\rho_a \, - \, \rho_p\right) ; \tag{2.23}$$

$$M_{or} = \frac{g\, \mu_a^4}{\rho_a^2\, \sigma^3} \left(\rho_a \, - \, \rho_p\right) ; \tag{2.24}$$

where ρ_p is the density of the droplet [kg/m^3], σ is the interfacial tension [N/m], $\mu_{a,0} = 9 \times 10^{-4} kg/m \cdot s$, D_c is the critical droplet diameter.

- To droplets type spherical cover (diameter greater then D_c)

$$w_p = 0,711 \sqrt{\frac{g\, d_p \left(\rho_a \, - \, \rho_p\right)}{\rho_a}} \, . \tag{2.25}$$

To avoid discontinuity in w_p, Zheng e Yapa (2000) developded a method to determine the value of D_c between shapes ellipsoidal and spherical cover.

2.5 Evaporation

Among weathering processes evaporation is the most important that oil undergoes after spillage, with a loss up to 75% of their volume for light crudes or refined products in a few days. An understanding of evaporation is important for practical actions, such as recovery strategies, and for the development of predictive models (FINGAS, 1995). Through evaporation, low boiling lighter components will rapidly be removed, reducing the volume of the remaining slick and increasing its density and viscosity. The change of oil properties due to evaporation is important to processes such as natural dispersion, emulsification, dissolution and sinking (check section 2.8) (SEBASTIAO; SOARES, 1995).

In many spill models, the so-called pseudo-components (chemical component groups) (PAYNE et al., 1984) are evaporated according to an evaporative exposure method, where the flux to the atmosphere is specific to the component's molar volume, vapor pressure, and molecular weight (SPAULDING, 2017).

In Reed (1989) evaporation was modelled using the pseudo-component approach known as "Model of Reed", which allows different fractions of oil to evaporate at different rates depending on the physical-chemical caracteristics of each component. This author used the method of Mackay e Matsugu (1973) to

calculate the mass transfer coefficient, and a variation of the method of Stiver e Mackay (1984) to calculate mass transfer rate (evaporation rate).

The mass transfer rate is given by

$$\frac{dM_j}{dt} = \frac{k_2 P_j A(t) f_j MW_j}{RT}, \tag{2.26}$$

where k_2 is the mass transfer coefficient, t is time (s), P_j is the vapor pressure for each pseudo-component j (atm), f_j is the mass fraction of pseudo-component, MW_j is the molecular weight (g mol^{-1}), R is the gas constant (8.206 x 10^{-5} atm m^3 mol^{-1}K^{-1}), T is the temperature (K).

The vapor pressure was obtained following the procedure in API (1997):

$$\ln(p^*) = (\ln p_r^*)^{(0)} + w(\ln p_r^*)^{(1)} \text{ at constant } T_r, \tag{2.27}$$

For computer calculations, the correlation terms are given by the following equations API (1997):

$$\begin{aligned} (\ln p_r^*)^{(0)} &= 5.92714 - 6.09648/T_r - 1.28862 \ln T_r + 0.169347 T_r^6, \\ (\ln p_r^*)^{(1)} &= 15.2518 - 15.6875/T_r - 13.4721 \ln T_r + 0.43577 T_r^6. \end{aligned} \tag{2.28}$$

where p_r^* is the reduced vapor pressure (p^*/p_c), p^* is the vapor pressure [atm], p_c is the critical pressure, $(\ln p_r^*)^{(0)}$ and $(\ln p_r^*)^{(1)}$ are correlation terms, w is the acentric factor of hydrocarbon, and T_r is the reduced temperature. The coefficient k_2 is the mass transfer coefficient given by Mackay e Matsugu (1973) as:

$$k_2 = 0.029 W^{0.78} d_{go}^{-0.11} S^{-0.67} \sqrt{\frac{MW_f + 29}{MW_f}} \tag{2.29}$$

where W is the wind magnitude [m/s].

The formulations of Reed (1989) takes into account the influence of oil composition, seawater temperatures, spill area, wind speed, solar radiation, slick thickness, with the rate of evaporation increasing due to the spreading of the oil,

seawater temperature and wind speed (CONCAWE, 1983).

The following assumptions are made: no diffusion limitation exists within the oil film, oil forms an ideal mixture, the partial pressure of the components in the air, compared to the vapor pressure, is negligible (CONCAWE, 1983).

2.6 Emulsification

Many oils tend to absorb water to form emulsions which may contain up to 80% water. With respect to the potential for emulsification of an oil and emulsion stability, it is generally agreed that a critical factor is the amount of natural surfactants present in the spilled oil, such as asphaltenes, resins and waxes (SEBASTIAO; SOARES, 1995).

The ability of crude oil to emulsify seems to be related to the level of asphaltenes in the oil, and the stability of emulsion is considered to be related to the presence of wax cristals. A crude oil with a relatively low asphaltene content is expected to be less likely to form a stable emulsion. However, stable emulsions are also associated with high wax contents (high pour points) (CONCAWE, 1983).

The result of emulsification is not only a large increase in volume (2 to 5 times the volume of the original stabilized oil) but also a significant increase in the density and in the viscosity. The density of the resulting emulsion can reach 1.03 g/ml compared to a starting density as low as 0.80 g/ml, and viscosity typically increases by a few orders of magnitude (FINGAS, 1995).

The emulsification of oil has a significant effect on recovery efforts. An emulsion with 80% water content has a volume that is five times the original spilled volume. There is more emulsified oil to be recovery than the parent oil. Special pumps are required to remove the oil due to the dramatic increase in viscosity (XIE et al., 2007).

Therefore, numericals models that reproduce emulsification are crucial in the development of clean up strategies for companies and government.

Emulsion formation and stability is poorly understood in the ocean due to the complexity of the process, and to its mutual relationship with other physical-chemical processes (XIE et al., 2007), increasing the difficulty in the implementation of this process in models.

The modelling of emulsification includes water uptake, emulsion stability, de-emulsification, and density and viscosity changes. Mackay et al. (1980) presented a model for simulating emulsification, which includes calculating water uptake. Mackay's equation is used in most oil spill models where emulsification is incorporated, and is formulated as:

$$\frac{dF_{wc}}{dt} = K_{em}\,(W+1)^2\,(1-\frac{F_w}{Y_{max}}), \tag{2.30}$$

where $\frac{dF_{wc}}{dt}$ is the rate of water incorporation, F_w is the fraction of water in oil [kg/kg], Y_{max} is the maximum fraction of water [kg/kg], K_{em} is the emulsion rate constant.

Wether an emulsion decomposes easily or not is determined by its stability. Mackay e Zagorski (1982) proposed a stability index to estimate emulsion stability. In this index, emulsion stability is determined by the temperature and fractions of asphaltenes, wax, and other components:

$$S = X_a \cdot \exp[K_{ao} \cdot (1 - X_a - X_w)^2 + K_{aw} \cdot X_w^2] \cdot \exp[-0.04 \cdot (T - 293))], \tag{2.31}$$

where a subscript represents asphaltenes, w subscript represents wax, o subscript represents other chemical components, $K_{ao} = 3.3$ at 293 K, $K_{aw} = 200$ at 293 K, X_a is the fraction of asphaltenes, X_w is the fraction of wax.

Stability is the determining factor in de-emulsification (the separation of an emulsion into water and oil). Fingas et al. (1997), Fingas (2001), Fingas et al. (2002) classified water-in-oil emulsion as: stable, meso-stable, and unstable. According to their findings, a stable emulsion has as asphaltene content of over 7% in weight. When the combined amount of asphaltene and resin is over 3%, meso-stable emulsions are formed. If these conditions are not met, the emulsions are unstable:

Stable emulsion, when $S > 1.22$;

Meso - stable emulsion, when $0.67 \leq S \leq 1.22$;

Unstable emulsion, when $S < \ 0.67$;

For unstable and meso-stable emulsions, de-emulsification can occur, resulting in the release of water. However, available information on de-emulsification is very limited. In order to model de-emulsification, a first order water release formula is assumed:

$$\text{Waterrelease} = -\alpha \cdot F_w, \tag{2.32}$$

where α is the water release rate.

Water release rate α changes with the parameter for emulsion stability S, and is assumed to have the following relationship with S:

$$\alpha = \begin{cases} \alpha_0 - (\alpha_0 - \alpha_{0.67})S/0.67 & \text{for } S<0.67 \\ \alpha_{0.67}[(1.22 - S)/(1.22 - 0.67)] & \text{for } 0.67 \leq S \leq 1.22 \\ 0 & \text{for } S > 1.22 \end{cases} \tag{2.33}$$

2.7 Three-Dimensional

The three-dimensional nature of an oil spill model is achived with the implementation of the vertical dispersion/entrainment process, resulting in the release of oil droplets to the water column from a basically two-dimensional oil slick. Numerically, the entrainment greatly increases the computation effort of the model, with the inclusion of more elements to the calculation, and the complexity of the model, with the calculation of the advection-diffusion and weathering processes acting on tiny droplets. Moreover, the 3D nature of the droplets demands an interpolation along the vertical layers of the hydrodinamic model, also increasing the computation effort.

Historically oil spill models have focused on surface trajectory (PROCTOR et al., 1994; REED et al., 1998) and weathering (DALING et al., 1997), primarily of oil on water surface. However, to evaluate the effects of subsurface oil, this trajectory and weathering analysis is not sufficient. For example, to evaluate the fates and impacts of a spill that is largely entrained into the water column (by waves or chemical dispersant application), subsurface oil must be explicitly tracked (REED et al., 2000). A prime example is the North Cape oil spill of January 1996, which occurred during a severe winter storm (FRENCH, 1998). The barge North Cape spilled 2696 metric tones (MT, 828,000 gallons) of home heating oil (No. 2 fuel oil)

into the surf zone on the south coast of Rhode Island, USA. Most of the oil was mixed into the water column by the heavy surf, resulting in high concentrations of the toxic components in shallow water that killed millions of water column and benthic organisms. While surface models may be useful in predicting the trajectory of slicks, they cannot evaluate the extent of biological impacts caused by subsurface oil. To accomplish this, it is necessary to simulate the vertical dispersion/entrainement of oil from the surface slick to the water column.

The importance of the explicit modeling of the entrainment was also verified by Rohrs et al. (2018), finding this process to be a crucial component affecting the horizontal transport of oil spills, controlling differences in the drift of various types of oil and in various weather conditions.

2.7.1 Vertical dispersion/entrainement

When evaluating the time evolution of a slick on the ocean surface, natural dispersion is a key process (JOHANSEN et al., 2015). Depending on the state of agitation of the ocean, a strong exchanging process between surface and water column establish, resulting in a great loss of the slick mass to the water column in the form of droplets, and vice versa, as stated by Huang (1983):

> The most common supposition is that breaking waves cause the oil layer to be propelled into the water column thus forming a 'shower' of oil droplets (figure 2.1). Most of the oil particles rise again to the slick and coalesce there, but some of the smaller oil droplets diffuse downward and become permanently incorporated into the water column. It is likely that the dispersion rate is a function of the oil slick thickness, oil-water interfacial tension, sea state, and in particular, the fraction of the sea which is covered by breaking waves.

How long oil will remain on the sea surface is a fundamental issue in evaluating alternative oil spill response strategies, determining the probability of impacting coastlines, and in estimating potential effects on sea birds and marine mammals in the path of the slick (JOHANSEN et al., 2015).

Figure 2.1 - Dispersion of oil droplets in the water column

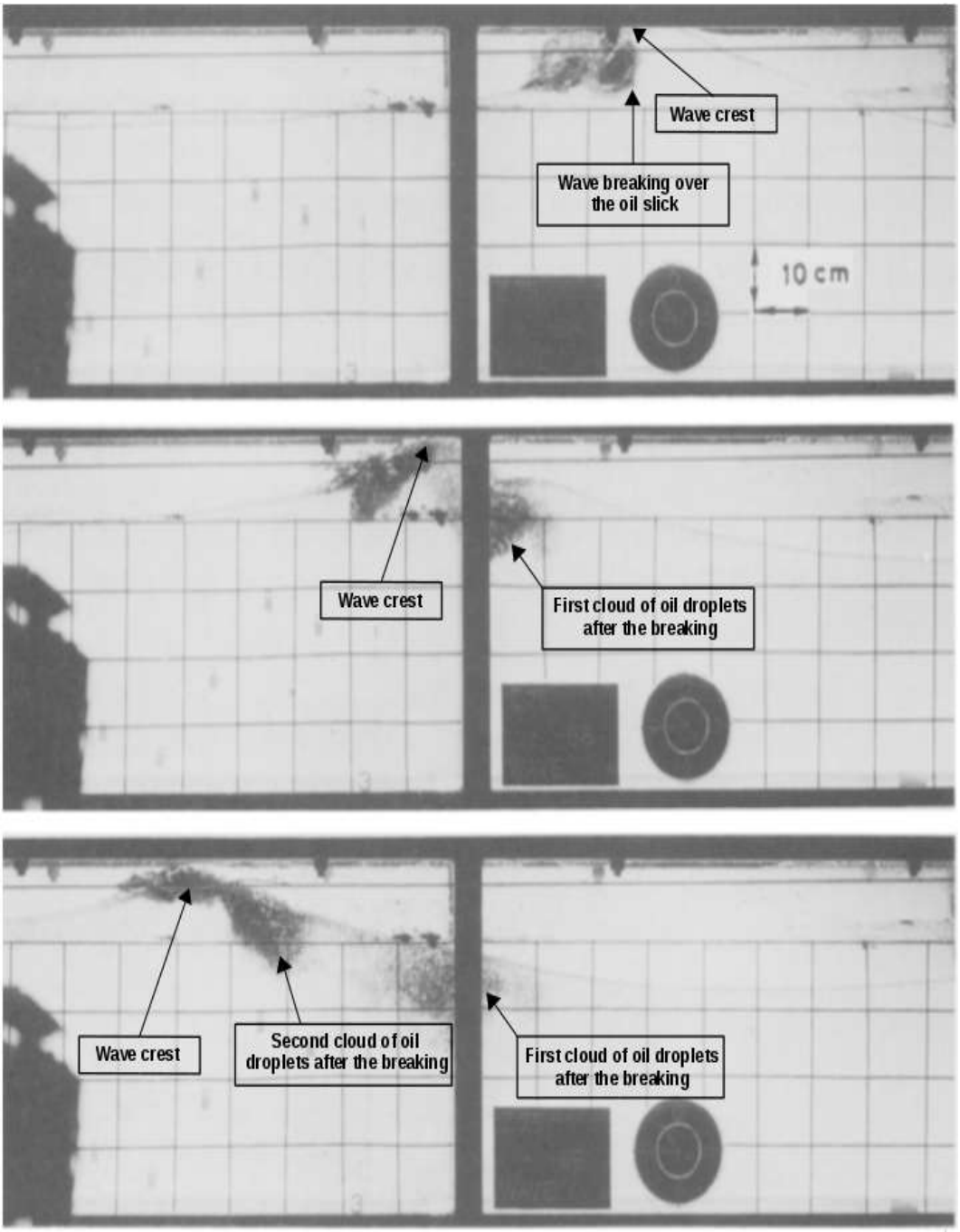

Passage of a breaking wave over an oil slick in a small flume, showing the ¨shower¨ (cloud) of oil droplets in the water column.

SOURCE: Modified from Delvigne e Sweeney (1988).

All models developed to study natural dispersion are based in following sub-processes:

- Fragmentation and entrainment of surface oil by breaking waves (droplet formation).
- Subsequent resurfacing of larger droplets and turbulent mixing of smaller droplets (vertical and horizontal).
- Accumulation of small oil droplets in the water masses as this process is repeated by subsequent breaking waves.
- Advection and dispersion of these droplets with ambient currents and turbulence (vertical and horizontal).

Using laboratory and flume experimental observation, Delvigne e Sweeney (1988) developed a relationship for entrainment rate $Q(kg/m^2/s)$ and oil droplet size distribution as a function of turbulent level and oil viscosity. The entrainment rate was formulated as:

$$Q = C^* D^{0.57} S F d_{go}^{0.7} \Delta d, \tag{2.34}$$

where C^* - empirical entrainment constant which depends on oil type and weathering state, D - dissipated breaking wave energy per unit surface area J/m^2, S - fraction of sea surface covered by oil, F - fraction of sea surface hit by breaking waves, Δd - oil droplet diameter interval (m).

Using a series of experimental data by Delvigne e Hulsen (1994), the entrainment constant, C^*, was parametrized to the following equations (FRENCH-MCCAY, 2004):

$$C^* = \exp(-0.1023\ \ln(\nu_{oil}) + 7.575) \ \text{ for } \ \nu_{oil} < 132\ (\text{cSt})\ ; \tag{2.35}$$

$$C^* = \exp(-1.8927\ \ln(\nu_{oil}) + 16.313) \ \text{ for } \ \nu_{oil} \geq 132\ (\text{cSt})\ ; \tag{2.36}$$

D is given by:

$$D = 0.0034\,\rho_w g H_b^2\ ; \tag{2.37}$$

where H_b - the breaking wave height (m), assumed to be equal to $1.5H_{sig}$ using the simple estimate of Liungman e Mattsson (2011), where H_{sig} is the significant wave height (m), and assuming a fully developed sea-state, can be calculated according to CERC (1984) as

$$H_{sig} = \left(\frac{0.243\,U_*^2}{g}\right)\ ; \tag{2.38}$$

where $U_*^2 = 0.71\,U_{wind}^{1.23}$ is the wind stress factor associated with the 10 m wind magnitude.

F is parameterised as:

$$\begin{aligned} F &= 3.0 \times 10^{-6}\left(W \quad {}^{3.5}/T_w\right) \quad \text{for } U_{wind} > U_{th}, \\ F &= 3.2 \times 10^{-2}\left[\left(W - U_{th}\right)/T_w\right] \quad \text{for } U_{wind} < U_{th}, \end{aligned} \tag{2.39}$$

where U_{th} is the threshold 10 m wind speed for the onset of breaking waves assumed as $5m/s$, T_w is the significant wave period and assuming a fully developed sea-state can be calculated according to CERC (1984):

$$T_w = 8.13\left(\frac{U_{wind}}{g}\right);; \tag{2.40}$$

The depth at which the dispersed droplets mix after a wave breaking event, Z_{mix} (m), is expressed as (BERRY et al., 2012):

$$Z_{mix} = max\left(\frac{D_{pz}}{w_p}, Z_i\right); \tag{2.41}$$

where Z_i is the intrusion depth (m) of the breaking wave equal to $1.5H_b$ after Delvigne e Hulsen (1994).

In applications over the past three decades, some of the key problems identified with Delvigne e Sweeney (1988) formulation include (LI et al., 2017):

a) *Model formulation is dimensional*
   The model coefficients depend on the units of the parameters used in the model, creating a chellenge in practical applications. It is also challenging to incorporate new insights into the model as advancements are made.

b) *Incorporation of droplet size into entrainment estimate*
   The entrainment formulation estimates the amount of oil entrained into the water column by droplet size class, , and hence has the droplet size distribution embedded in the entrainment formulation. This integration makes it impossible to estimate bulk entrainment without consideration of droplet formation processes. Conceptually it is simpler to separate these two processes into independent processes and models.

c) *No explicit procedure to address droplet resurfacing*
   The formulation has no explicit procedure to address resurfacing of dispersed droplets. This is typically handled by an ad-hoc adjustment so that droplets that are deemed to surface immediately after being injected into the water column are not dispersed in the first instance.

d) *Use of power law droplet size distribution*
   A power law formulation is used to represent dispersed oil droplet sizes. While the power law fits the original data used in the model development reasonably well, it is not typically used.

e) *Application of dispersants*
   The formulation has no provisions for cases when dispersants are applied to the spill. If this is to be modeled then the droplet size classes need to be adjusted. The dispersant to oil ratio (DOR) and dispersant efficiency (DE) need to be addressed as separate calculations.

f) *Ad hoc adjustment for oil viscosity*
   Viscous effects are addressed through an ad hoc adjustment of one of the coefficients in the empirical model formulation and not explicitly incorporated into the model formulation.

The overcome these and other problems, Li et al. (2017) developed an adimensional entrainment rate Q_0 formulation:

$$Q_0 = aWe^b Oh^c \; ; \tag{2.42}$$

where a, b, c are constants, We is the dimensionless Weber number, and Oh the dimensionless Ohnesorge number.

A common assumption applied here is that the action of each breaking wave can be seen as independent of the previous breaking events, and that (vertical) advection and turbulent mixing of oil droplets are dominated by the long term averaged turbulence (induced by wind stress and wave motion). This assumption is supported by the rapid dissipation of the turbulent energy related to each breaking wave event both in time and space.

The Weber number, We, is the ratio of disruptive momentum (hydrodynamic) forces to restorative interfacial tension forces, and is a function of seawater density, gravity, wave height, the oil-water interfacial tension, and the Rayleigh-Taylor (R-T) instability maximum diameter, d_0, which is given by Grace et al. (1978) as:

$$d_0 = 4 \left(\frac{\sigma_{o-w}}{\triangle \rho \, g} \right)^{0.5} \; ; \tag{2.43}$$

where σ_{o-w} is the oil-water interfacial tension.

Assuming that the product gH_{sig} represents the potential energy in the breaking waves, the Weber number can be expressed as (REED et al., 2009):

$$We = \frac{\rho_w \, g \, H_{sig} d_0}{\sigma_{o-w}} \; ; \tag{2.44}$$

The Ohnesorge number (LEFEBVRE, 1989; OHNESORGE, 1936) is the ratio of viscous to interfacial tension forces and is a function of the oil dynamic viscosity, the oil density, the oil-water interfacial tension, and the R-T instability maximum diameter.

$$Oh = \frac{\mu_0}{\sqrt{\rho_0 \sigma_{o-w} d_0}} \; ; \tag{2.45}$$

Recently Li et al. (2016) has presented a unified oil droplet size model that was developed for a variety of turbulent conditions based on non-dimensional analysis of disruptive and restorative forces, which is applicable to oil droplet formation under both surface breaking-wave and subsurface-blowout conditions, with or without dispersant application. This new model was calibrated and successfully validated with dispersant-treated and non-treated oil droplet size data obtained from controlled laboratory studies of dispersant-treated and non-treated oil in API (industry)- and BSEE (government)-sponsored subsea dispersant tank tests. The model was also validated against results from field surveys, including the Deep Spill experimental release and the Deepwater Horizon blowout oil spill. This model is an advancement over prior models, as it explicitly addresses the dispersed phase viscosity effects resulting from dispersant application and constrains the maximum stable droplet size based on Rayleigh-Taylor instability that needs to be invoked for a release from a large aperture.

To address the problem of resurfacing of dispersed oil droplets, a protocol has been developed that balances the return of oil droplets to the sea surface by buoyancy and the energetic dispersion that occurs in the near surface region in the presence of breaking waves. This replaces the ad hoc method used in Delvigne e Sweeney (1988).

2.8 Coupled Physical-chemical processes

In the numerical study of weathering precesses associated with oil-in-water bodies, effort are not only spent in the implementation of the process itself, but also in understanding the interactions between these processeses, since there are mutual relationships among physical-chemical transformations undergone by the oil/emulsion, as depicted in figure 2.2.

Figure 2.2 - Coupling of physical-chemical processes

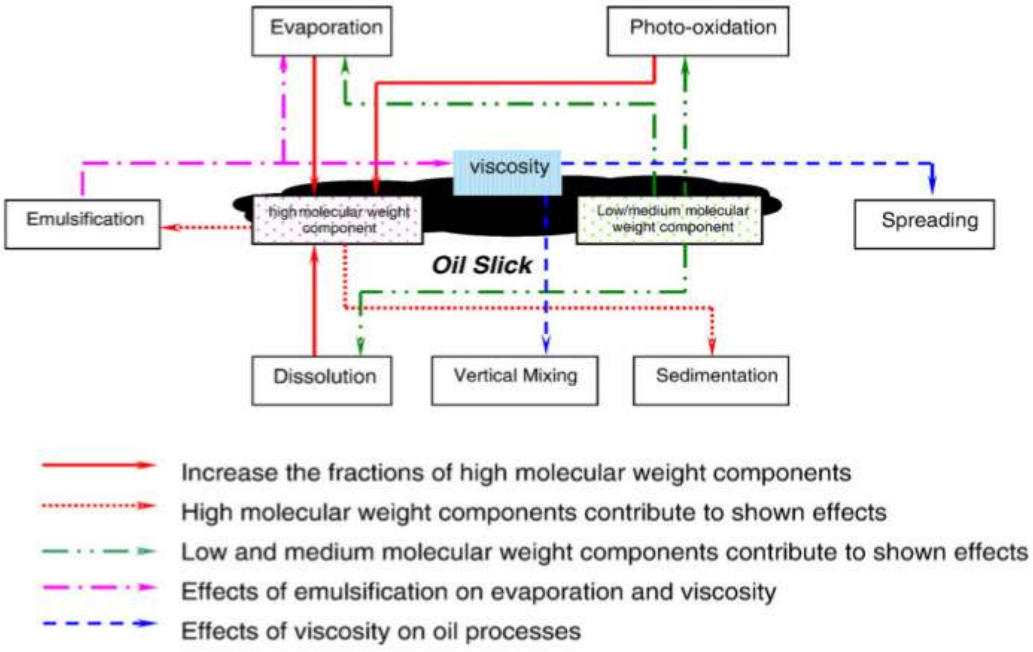

Representation of the physical-chemical processes acting on a slick on the ocean surface with the coupling among them indicated by arrows

SOURCE: Adapted de Xie et al. (2007).

Oil is a complex mixture of multiple hydrocarbons components with differents molecular weights. Processes act on components with different intensities, which changes the physical-chemical properties of the oil, affecting all weathering processes.

As gravitational spreading occurs to a minimum thickness, the area exposed to evaporation is high relative to the oil volume, greatly increasing the importance of evaporation over dissolution. Spreading can also affect entrainment process, since its flux rate is dependent on slick thickness through the terms of the Weber number and Ohnesorger number, used in the formulation of Li et al. (2017).

For surface slicks, since the partial pressures tend to exceed the solubility of the lower molecular weight compounds, evaporation accounts for a larger portion of the mass lost than dissolution (MCAULIFFE, 1989). Dissolution and evaporation are competitive processes though. The dissolved component concentration of

hydrocarbons in water under a surface slick shows an initial increase followed by a rapid decrease after some hours due to the evaporative loss of components. Most soluble components are also volatile and direct evaporation (volatilization) from the water column depletes their concentrations in the water. Dissolution is particularly important where evaporation is low (from dispersed oil droplets and in ice-covered surfaces) (SPAULDING, 2017). Dissolution can be significant from subsurface droplets due to the lack of atmospheric exposure and the higher surface area per unit of volume (FRENCH-MCCAY; PAYNE, 2001).

Evaporation and dissolution remove low and medium molecular weight (MW) components from the oil slick, increasing high MW components in the oil (YANG; WANG, 1977, 1977; XIE et al., 2007). Among these high MW are the surfactants, such as asphaltenes, resins, and waxes, that greatly influence the emulsification (see 2.6). Since the evaporation of surfactants are very limited (close to zero), volatile components are removed from the oil, increasing the fraction of X_a and X_w in equation 2.31, and modifying the stability of the emulsion. Bobra (1991) explained that surfactant materials lower the interfacial tension as they migrate to the interface, prevent water-water droplet coalescence in the emulsion, and hence make the emulsion more stable.

In their experiments, Fingas e Fieldhouse (2004) found that Carpenteria crude oil does not form any type of emulsion at 0% evaporation, but forms a mesostable emulsion after 10% is lost through evaporation. Therefore, an oil that initially was uncapable of producing a stable emulsion can become capable through evaporation.

With the onset of emulsification, not only viscosity is affected (and therefore the entrainment process), but also evaporation and spreading of the slick. The National Research Council (2003) and Fingas (1995) found that evaporation and spreading slow down due to emulsification. An experimental study by Ross e Buist (1995) found that oil evaporation is reduced when oil is mixed with water to form a stable water-in-oil emulsion. The inhibition of evaporation increases with increasing water content and slick thickness.

The deleterious influence of emulsification on evaporation was quantified by Ross e Buist (1995) as

$$F_{ew} = \frac{C_2 - F_{wc}}{C_2} F_{vol}; \tag{2.46}$$

Where F_{vol} is the volatile fraction, F_{ew} is the adapted volatile fraction, F_{wc} is the water fraction, and C_2 is the maximum allowed water fraction.

The effect of emulsufication on the mechanical spreading is computed in equation 2.3, with the increase in the emulsion viscosity leading to a reduction in the area growth rate.

In this section only part of the interactions among the processes were mentioned. Some physical-chemical reactions between the processes are still poorly understood, like the influence of viscosity increase on entrainment, and can become more complex if sedimentation, bioxidation and biodegradion are added to the equation.

3 METHODOLOGY

3.1 Study area

The study area of this thesis comprises the water body defined as the Estuarine System of Vitória Island (Sistema Estuarino da Ilha de Vitória, SEIV), which is commonly divided in Espírito Santo bay (Baía do Espírito Santo, BES) and Vit́oria bay (VERONEZ et al., 2009). As part of this system are the Vitória Port and its channel, the Canal da Passagem, and the Tubarão port (Figure 3.1).

At the beggining of 2019, one year after the conclusion of the dredging of Vitória channel, it was allowed the access of ships with an upper weight limit of 70 thousand tons to Vitória Port. Before that, the limit was of 30 thousand tons. Meanwhile, Tubarão port is a private port owning to Vale, one of the largest in the world in the transport of iron ore and pellets, with a capacity to receive vessels with a weight limit up to 300 thousand tons.

The hydrodinamics of the SEIV is strongly controlled by the astronomic tide and the Santa Maria da Vitória river discharge, as described by Nascimento et al. (2013). The tidal regime is classified as semidiurnal micro-tidal. The wind regime in the region is dominated by northeast, east and southeast directions.

Figure 3.1 - Study area

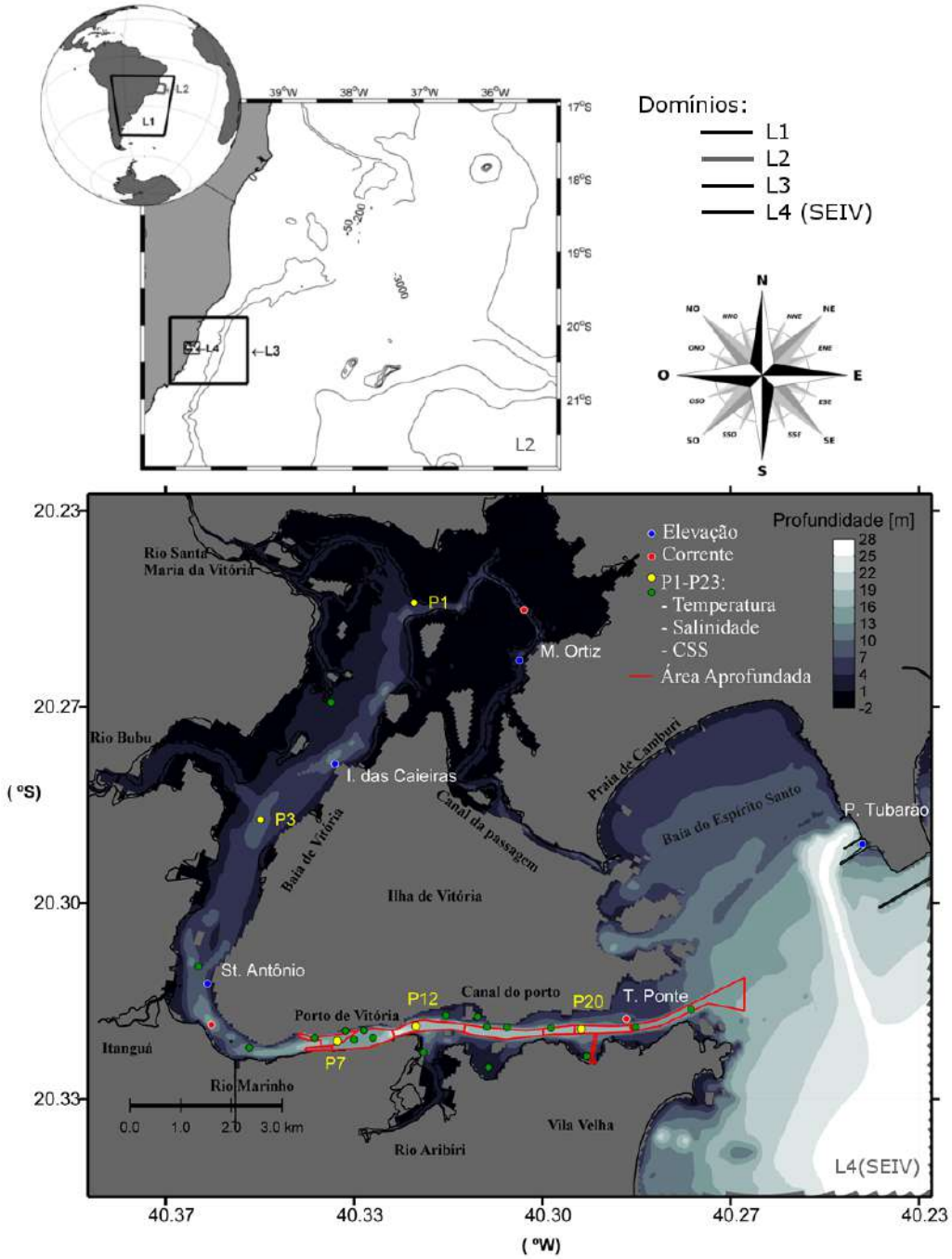

Location of the study area. In the map the gauging stations for current (T. Ponte) and elevation (P. Tubarão, St. Antonio, I. Das Caieiras, M. Ortiz) are indicated. The computational domains are also defined.

3.2 Hydrodinamic model setup

The hydrodynamic model chosen to couple with the oil spill model is the Delft3D, a three-dimensional Boussinesq based model widely used for research and economical purposes. For information regarding the physical-mathematical description of the model, check Deltares (2014).

To implement the hydrodynamic model in the study region, a nested grid system made by four grids was used to transpose the oceanographic information from offshore to the SEIV (Table 3.2, Figure 3.2). For the innermost region was built a curvilinear grid (L4 in Figure 3.2) to optimize the highly irregular morphology of the study region, allowing higher resolution in some specific areas of interest (Figure 3.3). Regarding the vertical grid, it was used $10\,\sigma$ layers.

Table 3.1 - Description of the nested grid system

Domain	**Geographic coordinates**		**Horizontal resolution**
	Latitude	**Longitude**	
L1	-46,004990 °	67,683432 °	1/12 °
	-11,107052 °	-30,000000 °	
L2	-21,966058 °	-40,998266 °	1/36 °
	-16,906462 °	-35,049066 °	
L3	-20,793688 °	-40,582035 °	1/108 °
	-19,891591 °	-39,484633 °	
L4	-20,391339 °	-40,249387 °	Variable (14-270 m)
	-20,217141 °	-40,203001 °	

Figure 3.2 - Nested grids

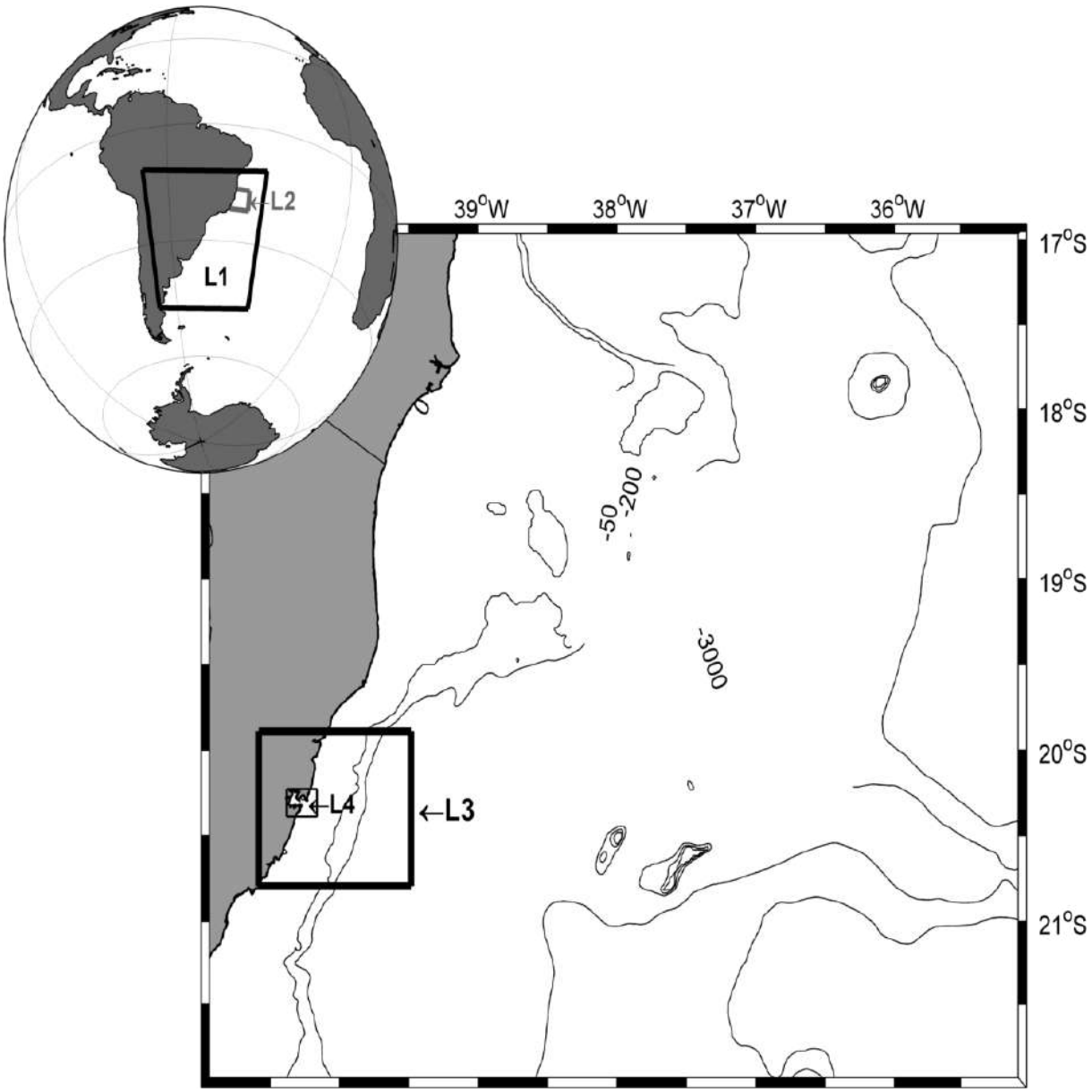

System of nested grids used in the hydrodynamic simulation

Figure 3.3 - L4 grid

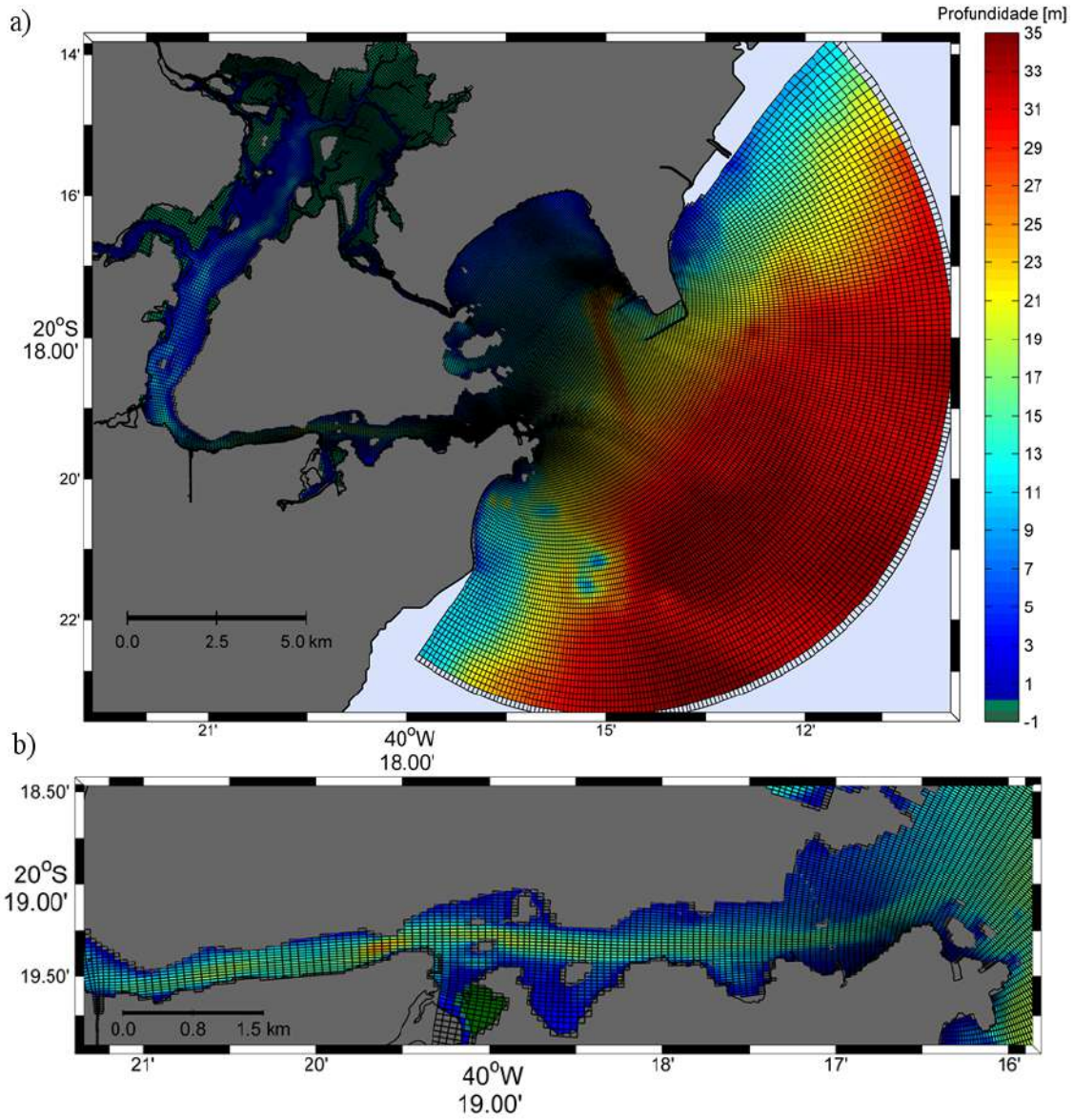

Curvilinear L4 grid. At bottom a zoom in part of the Vitória bay.

At the offshore open boundaries, it was used the characteristics based Riemann boundary condition (VERBOOM; SLOB, 1984) at each grid point. In this boundary condition, Riemann invariants are built from water level and current velocity data (equation 3.1):

$$R = U \pm \eta\sqrt{\frac{g}{h}}\,, \tag{3.1}$$

where U is the current velocity normal to the boundary section, η is the water level, and h the depth in relation to the mean level.

The water level and velocity data were obtained through the nesting between L2 and L1. From L2 to inner domains, it was transposed riemann invariant values.

At the domain L1, hydrodynamic information were calculated from 13 tidal harmonics (i.e., M2, S2, N2, K1, O1, Q1, Mf, Mm, M4, MS4, MN4). The values of phase and amplitude are from the global model TPXO (EGBERT; EROFEEVA, 2002), interpolated to L1.

The atmospheric fluxes were parameterized through the quadratic law for wind velocity, with the friction coefficient calculated by the formulation of Large e Pond (1981) for the domains L1, L2, L3 and of Smith e Banke (1975) for the L4. For these calculations were used x and y components of wind velocity at 10m and atmospheric pressure at sea level, obtained from reanalysis 2 of NCEP (NCEP2), with temporal resolution of 6h and spatial of $2,5°$.

To calculate the turbulent diffusion coefficients, crucial in the parametrization of the parcels dispersion through the *random walk*, it was choosen the second-order turbulence closure model $k - \varepsilon$. In this model, both the turbulent kinetic energy k and the turbulent kinetic dissipation ε are prescribed by a transport equation. For more information regarding the 4 turbulence models implemented in Delft3D and their especifications, check Deltares (2014)

The bathymetric information used in domains L1, L2, L3 was interpolated from the global bathymetric data GEBCO08, and from nautical charts (n° 1400, 1402 and 1403), available by DHN (Diretório de Hidrografia e Navegação da Marinha do Brasil). For the domain L4, bathymetric and altimetric data were constructed from a digital elevation model made availabel by Laboratório de Simulação de Escoamento com Superfície Livre (LABESUL), with input data from nautical chart n° 1401, and depth gauging of the channels (RIGO, 2001).

Regarding the termohaline information in the offshore region, values of temperature and salinity were interpolated from the HYMCOM + NCODA global $1/12°$ reanalysis, available at `https://www.hycom.org/dataserver/gofs-3pt0/`

reanalysis.

At the inland open boundaries were imposed river discharges from Instituto Estadual de Meio Ambiente (IEMA) (Table 3.2), with the stationary values applied over the simulation.

After the establishment of all input data, the model was run for 60 days, including 30 days of spin up time and 30 days for data validation and oil spill simulations. The long period for spin up is necessary due to the baroclinicity of the model.

Table 3.2 - Description of the tributaries of Vitória bay

Tributary	**Date**	**Flow rate (m^3/s)**	**Temperature ($^\circ C$)**	**Salinity**
Bubu	17/10/12	0,598	24	0
Marinho	16/10/12	1,537	23	17
Aribiri	19/10/12	1,34	26	20
St. Maria da Vitória	18/10/12	13,75	24	0

3.2.1 Validation

The modelled results were compared against measured data of current and elevation for the period between 3/04/1999 and 18/04/1999. The current data was collected at the Terceira ponte station (Figure 3.1), and elevation at the Porto de Tubarão, Santo antonio, Maria Ortiz, and Ilha das Caieiras stations (Figure 3.1). The validation for temperature and salinity was performed against the measured data made available by IEMA for 23 gauging locations along Vitória bay (Figure 3.4). For each station was measured a data at the surface and bottom between 9/10/2012 and 11/10/2012.

Five experiments with different setups of boundary and surface conditions were stablished to evaluate the response of the model to different degrees of sofistication of the input conditions. The five experiments are differentiated as following: WL - astronomical tide, WWL - tide (astronomical and meteorological), TS - tide, temperature, salinity, W - tide, wind, atmospheric pressure, 2DH - tide, temperature, salinity, wind, atmospheric pressure, 3D - tide, temperature, salinity, wind, atmospheric pressure.

The comparison between modelled and measured data was performed from the

analysis of the following statistical parameters: Willmott´s index of agreement (Id or IAS), Mean Absolut Error (MAE), Root Mean Square (RMS), Pearson Correlation Index (r), and Bias.

After the validation of the hydrodynamic model, paramount in the correct calculation of particles and droplets advection/dispersion, theoretical oil spill simulations were performed with the oil model to fullfill all objectives.

Figure 3.4 - Gauging stations

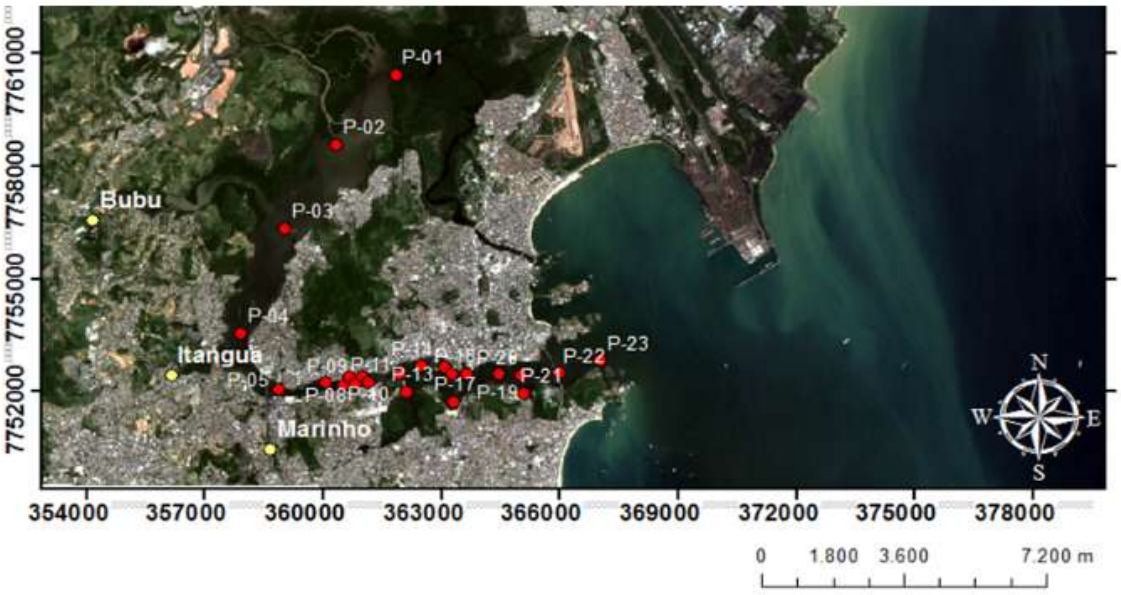

Location of the gauging stations for the thermohaline data (P-01 to P-23.)
SOURCE: Produção do autor

3.3 Wind data

The x and y wind velocity components used in the transport equations (equations 2.10 and 2.11) were interpolated from the ERA 5 reanalysis. ERA5 provides hourly estimates of a large number of atmospheric, land and oceanic climate variables. The data cover the Earth on a 30km grid and resolve the atmosphere using 137 levels from the surface up to a height of 80km. ERA5 includes information about uncertainties for all variables at reduced spatial and temporal

resolutions (ECMWF, 2019).

3.4 Oil Model

In this thesis, an open source three-dimensional oil spill model based on the lagrangian parcel method was built to simulate the dynamics of oil spilled on the ocean surface, using the advection from the meteo-oceanographic forcings and the random walk technique to resolve the three-dimensional transport of particles and droplets, and state-of-art parametrizations to compute the physical-chemical transformation undergone by the oil. Furthermore, to gain a better understanding of the impacts from potential oil spills, we implemented a probabilistic method, which simulates numerous oil spill trajectories under varying environmental conditions. From this probabilistic simulation were calculated statistical parameters to be used as a tool for management, mitigation, and response analysis.

The oil spill model was written in Fortran, with the pre- and post-processing realized in Python. Fortran was chosen due to its computational performance, essential in lagrangian models that require a great number of calculations in each timestep. Python was chosen due to its widespread usage in data analysis and straightforward installation procedure.

The pre-processing is the gathering and reshaping of all meteo-oceanographic data used by the oil model, corresponding to an offline coupling between Delft3D/wind data and the oil spill model. Hourly files for 3D fields of temperature and salinity, x, y and z velocity components, x and y wind components, and vertical and horizontal eddy diffusivities are created from the output data of the hydrodinamic model and the ERA 5 reanalysis, being all interpolations resolved inside the oil model.

In lagrangian models the interpolations are the most time-consuming part of the simulation, as the fields of properties are interpolated to all particles and droplets at each timestep. After each displacement, the new coordinate of a parcel is located in the hydrodynamic and atmospheric grid, from which the nearby information are loaded for interpolation.

Post-processing involves codes designed for data analysis and visualization methods.

The model was structured following the recomendation of Spaulding (2017),

which stated that it is best to have each fate process as a separate algorithm with supporting data provided from other algorithms as appropriate. This allows a straightfoward accomodation of potential algorithms for each fate process, essential for the improvement of the model.

In its current implementation the oil model presents 2 main programs, for continuous and instantaneous sources, and 10 modules. The weathering processes can be activated independently, depending on the purpose of the research. If all weathering processes are deactivated, the particles are deemed as conservative parcels.

In order to facilitate future contributions to the oil model, the code was uploaded to the github repository `https://github.com/fernandotcbarreto/SYMOS-model`. A github system allows developers to easily collaborate, as they can download the current version of the code, make changes, and upload the newest revision, keeping the records of all changes.

Figure 3.5 shows a flow chart of the mean structure of the oil model. After the pre-processing of the input data, the model splits into two sources, continuous, where a group particles are released in some frequency, and instantaneous, where a group of particles is only released in the initial timestep.

Two types of timestep were implemented in the model, one to resolve the turbulent diffusion of particle and droplets, called difusion timestep (DTS), and one to resolve the advection equation and processes calculations, called simply timestep (TS). Due to the rapid nature of turbulent motion, DTS is usually much smaller than TS, requiring for the advection-diffusion equation to be resolved using two timesteps. Time evolution was resolved using the Euler method, that constrains small values to be used for the TS.

The instantaneous source was designed to be a section in the model where the new implementations are coded and tested, since the workflow in this section is simpler and easier to modify. After the validation of the processes they can be implemented in the continuous source, the main core of the model.

For the continuous source, two modes of release were implemented. In the classical mode, subsequent group of particles are added to previous ones, increasing the number of particles in the domain at each release. In the probabilistic mode, with a new release the old parcels are erased from the

simulation after the record of their information, similar to multiple instantaneous releases.

Figure 3.5 - Flowchart of the main modules inside the oil module

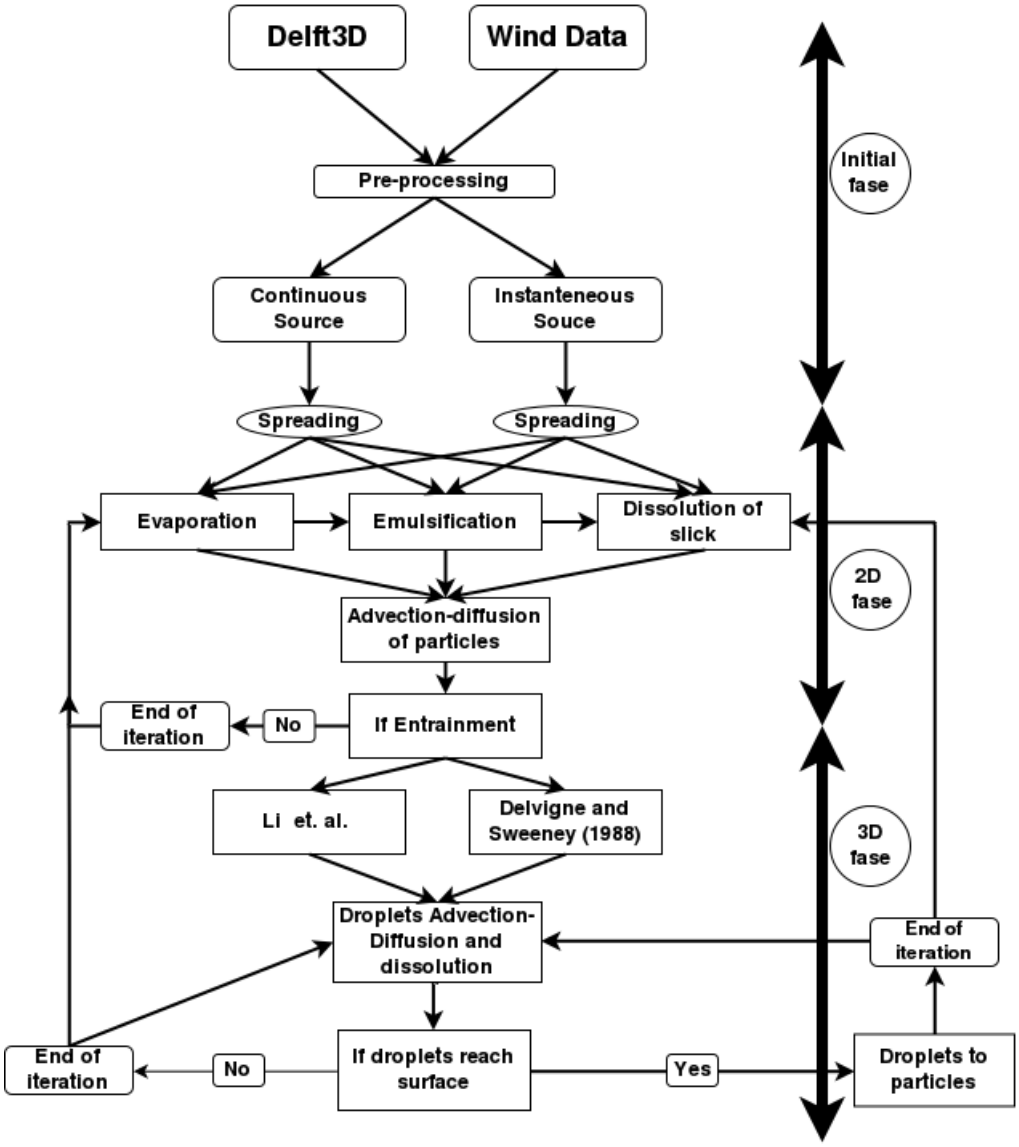

SOURCE: Produção do autor

After the initial fase, the model splits into 4 weathering processes. The processes were implemented in the following order: evaporation (REED, 1989), emulsification

(MACKAY et al., 1980), dissolution (JOHANSEN, 2003) and entrainment (DELVIGNE; HULSEN, 1994; LI et al., 2017). If entrainment is deactivated, it is only calculated the horizontal advection and diffusion of particles, in a 2D simulation, since no oil is exchanged with the water column (no droplets are generated).

Two state-of-art formulations were implemented for the calculation of the entrainment rate, Delvigne e Sweeney (1988) and Li et al. (2017). The diameter of the oil droplets (in m) injected in the water column by entrainment was defined as in Reed et al. (1995) (equation 3.2). Droplet size distribution is not implemented in the model.

$$d_0 = C_0 \, \nu_{oil}^{0.34} e^{-0.4} \tag{3.2}$$

where $e \, (J/m^3 \cdot s)$ is the energy dissipation rate.

At each timestep the entrainment rate is calculated for each particle, with droplets being generated from each positive flux value. Once in the water column, oil droplets go through dissolution, buoyancy, advection, and diffusion. If in subsequente timesteps the oil droplet resurfaces, it returns to the 2D fase, being subject to the same processes as the particles, including entrainment.

Regarding advection, it was resolved from the current data of the Delft3D and the wind data from ERA5 reanalysis. The advection by waves, also know as Stokes drift, was not computed, since it requires the coupling with a wave model.

An important boundary condition in an oil model is the interaction of the parcels with the shoreline, ocean floor, or any other hard surface, a process called stranding or beaching. In the current implementation of the model, when reaching a hard surface the parcel presents 100% probability of adhering to it. Regarding the ocean-atmosphere interface, it was used a non-penetrative boundary condition.

To validate all four physical-chemical processes implemented in this model, were performed simulations with 1000 particles released as an instantanuous source. This kind of source was chosen to facilitate the tracking of particles. Since validations are usually made against data collected in controled experiments, in this fase the values of sea temperature, salinity, and wind velocity used were uniform all over $\mathrm{L}4$ grid and stationary in time, aiming to reproduce a controlled

environment. As a result all particles experienced the same weathering rates.

In the emulsification section, changes to the slick viscosity and density as result of water inflow are calculated using Mooney equation, following Sebastiao e Soares (1995):

$$\mu = \mu_0 \cdot \exp\left[\left(\frac{2.5 \cdot F_{wc}}{1 - C_2 \cdot F_{wc}}\right)\right]; \tag{3.3}$$

where μ_0 is the parent oil viscosity $[cP]$.

$$\rho_e = F_{wc}\rho_a + (1 - F_{wc})\,\rho_o; \tag{3.4}$$

where ρ_e is the emulsion density (Kg/m^3), and ρ_o the oil density.

The simulations were performed for two types of oil, Ekofisk ($^\circ$API $= 44.5$), and Kuwait ($^\circ$API $= 31.1$), often used in experiments reported in literature. In the model the oil composition was implemented following the 25 pseudo-components of Johansen (2003). With this method any type of oil can be reproduced by modifications in the pseudo-components, with resultant modifications in the oil properties. The properties of the pseudo-components are shown in Table 3.3.

Table 3.3 - Properties of pseudo-componentes used to specify the oil composition in the model.

Group	Description	Molar mass (kg/kmol)	Solubility (10^{-3} kg/m^3)	Density (kg/m^3)
1	C1-C4 (dissolved in oil)	37,0	40,0	615,0
2	C5-saturates	66,0	95,0	673,0
3	C6-saturates	80,5	32,5	697,0
4	C7-saturated	99,0	9,0	712,0
5	C8-saturates	113,0	4,35	753,0
6	C9-saturates	127,0	0,205	764,0
7	Benzene	78,0	1780,0	884,0
8	C1-benzene (Toluene)	92,0	515,0	880,0
9	C2-benzene (Xylene)	106,0	175,0	875,0
10	C3-benzene	120,0	57,5	875,0
11	C4 e C5-benzenes	141,5	12,5	880,0
12	C10-saturates	140,5	0,0575	773,0

(Continue)

Table 3.3 - Conclusion

Group	Description	Molar mass (kg/kmol)	Solubility (10^{-3} kg/m^3)	Density (kg/m^3)
13	C11-C12 (total sat + aromats	156,5	0,022	810,0
14	C13-C14 (total sat + aromats)	185,5	0,0025	816,0
15	C15-C16 (saturated + aromatic)	215,5	0,01	823,0
16	C17-C18 (total sat + aromats)	238,0	0,001	828,0
17	C19-C20 (total sat + aromats)	273,0	0,001	818,0
18	C21-C25 (total sat + aromats)	317,5	0,001	823,0
19	C25+ (total sat + aromats)	465,0	0,001	950,0
20	Naphthalenes (C0-C1 Alkylated)	135,0	27,5	1015,0
21	Naphthalenes 2 (C2-C3 Alkylated)	163,0	5,5	1016,0
22	PAH 1[a]	177,0	3,65	980,0
23	PAH 2[b]	222,5	0,1005	980,0
24	Phenols (C0-C4 alkylated)	130,0	51000,0	986,0
25	Polars (C10-C36)	215,0	150,0	1015,0

[a] Medium soluble polyaromatic hydrocarbons, 3 rings-non-alkylated.

[b] Low soluble polyaromatic hydrocarbons, 3 rings-alkylated, 4-5+ rings.

Fonte: Adapted from Johansen (2003).

To evaluate the horizontal advection of oil particles, a numerical flume was established (Figure 3.6), over which were applied known current conditions to a hipothetical slick for both instantaneous and continuous spill. Since particles are passive under hydrodynamic processes, it is expected for the particles to follow the mean flow with smalls variations of position due to turbulent diffusion.

The flume is 1000 m long and high, presenting a hard boundary 300 m long at the right end (land in Figure 3.6). The current used for the testing resembles a fully developed flow, with maximum velocity of 0.5 m/s at the center and 0 in upper and bottom limits. This configuration was chosen to observe the effect of the current shear in the oil slick. Three directions for the current were used, parallel to the x axis, $15\,^\circ$ rotated upwards, $15\,^\circ$ rotated downwards.

Figure 3.6 - Numerical flume

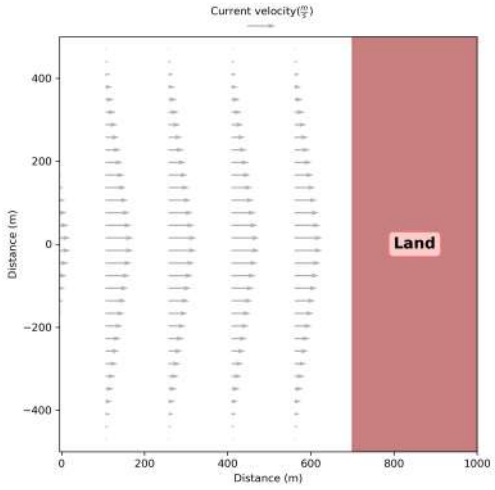

Numerical flume over which will be performed the validation of the advection of oil particles. A vector field parallel to the x axis is plotted on the figure.

After the validation of the four physical-chemical processes and of the advection, were performed simulations in the probabilistic and in the continuous mode to assess the susceptibility of the study region in oil spill events. In mitigation studies some statistical parameters are crucial when developing strategies to address in the aftermath, as the probability of an area being affected by the slick, the distribution of slick in the region, among others. These parameters are calculated from the data analysis of the results of probabilistic simulations.

In the probabilistic simulation were performed 120 deterministic runs with a period of 60 hours each, starting in randomly selected starting points along 1 month of hydrodynamic data, with the slick discretized as 5000 particles. Every event spilled 200^3 of oil to the environment. The period of each run was defined based on CONAMA resolution №6 398/08, which states the maximum time for the avaibility of resources for containment/cleaning as being 60 hours.

The number of simulations and particles were defined based in the current optimization level of the code, and in memory constraits.

In the continuous simulation, 1000 particles were released at each 12 hours for 15 days, starting at the first timestep, with a total of 30000 oil particles in the domain

by the end of the simulation. The total volume of oil spilled in the continuous source was 500^3. The continuous simulation was performed to evaluate the transport behavior of the slick in longer periods.

To account for seasonal variations in the study region the cases were run for periods of summer and winter, from 01/01/2013 to 01/02/2013 for summer, and from 01/07/2013 to 01/08/2013 for winter. The greatest difference between these two seasons is related to the wind regime, northeast dominated in the summer, and east/southeast dominated in winter, and to the flow rates of the tributaries, with the highest values found in summer, the wet season.

To reckon the sensibility of the study region to oil spill damages, in the following paragraphs are presented the parameters calculated from the output data of the probabilistic simulation.

In the distribution of the oil slick ($\%$) (equation {equacao:distri), it is stored the amount and position of particles in the hydrodynamic grid at the end of each run (60 hours). By the end of the simulation, a spatial map of the distribution of the slick was obtained by the fraction of the number of particles found in each position, by the total number of particles released along the simulation. This map allow us to analyse the shape of the slick considering n environmental conditions. A great percentage means more particles, holding no correlation to weathering processes.

$$\frac{\sum^{D} Np}{Tp}|_{\text{grid cell}}; \tag{3.5}$$

where D is the number of deterministic simulations, Np is the number of particles in each grid cell by the end of the deterministic simulation, and Tp is the total number of particles released in the probabilistic simulation.

To calculate the probability of ocurrence ($\%$) of the slick in the study region (equation 3.6), at each time step it was tracked the position of each oil particle. At the end of the simulation, it was analysed if, at least once in each run, a region was affected by the oil slick. The sum of the number of times a region was reached by the slick was divided by the total number of runs (120), indicating how often a region was affected by the spill considering the many environmental conditions. A 100% value means that the oil reached some region in all runs at least once.

$$\frac{\sum Pc}{D}|_{\text{grid cell}}; \tag{3.6}$$

where Pc is a 1 dimensional array of 1 and 0 with a length equals to D. An integer 1 means that a grid cell was reached by an oil particle at least once in the deterministic simulation, and 0 that it was not.

In the area density analysis (kg/m^2) (equation 3.7), it was recorded the mass of the slick present at each grid cell by the end of the deterministic run. At the end of the simulation the D-averaged mass was divided by the area of each grid, giving the mass of oil per unit area. This index is important when planning cleaning strategies, and is highly dependent on the weathering processes.

$$\frac{(Tm/D)}{A}|_{\text{grid cell}}; \tag{3.7}$$

where Tm is the total mass of oil defined as $\sum^D Md$, Md is the mass of oil in each grid cell by the end of the deterministic simulation, A is the area of the grid cell.

In the time percentage analysis ($\%$) (equation 3.8) it was reckoned how long a region was affected by the oil slick. For that it was recordedthe amount of time a region was in contact with the oil slick along the simulation. At the end, a percentage was calculated by the fraction of the values at each cell by the timespan of the simulation. The greater the percentage, the longer the location was affected by the slick.

$$\frac{\sum^D Tg}{Tp}|_{\text{grid cell}}; \tag{3.8}$$

where Tg is the time a grid cell is in contact with the oil slick in each deterministic simulation, and Tp is the total time of the probabilisitic simulation.

All simulations were performed for 2 strategical spill locations in the study region (figure 3.7), one near the Tubarão Port (known as "Tuburão port spill"), and the other at the entrance of the Vitória bay (Known as "Vitória bay spill"). These 2 regions are characterized by an intense movement of vessels. For the Tuburão port spill two scenarios were simulated, with and without considering the effect of the port piers in the oil transport.

Figure 3.7 - Spill locations

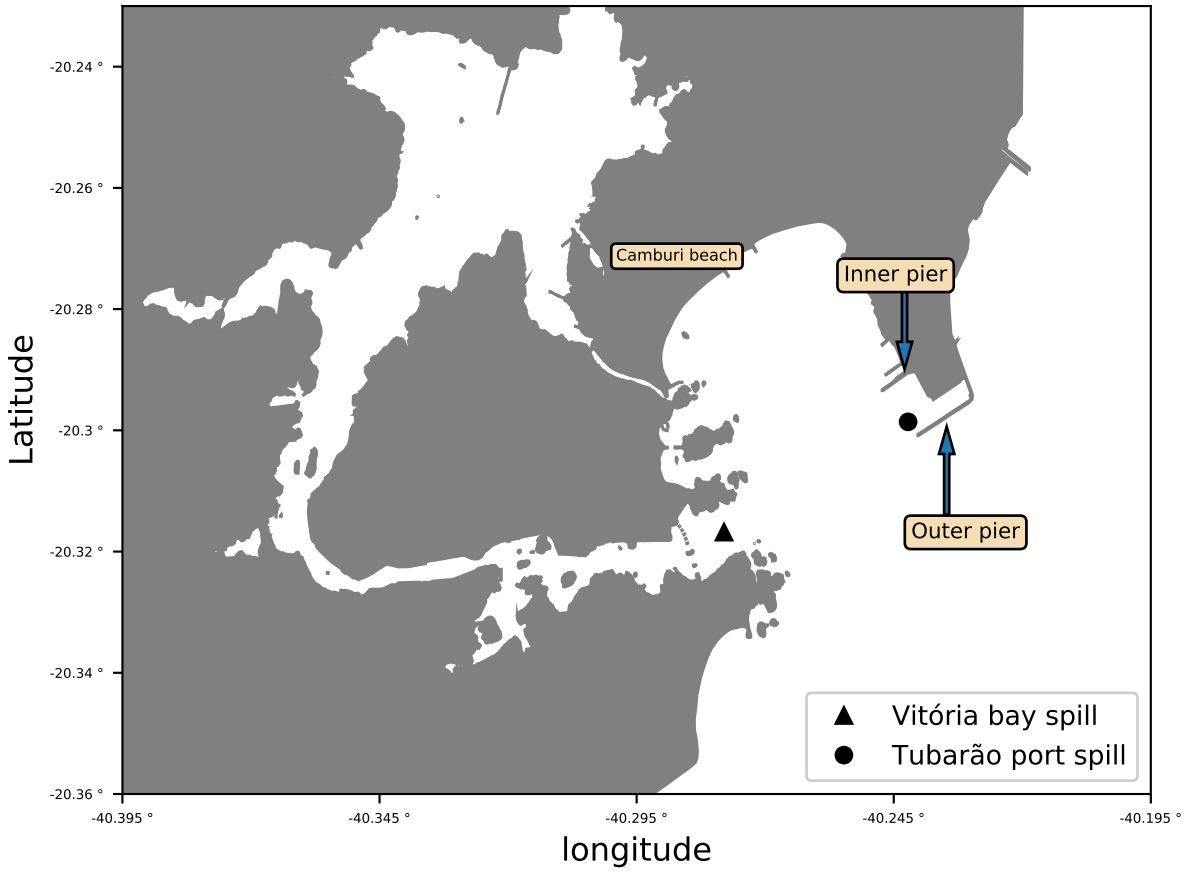

Location in the study area of the Vitória bay spill and the Tubarão port spill. At the Tubarão port the inner and outer piers are indicated

SOURCE: Produção do autor.

3.5 Numerical procedure

The formulations described in the theoretical revision (section 2) and the structure described in section 3.4 were used to determine the behaviour of oil spilled on the ocean surface. After the release of oil, the transformations resultant from the physical-chemical processes modifies the chemical composition of the oil (evaporation and dissolution), and the properties of the slick (emulsification, vertical dispersion). From the time evolution of the position of the parcels (particles and droplets in the lagrangian parcel method), and the concentration

of each of the 25 oil pseudo-components, we can evaluate the influence of the environmental conditions in the evolution of the oil slick, inducing or hampering the physical-chemical processes and the transport of the parcels.

The numerical model was split in two stages, the surface stage (oil slick represented by particles) and the water column stage (entrained oil represented by droplets). In 2D simulations the water column stage is not resolved.

At the moment of release, it is used the volume and the location of the spill, the chemical composition of the oil (API and the mass fraction of the pseudo-components), and the number of parcels to construct the oil slick from the radius given by the gravity-inertial spreading equation (section 2.2), with the oil particles randomly located inside the slick. The gravity-viscous spreading of each particle was computed following Aamo et al. (1997), setting a mininum thickness under which spreading ceases.

From a numerical point of view each particle may be understood as a ¨mini-slick¨, since the modifications in the slick are calculated from the sum of the properties of each particle, as in equation 3.9.

$$M_S = M_1^p + M_2^p + M_3^p \cdots + M_n^p; \tag{3.9}$$

where M_S is the mass of the slick, M^p is the mass of the particles, and n the number of particles.

In the water column, since the diameter of the droplets is too small (with values ranging from 1 and 1000μ), at each entrainment process all droplets with the same diameter are grouped in the same parcel, with the dissolution rate and transport equally affecting all droplets in this parcel. Without this numerical procedure, it would be impossible to apply the lagrangian method in the water column, due to the incredibly large number (in the thousands) of droplets generated at each entrainment process.

At each time step, the workflow can be schematized in the following routine:

a) Surface stage:

- Properties of each particle:
  - coordinates (x_0, y_0);
  - mass fractions of each oil pseudo-component;

  - fractions of oil mass and water in the particle (result of emulsification);
  - mass of the oil and the emulsion in the particle;
  - specific mass and viscosity of oil and emulsion;
  - thickness, radius, and volume of the particle.
- from the coordinates, the physical properties of the environmet (current and wind velocity, temperature, salinity, diffusity) are interpolated;
- Evaporation is computed using as input the atmospheric information, with the evaporation rate resolved for each pseudo-component. Since the mass fraction of the components are modified, the particle properties are recalculated;
- Dissolution is computed using as input the atmospheric and termohaline information, with the dissolution rate resolved for each pseudo-component. Since the mass fraction of the components are modified, the particle properties are recalculated ;
- Emulsification is computed using as input the atmospheric and termohaline information, resulting in the uptake and release of water to/from the slick. Since the oil composition is not modified during emulsification, only the emulsition properties are recalculated;
- Vertical dispersion is computed using the atmospheric information, being this a source of mass loss to the water column stage. Since it is assumed the entrained oil as having the same chemical composition of the origin particle, the chemical properties of the oil are not modified. The size of the oil droplets are calculated as stated in equation 3.2;
- The advection of the particles are resolved from current and wind velocity, and the turbulent diffusion (random walk) from the diffusity;
- Check whether the continuous or probabilistic condition is satisfied, applying the appropriate modification in the variables, as the reinitialization of all particles properties for the probabilistic case, and the inclusion of new particles in the continuous one;
- Check whether there are resurfaced droplets. If yes, resize the variables and compute the coordinates and the chemical properties of the new particle. Resurfaced droplets is a source of mass gain from the water column stage.

b) Water column stage:

- After each entrainment process new parcels are included in the water column stage;
- Properties of droplets:
  - coordinates, including the vertical position in the water column (x_0, y_0, z_0);
  - mass fractions of each oil pseudo-component;
  - mass of oil in the droplet;
  - specific mass and viscosity of the oil;
  - radius and volume of the droplet.
- Properties of parcels:
  - coordinates, including vertical position in the water column (x_0, y_0, z_0);
  - number and diameter of droplets.
- Each parcel is formed by thousands of droplets, all with the same properties;
- From the coordinates, the physical properties of the environmet (current and wind velocity, temperature, salinity, diffusity) are interpolated;
- Dissolution is computed using as input the termohaline information, with the dissolution rate resolved for each pseudo-component. All droplets of a parcel undergo the same dissoluton rate, resulting in a decrease in radius. Since the mass fraction of the components are modified, all droplet properties are recalculated;
- The advection of the parcels are calculated from current velocity, the buoyancy from the termohaline information, and the turbulent diffusion (random walk) from the diffusity;
- Check whether there are resurfaced parcels. If yes, this parcel is transfered to the surface stage. Resurfaced parcels is a source of mass loss to the surface stage.

3.6 Probabilistic module

The probabilistic module was implemented to account for the great number of runs necessary to obtain a steady probability distribution, from which are calculate

the parameters to be used in the sensibility analysis. Since the ocurrence of an oil spill is unpredictable, it is simulated a great number of cases to resolve the transport and weathering processes under varying oceanographic and atmospheric conditions, allowing a more adequate assessment of the susceptibility of the study region to oil spill damage. In this kind of simulation the probabilistic module is responsible to control the modifications in the workflow of the algorithm and in the variables, setting the onset of the deterministic runs in a random timepoint along the simulation period.

In a probabilistic simulation, each deterministic run is independent, with no information nor parcels being transfered to subsequent runs. As a result, a small variation of the computation effort is observed along the simulation, resultant from the fluctuations of the number of droplets between the deterministic runs.

The workflow for the probabilistic module can be schematized in the following routine:

- Define the oil properties of leaking oil (density, viscosity, surface tension, volatility, etc), and the spill size;
- Compute the properties of the parcels (height, diamater, volume, coordinates);
- Define the period of the deterministic run;
- Define the number of deterministic runs (length of the probabilistic simulation);
- Define the number of parcels;
- Provide accurate information of temporal environmental conditions (temperature, salinity, currents, diffusivity, and winds);
- Simulate the processes of oil-slick transport and fate, recording relevant information (each grid cell will be polluted or not throughout the spill scenario, the duration of each cell exposed to slick, the final quantity of particles and mass at each cell, etc.);
- Repeated running abundant times of indenpendt oil-spilll events to obtain steady probability distribution;
- If the end of a deterministic run is reached:

  - Erase the parcels;
  - Define the new slick;
  - Reinitialize the variables;
  - Randomly selects a new starting point along the simulation period.
- If the number of deterministic runs is reached:
  - Statistical analysis of data from every hypothetical spill event;
  - End the probabilistic simulation.

3.7 Continuous Simulation

A continuous simulation was designed to reproduce a continuous spill, in which oil is spilled on the ocean surface at some frequency. In management studies, continuous simulations are often used to evaluate worst case cenarios, since more damage is expected from releases of oil in larger periods of time.

In the numerical model, the continuous simulation is represented by the release of new particles in the domain, adding up to old particles and droplets. As a result, a crescent computational effort establishes, since more calculations are resolved after each release.

The workflow for the continuous simulation can be schematized in the following routine:

- Define the period of the simulation;
- Define the frequency of releases (timespan between each spillage);
- Define the number of parcels;
- Define the oil properties of leaking oil;
- Compute the properties of the parcels (height, diamater, volume, coordinates);
- Interpolate the meteoceanographic conditions;
- Simulate the processes of oil-slick transport and fate;
- If the timepoint a new spillage is reached:
  - Release new parcels;

- Define the oil properties of leaking oil;
- Compute the properties of the new parcels (height, diamater, volume, coordinates);
- Resize the variables, increasing the dimension along the particles index;
- Modifies the loop along the particles;

4 RESULTS AND DISCUSSION

4.1 Validation

4.1.1 Validation of the hydrodynamic model

In this section the results from the simulations with Delft3D are compared against measured data to assess the ability of the model in reproducing the hydrodynamic and termohaline fields in the study region, crucial in the transport and in the physical-chemical processes undergone by the oil slick .

In table 4.1.1 are presented the results of the six statistical parameters, Willmott´s index of agreement (Id or IAS), Mean Absolut Error (MAE), Root Mean Square (RMS), Pearson Correlation Index (r), and Bias, for the six experiments, WL (astronomical tide), WWL (astronomical and meteorological tide), TS (tide, temperature, salinity), W (tide, wind, atmospheric pressure), 2DH (tide, temperature, salinity, wind, atmospheric pressure), and 3D (tide, temperature, salinity, wind, atmospheric pressure), at two stations, Terceira ponte (current data), and Vitória Port (Water level).

Table 4.1 - Statistical analysis of the experiments performed for validation

Station	Experiment	Id or IAS	MAE (S.I.)	RMS (S.I.)	r	Bias (S.I.)
Vitória Port (Water level)	WL	0,9873	0,0682	0,0823	0,9811	0,0411
	WWL	0,9935	0,0468	0,0598	0,9882	0,0174
	TS	0,9935	0,0469	0,0598	0,9881	0,0166
	W	0,9935	0,0466	0,0596	0,9883	0,0176
	2HD	0,9934	0,0471	0,0604	0,9881	0,0186
	3D	0,9935	0,0462	0,0594	0,9883	0,0160
Terceira ponte (Current)	WL	0,8968	0,0663	0,0844	0,8081	-0,0052
	WWL	0,8897	0,0682	0,0873	0,7942	0,0009
	TS	0,8908	0,0676	0,0869	0,7962	0,0014
	W	0,8893	0,0683	0,0874	0,7935	0,0016
	2HD	0,8886	0,0690	0,0881	0,7925	-0,0005
	3D	0,8972	0,0658	0,0832	0,8097	-0,0075

In general, the IAS parameter indicates that the simulations reproduced the gauged water level (IAS of 0.99) and and current (IAS of 0.89) satisfactorilly. Modelled water level also presented high correlation (r, ≈ 0.99), and small values of MAE, of $\approx 0.047\,m$. In this case MAE represents about 6% of the maximum amplitudes.

The modelled current values presented correlation of ≈ 0.8, and MAE of $\approx$

$0.07\,m/s$. MAE represents the 10% of the greatest velocities that ocurried during the ebbing of spring tides, with values up to $0.7\,m/s$.

The IAS obtained for elevation (0.993), is similar to the results of Li e Reidenbach (2014) to simulations performed for the coastal region of Bocas del Toro archipelago, with the best result for elevation being 0.937, and by Nascimento et al. (2013) for the SEIV region, with a maximum IAS of 0.981

The IAS obtained for current magnitude (0.889 - 2DH) is inside the range obtained by Nascimento et al. (2013), $0,791 - 0,949$

The value of $0.088\,m/s$ for the RMS is similar to the values found by Barth et al. (2008), between $0,791$ and $0,949$, when comparing different configurations of a regional model against *in situ* data.

Figure 4.1 shows time series of modelled and observed current velocities at Terceira Ponte station, with a good agreement for both phase and magnitudes, and an ebb dominance with the greatest velocities occurying durring the ebbing period. The largest differences occuried in a neap tide period at $08/04$.

Figure 4.1 - Magnitude of currents - case 2DH

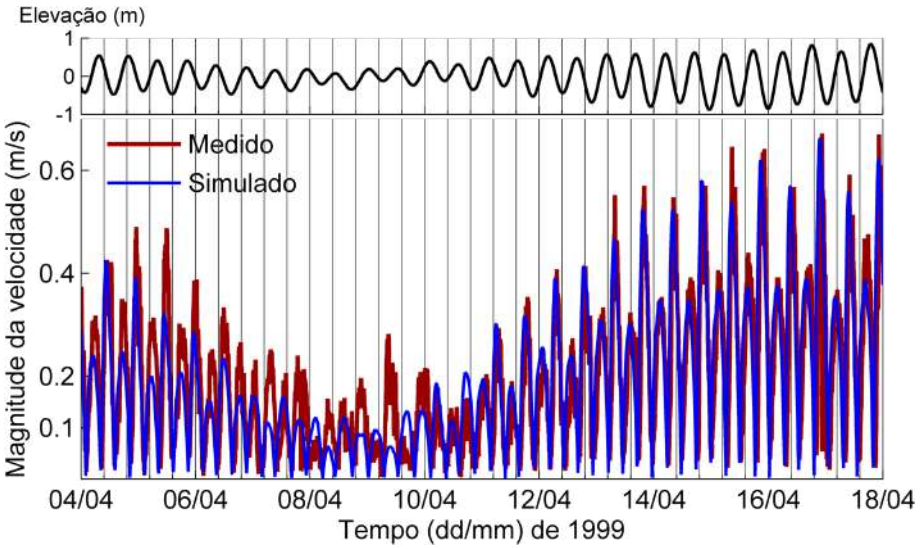

Magnitude of currents in Terceira ponte, for measured (red) and case 2DH (blue) data. At the top, in black, was plotted the series for simulated water level.

The WL case presented the largest errors for water level modelling, in average 30% greater than other cases, with the greater value of MAE and smaller of IAS. Since this was the only case without atmospheric forcing, we can conclude that the inclusion of wind and horizontal gradients of pressure improved the modelling of water level.

The improvement observed with the inclusion of atmospheric forcing in the modelling of water level around Vitória port was not observed in the modelling of currents around Terceira ponte. Instead, WL case presented the best values for current (table 4.1.1). To verify if these unexspected results were associated to the difference in the location of the measurements, time series of water level with the astronomical tide filtered out were compared for different sites in Vitória bay, including Terceira ponte and Vitória port (figure 4.2).

Figure 4.2 - Averaged water level

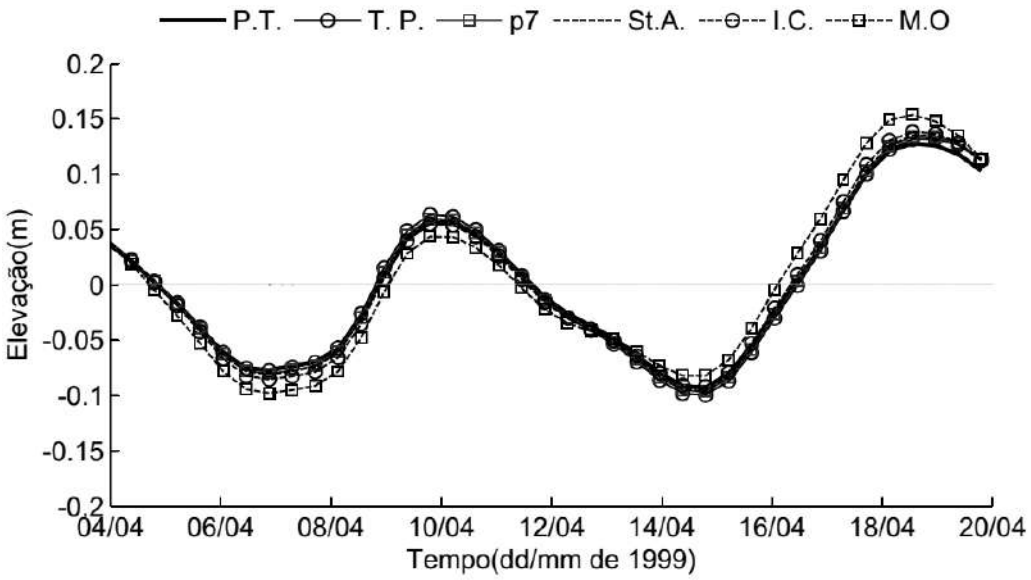

Mean oscilation for the following locations: Tubarão port (P.T.), Terceira ponte (T.P.), Vitória port (p7), Santo Antônio (St.A.), Ilha das Caieiras (I.C.), and Maria Ortiz (M.O.).

The small differences between the 6 time series indicate a covariation of the water level from Terceira ponte to the interior of the estuary, which suggests that the error increase for the simulation of currents with atmospheric forcing in Terceira ponte is not related to the bad representation of meteorological tide.

In figure 4.3 the time series of water level for gauged and modelled data are compared, showing a good representation by the model for both filtered (mean level) and unfiltered data. The model satisfactorily simulated the phase and amplitude of the perturbations of mean level for most period of time.

Figure 4.3 - Water level time series

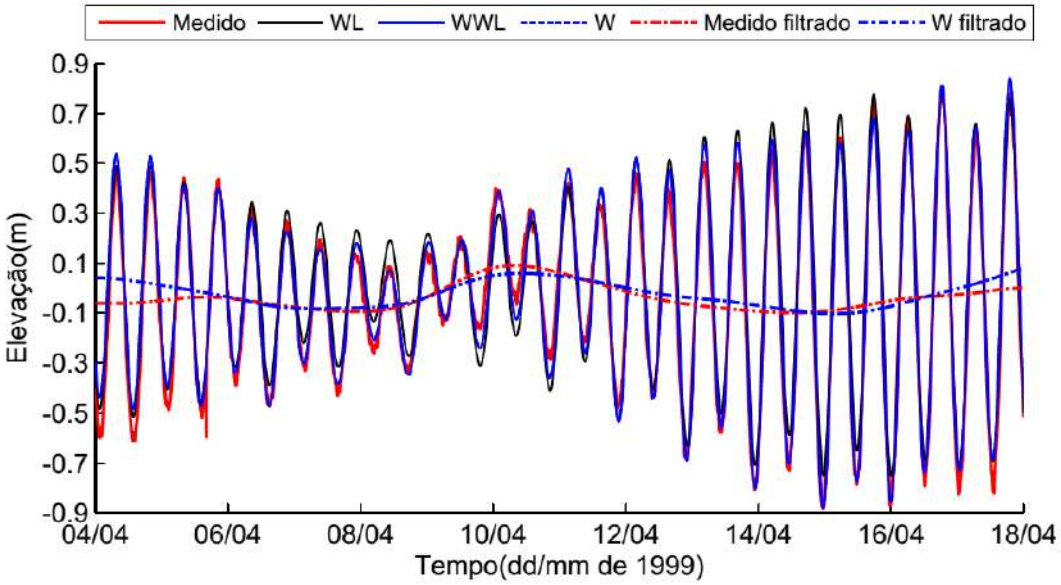

Time series for measured and simulated (WL, WWL, W) water level, and for filtered measured and simulated (W) water level.

The representation of the termohaline field by the model was evaluated against measured data collected along the Vitória bay for 23 gauging points(figures 4.4 and 4.5), with 1 being the innermost point, and 23 the outermost (nearest to Espírito Santo bay). The MAE calculated from gauged and modelled data were 2.4 for salininity and 0.92°C for temperature. The poorer representantation of the termohaline field in comparison to the hydrodynamic one is meanly related to lack of information of river tributaries discharging into Vitória bay and to the lack of calibration of the heat flux parametrization between water body and atmosphere.

Figure 4.4 - Termohaline validation - Salinity

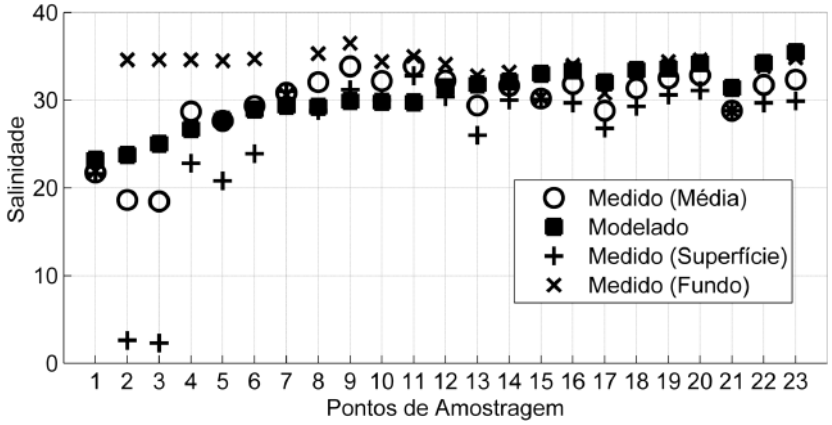

Measured and simulated salinity values for 23 gauging points inside Vitória bay. Values collected between october 7th and 9th.

Figure 4.5 - Termohaline validation - temperature

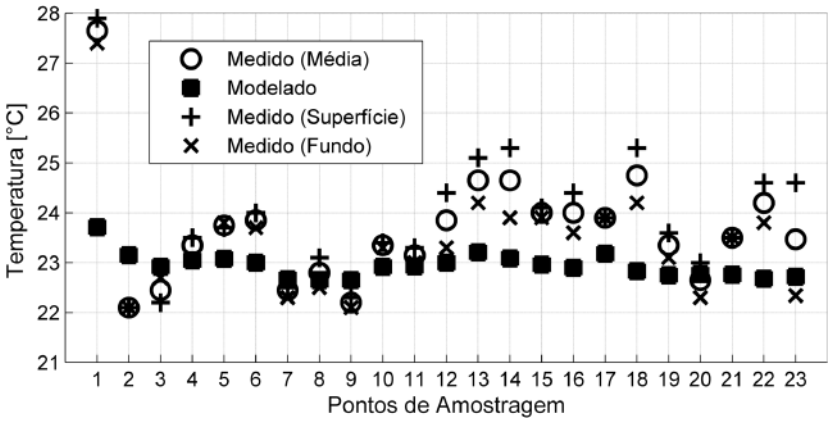

Measured and simulated temperature values for 23 gauging points inside Vitória bay. Values collected between october 7th and 9th.

In spite of the dominance in the modelling of water level and velocity by the astronomical tide, results shows that the inclusion of the meteorological tide in simulations was responsible for a reduction of 31% in the error associated with the water level (4.1.1). The 3D simulation, when compared to 2DH, was responsible for improvements of 2% in water level, and 5% current velocity.

4.1.2 Evaporation

Figures 4.6 and 4.7 depict the curve of the volume loss due to evaporation alone, and measured data from CONCAVE (1983), for two oils with different °API, Ekofisk (°API $= 44.5$), and Kuwait (°API $= 31.1$). It was spilled 500m^3 of oil in an environment with a wind velocity of 15.8km/h and a temperature of 7°C.

The figures show a good agreement between modelled and gauged data for both oils, with a high evaporation rate in the first 24 h for the Ekofisk oil, and in the first 2 h for the Kuwait oil, due to the rapid evaporation of low molecular weight (MW) components (with the greatest vapor pressure), and a stabilization after this period with the volatization of the high MW components (components with low vapor pressure) and the remaining low MW components.

Figure 4.6 - Evaporation curve for Ekofisk oil.

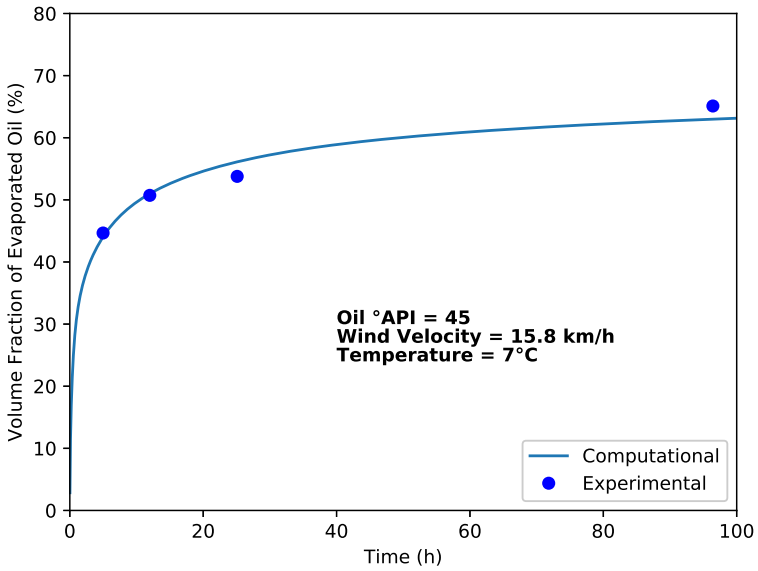

Simulated and observed values for the fraction of volume evaporated for the Ekofisk oil

Figure 4.7 - Evaporation curve for Kuwait oil.

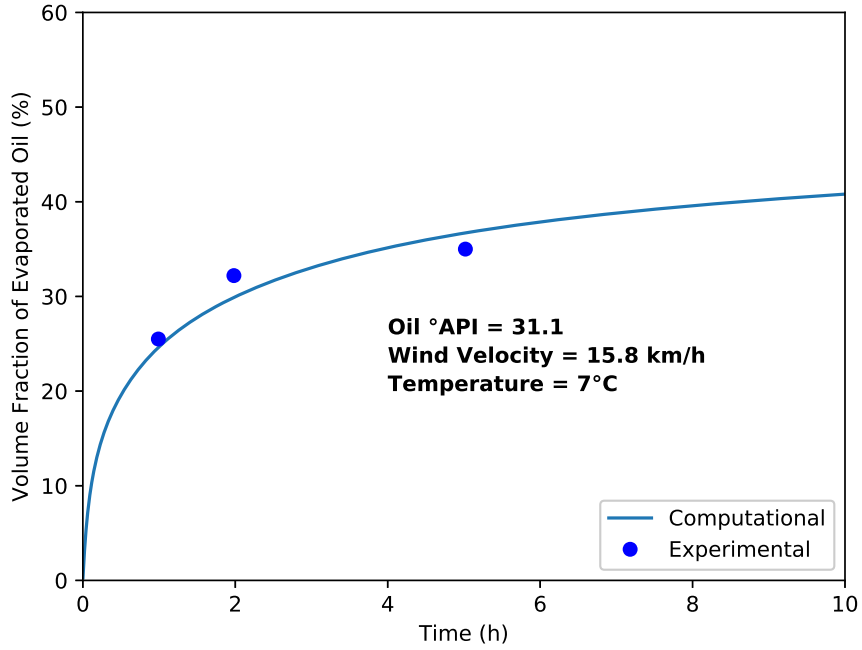

Simulated and observed values for the fraction of volume evaporated for the Kwuait oil

The differences between predicted and measured data are significantly related to the difference in chemical composition of the experimental and modelled oils, since an °API only reflects the proportions between low and high MW fractions, and not the exact chemical composition. The chemical composition of a numerical oil greatly depends in the discretization used, in this model the 25 fractions from Johansen (2003).

Comparing Figures 4.6 and 4.7 it is also possible to conclude that a greater volume loss ocurred with Ekofisk oil, the lighter one, in agreement with the data found in CONCAVE (1983).

In Figure 4.8, three curves are plotted of fraction of evaporated oil mass against time, for Ekofisk oil (°API $= 45$), in an environment with W $= 15.8$km/h, for 3 different configuratios of temperature (7°C, 15°C, and 30°C). And in figure 4.9, three curves are plotted of fraction of evaporated oil mass againt time, for Ekofisk oil (°API $= 45$), in an environment with temperature of 7°C, for three configurations

of wind speed, 15km/h, 30km/h, and 40km/h.

As expected the rate of evaporation increases with temperature and wind speed. For temperature, greater values of vapor pressure with greater temperature explain the direct relationship, and for wind the greater transference of kinect energy associated with high wind speeds (Speight & Arjoon 2012)

Figure 4.8 - Effect of temperature on evaporation curves

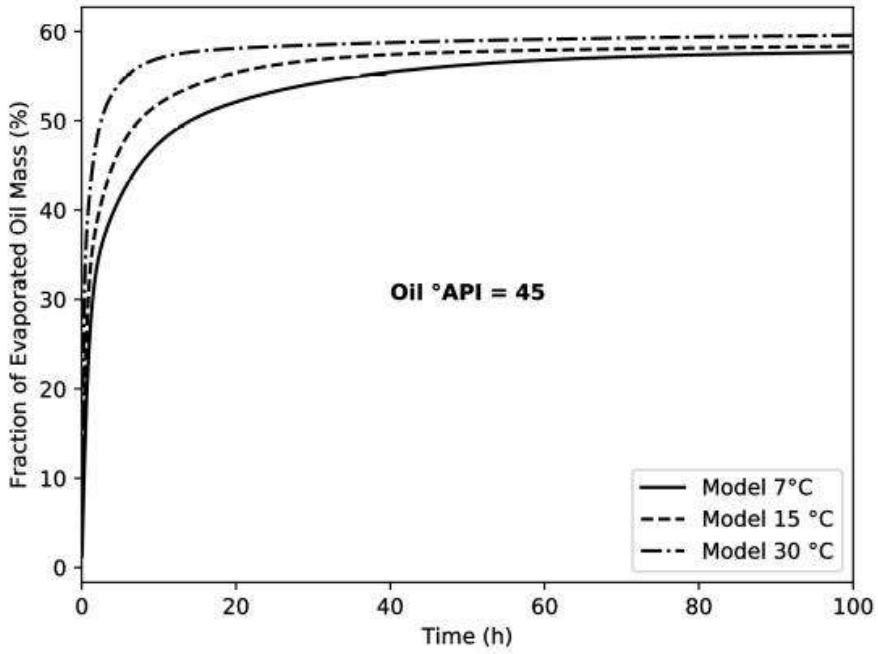

Effect of temperature on evaporations curves, for an Ekofisk oil spill of $500\,m^3$ at a wind speed of 15.8 km/h

Figure 4.9 - Effect of wind speed on evaporation curves

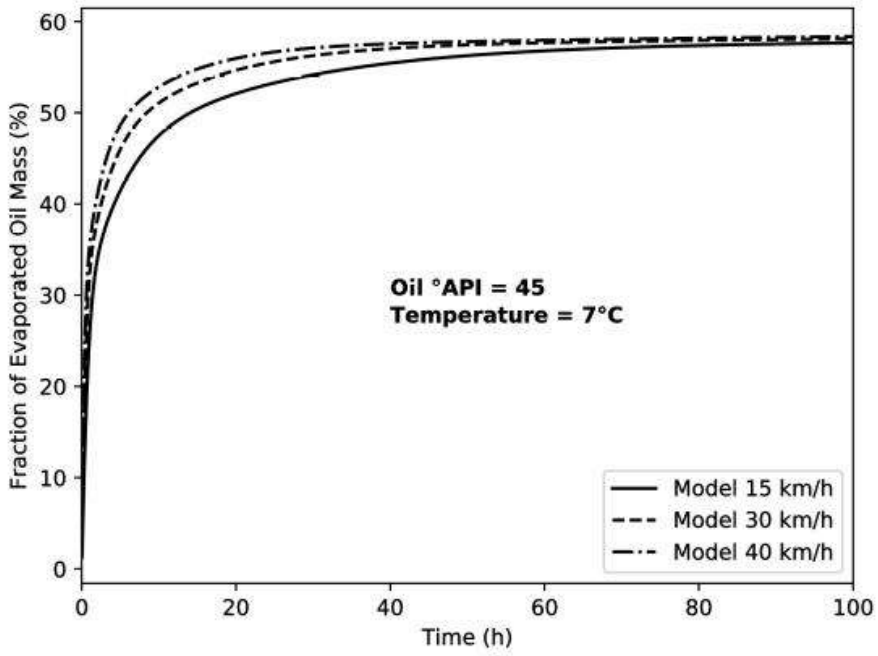

Effect of wind on evaporation curvesm for an ekofisk oil spill of $500\,m^3$ at a temperature of $7°$C

4.1.3 Dissolution of oil

In dissolution, portions of the oil mass are transfered to the environment through a process controlled by the solubility of each oil fraction. Since some components of oil are very toxic for aquatica life, it is extremelly important to reckon dissolution in mathematical models.

As shown in section 2.3, solubility and mass transfer coefficient are paramount when determining the amount of dissolved fraction. According to Johansen (2003), temperature and pressure can be kept constant, as their variations do not affect liquid solubility significantly. Since the mass transfer coefficient is determined by the difusion coefficient and the Sherwood number (S_h), it is necessary to evaluate the performance of the model in the calcutation of these two parameters.

The values of diffusion coefficients calcutated by the model for different

temperatures were compared against the data from experiments performed by Witherspoon e Bonoli (1969) for some petroleum hydrocarbons (figure 4.10). There was a good agreement between both data, with a slight underestimation for aromatic hydrocarbons, and overestimation for ciclic hydrocarbons. In addition, there is a positive correlation of the diffusion coefficent against temperature and a negative correlation against molar mass.

The transfer of mass from droplets of organic liquids was studied by Garner et al. (1959) e Heertjes et al. (1954), considering the binary systems furfural-water and isobutanol -water, respectively. The correlation between the Sherwood number, Reynold number (R_e), and Schmidt number (S_c), presented by the authors were used to evaluate this model (Figure 4.11), showing a good agreement for both binary systems.

Figure 4.10 - Difusivity of hydrocarbons in water.

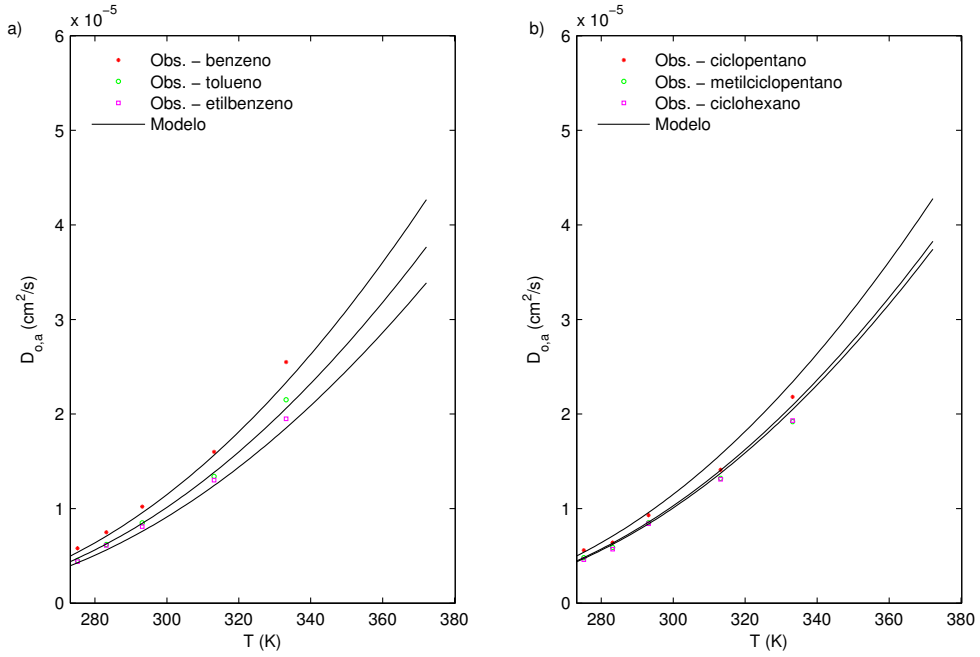

Simulated and observed values of the diffusion coefficient to different hydrocarbons as a function of temperature: a) benzene, toluene e ethylbenzene; b) cyclepentane, methylcyclepentane and cyclohexane. Simulated results are shown by continuous lines and observed data by "⋆", "○", "□" e "×".

Figure 4.11 - Mass transference to water.

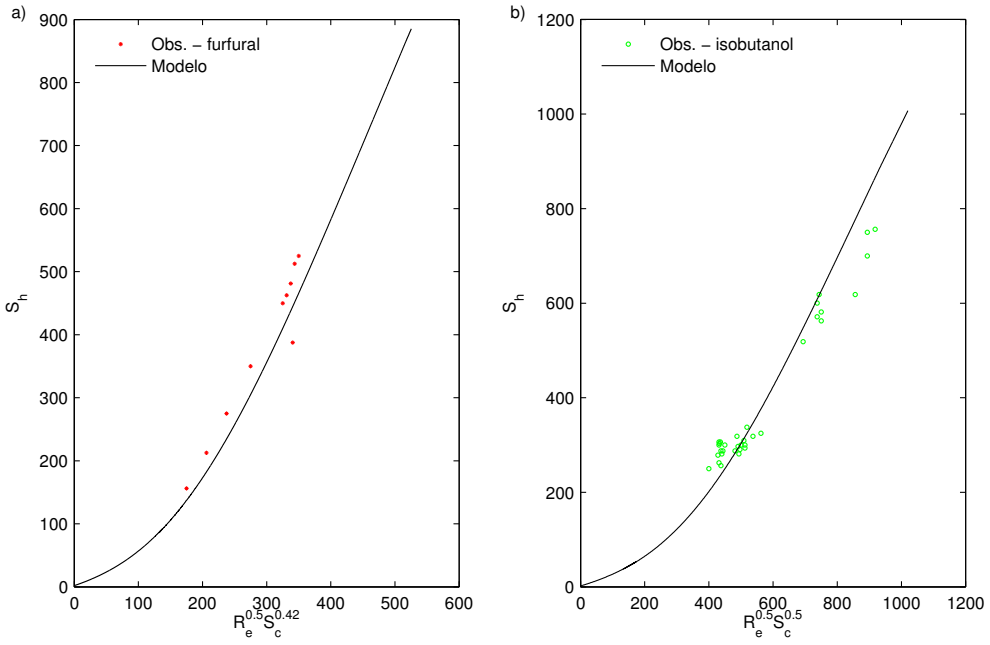

Data of S_h as function of R_e e S_c simulated by the model and gauged by Garner et al. (1959) and Heertjes et al. (1954), respectivelly, to the following organic compounds: a) furfural; b) isobutanol. Simulated results are shown by continous lines and gauged data by "$\star$" e "$\circ$".

The experiments performed by Su e Needham (2013) were used to validate the performance of the dissolution equation implemented in this model. In these experiments, compounds of butyl acetate, ethyl acetate and amyl acetate were injected in a water medium, being gauged the variation of the droplet radius. The simulated and observed profiles of the time evolution of the droplet radius (r_{go}) are present in figure 4.12, showing a good agreement for all cases. The most soluble compound, ethyl acetate (Figure 4.12a), presented the hightest dissolution rate, confirming the correctness of the mathematical model for dissolution of a droplet implemented in this model.

Figure 4.12 - Dissolution of droplets in water.

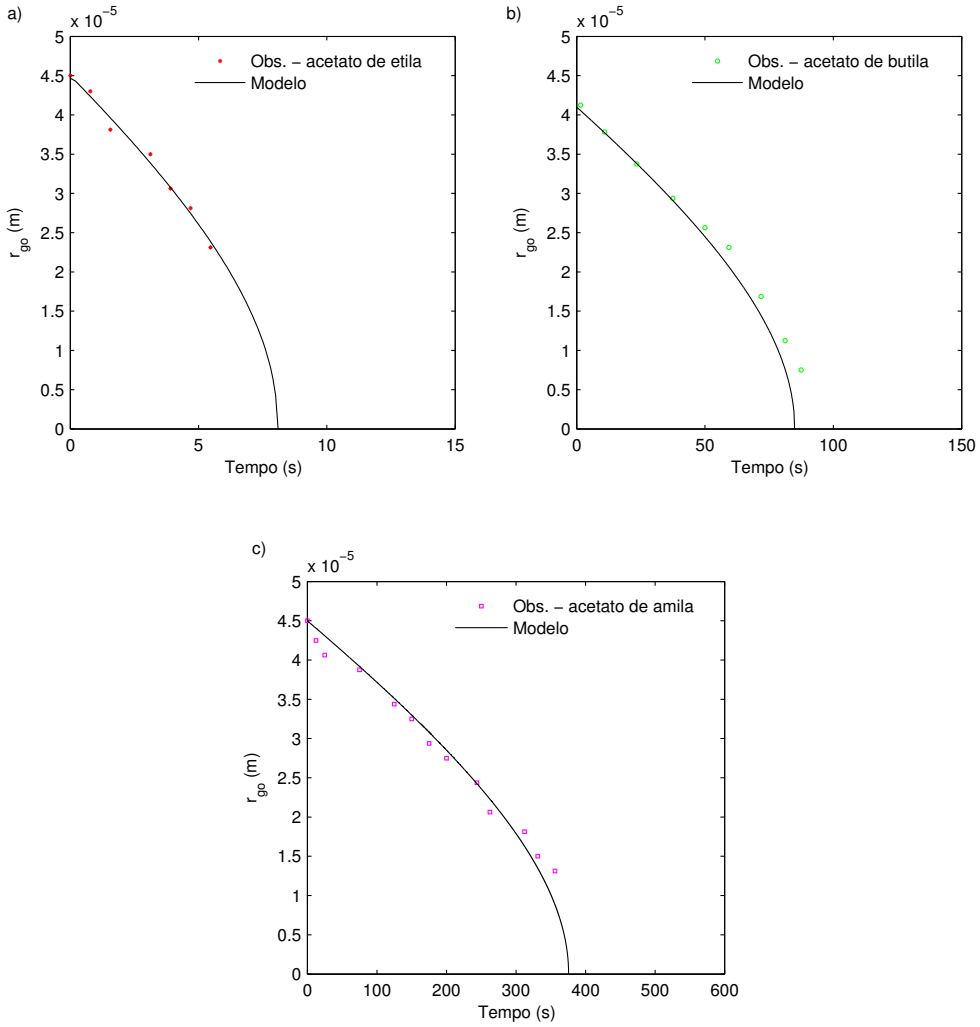

Decreasing of droplet radius for the following compounds: a) ethyl acetate; b) butyl acetate; c) amyl acetate. Simulated results are shown by continous lines and gauged data by "⋆", "○" e "□".

Regarding the dissolution of an oil slick, it is well stablished that the porcentage of volume dissolved is usually no greater than 1%. In Riazi e Al-Enezi (1999) the author presented some experimental results for the rate of disappearance of Kuwait crude oil at $42°$. After 175 h only 0.18% of the volume of the initial oil slick had dissolved. This low pocentage is probably explained by the presence of evaporation, that swiflty consumes low weight fractions.

The experiment with the Kuwait oil performed in evaporation section was run with

a temperature of $42°$. The evolution of the percentage of oil volume loss due to dissolution is present in figure 4.13. After 174 h, 0.2769% of initial oil volume had evaporated, similar to the experimental results.

The increasing dissolution observed in the figure 4.13 is associated with the presence of heavier fractions with medium solubility not evaporated in the first 24 h. It was observed a stabilization of the dissolution curve after 400 h (not shown), after only low solubility fractions are left.

Figure 4.13 - Evolution of the percentage of oil volume loss .

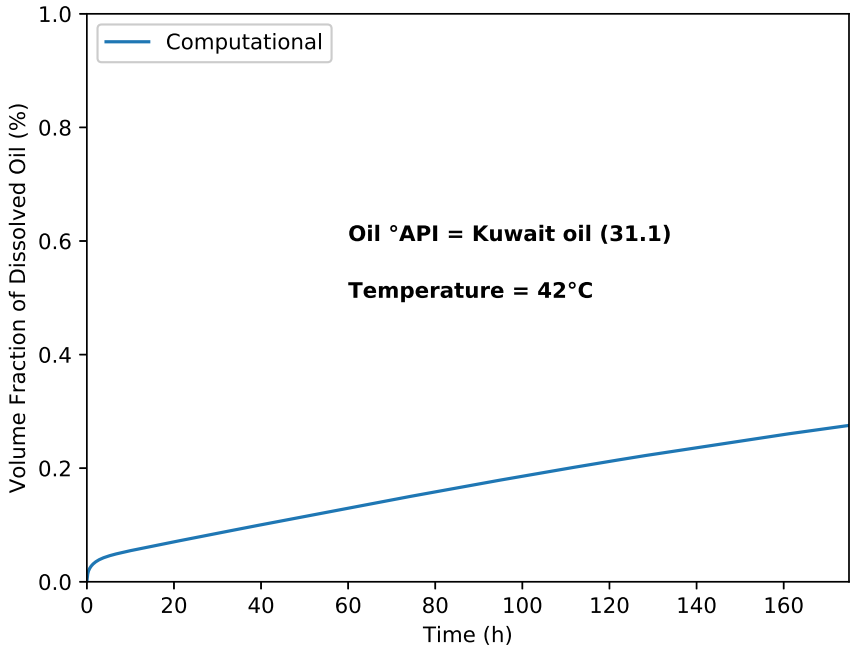

4.1.4 Emulsification

The main way to validate the ability of a model to reproduce the emulsification process is to measure the evolution of water intake by the slick. To this end it was used the Large scale experimental oil spill conducted at Haltenbanken offshore Norway in July (1982) (AUNDUNSON et al., 1984). This experiment envolved a controlled release of $100\,m^3$ of crude oil discharged over a period of $2\,h$. The oil

slick was observed for a period of 7 days with surface vessels and aircraft. During this period, oil samples were taken on a regular basis within the slick.

Since we are comparing modelled data with field experimental data, the processes of evaporation and dissolution were also activated in this run. The influence of evaporation and dissolution was not assessed in the following results though.

In the figure 4.14 is depicted the evolution of the water content (in %) in a slick due to emulsification. The modelled results are shown by continuous line, and the experimental data by Aundunson et al. (1984) in dots.

Figure 4.14 - Water content evolution in an oil slick

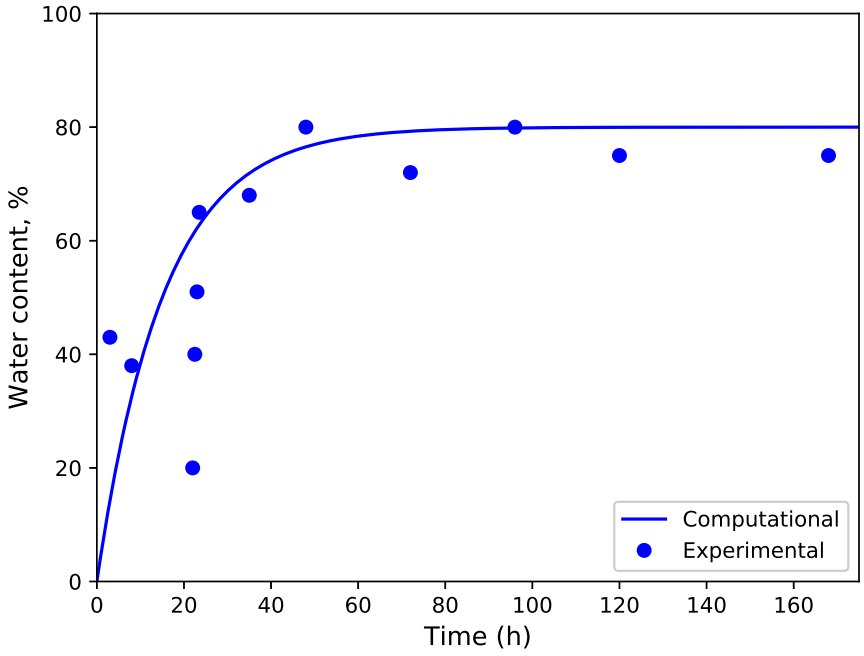

Evolution of the water content (in %) in a water slick due to emulsification. The modelled results are shown by continuous line, and the experimental data in dots.

The figures shows that the model reproduced the increase in water content with time, with better results reproduced after 24 hours. The water content decrease in the first hours (with negative pick approximately 20 hours) was not captured

by the model. Similar results were found by Johansen et al. (2015), that justified the poor reproduction of the model in the first day to the presence of unstable emulsion samples. According to the authors, the release of oil over a period of $2\,h$ (differently from the instantaneous release of the model), may explain some difference between modelled and gauged.

In figure 4.15 is depicted the evolution of the viscosity (cP) of the emulsion as a function of time. A great viscosity increase was reproduced by the model, as in the measured data by Aundunson et al. (1984). This increase is the most proeminent feature during an emulsion formation, and have been cited by Reed e Gundlach (1989), Fingas (1995), Fingas e Fieldhouse (2004), among others.

Figure 4.15 - Viscosity (cP) evolution of the emulsion

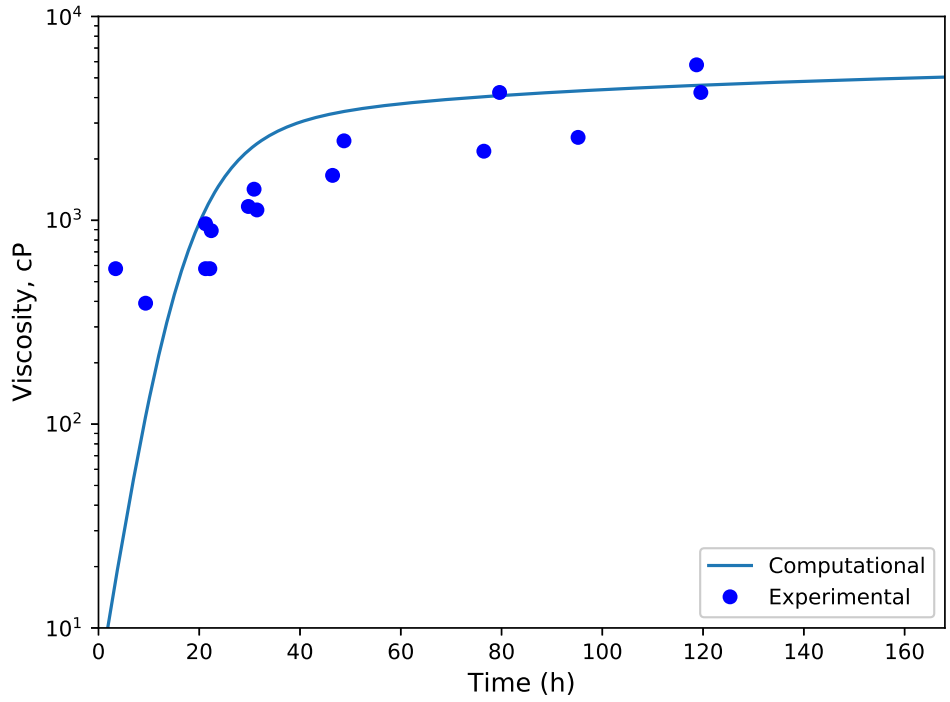

Evolution of the viscosity (cP). The modelled results are shown by continuous line, and the experimental data in dots.

In the figure 4.16 is present the evolution of the density (km/m^3) of the emulsion as a function of time. A great density increase was reproduced by the model, as in the measured data by Aundunson et al. (1984). Differences in the first 24

hours may be due to the same factor as presented by Johansen et al. (2015) for the emulsification The decrease in the emulsion density after 100 h is a result of the de-emulsification undergone by the slick in the experimental site. The same overestimation is observed in the results of Johansen et al. (2015), and is associated to the lack of detailed information of the experiment performed by citeaundunson1984

Figure 4.16 - Density (km/m^3) evolution of the emulsion

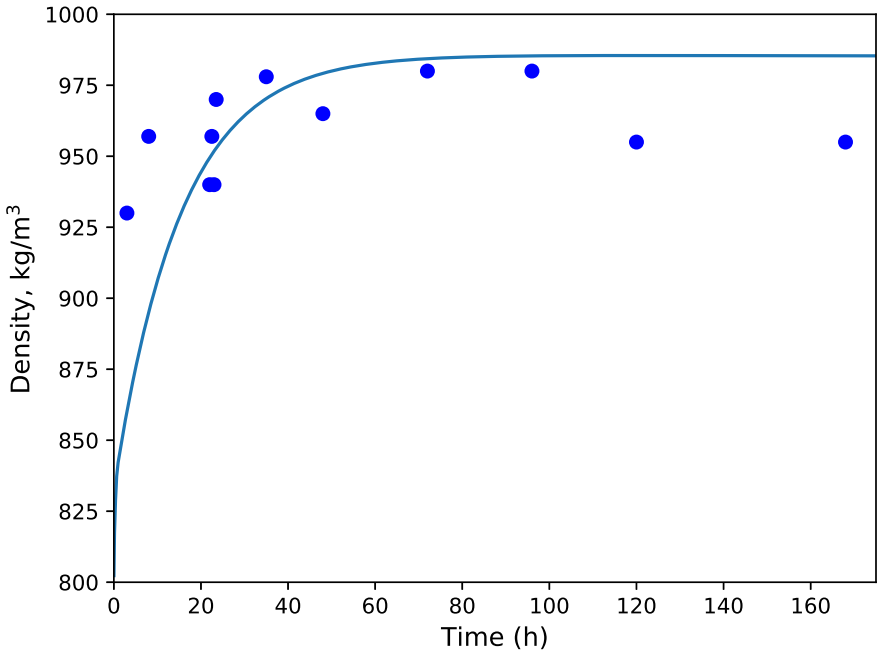

Evolution of the emulsion density (km/m^3). The modelled results are shown by continuous line, and the experimental data in dots.

SOURCE: Produção do autor.

After many tests it was verified the great dependence of emulsification to the emulsification rate constant (K_{em} in equation 2.30), being found, for the oil composition tested in this thesis, an optimal value of 5×10^{-7}.

4.1.5 Horizontal advection

Following are the figures (Figure 4.29 to 4.30) of the position of the oil particles at the numerical flume released from continuous and instantaneous sources, for three directions of current, parallel to x axis, $15\,^{\circ}$ rotated upwards, and $15\,^{\circ}$ rotated downwards. For both spills was discharged 500 m^3 of crude oil with $^{\circ}$API $= 45$ (oil physical-chemical characteristics are irrelevant in horizontal advection-diffusion). No weathering processes were activated in this section.

To evaluate the evolution of the trajectories of oil particles, were taken snapshots at the initial step, when the slick reaches the middle of the aquaous domain, and when the slick reaches the land.

Spreading was not applied in this case. Instead, particles were randomingly positioned in a square-shaped initial slick.

Figure 4.17 - Propagation of an oil slick

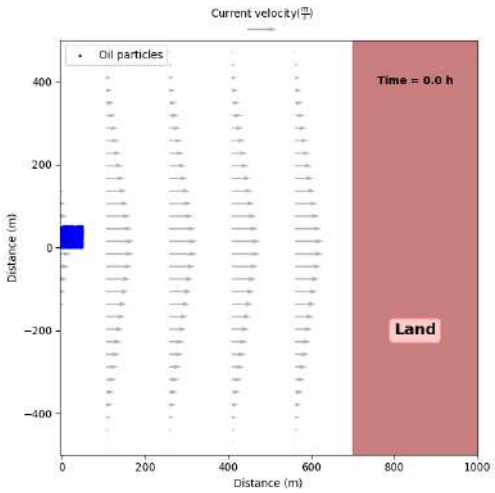

Propagation of an oil slick, instantaneous source. First time step.

Figure 4.18 - Propagation of an oil slick

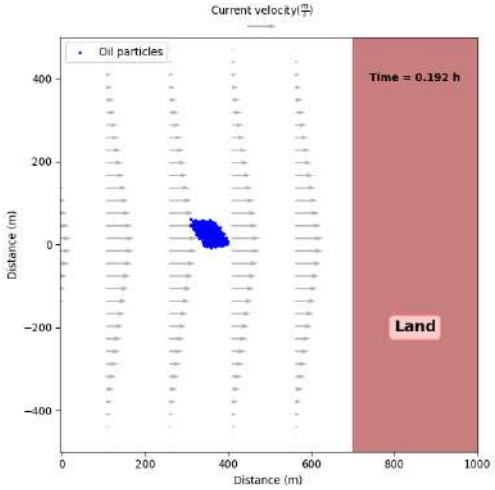

Propagation of an oil slick on a parallel current, instantaneous source. After 0.192 h.

Figure 4.19 - Propagation of an oil slick

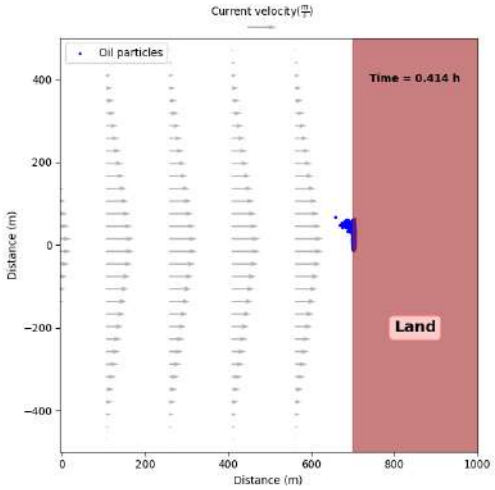

Propagation of an oil slick on a parallel current, instantaneous source. After 0.414 h.

Figure 4.20 - Propagation of an oil slick

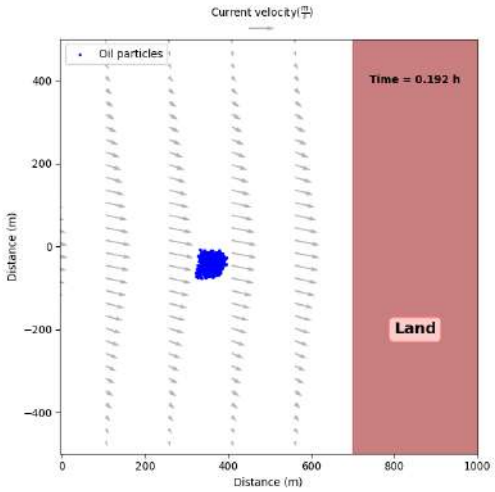

Propagation of an oil slick on a current rotated downwards, instantaneous source. After 0.192 h.

Figure 4.21 - Propagation of an oil slick

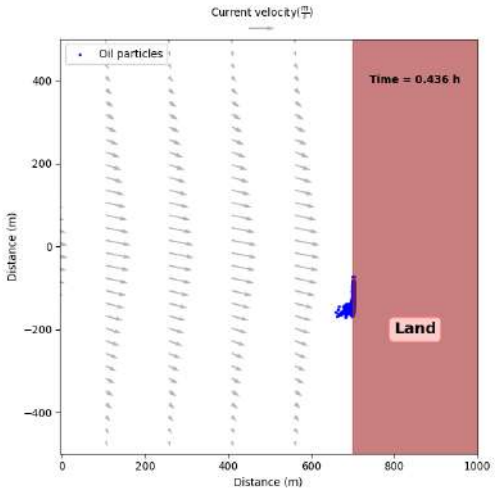

Propagation of an oil slick on a current rotated downwards, instantaneous source. After 0.436 h.

Figure 4.22 - Propagation of an oil slick

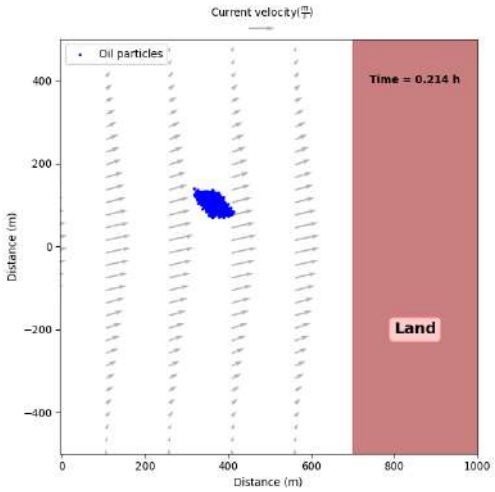

Propagation of an oil slick on a current rotated upwards, instantaneous source. After 0.214 h.

Figure 4.23 - Propagation of an oil slick

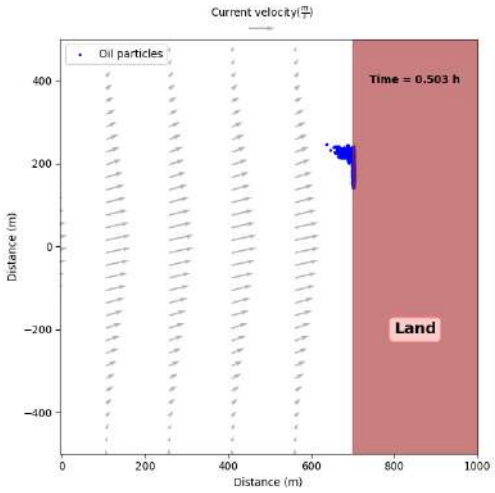

Propagation of an oil slick on a current rotated upwards, instantaneous source. After 0.503 h.

Figure 4.24 - Propagation of an oil slick

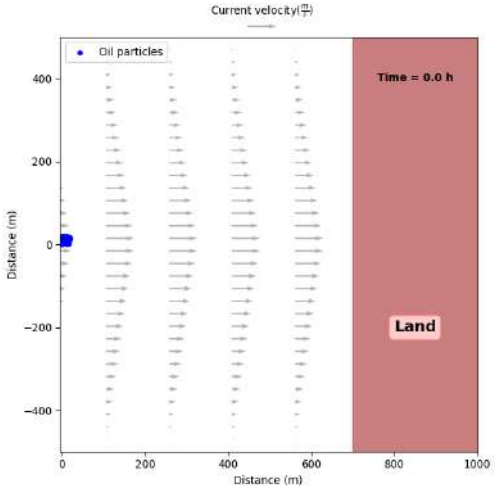

Propagation of an oil slick, continuous source. Initial time step.

Figure 4.25 - Propagation of an oil slick

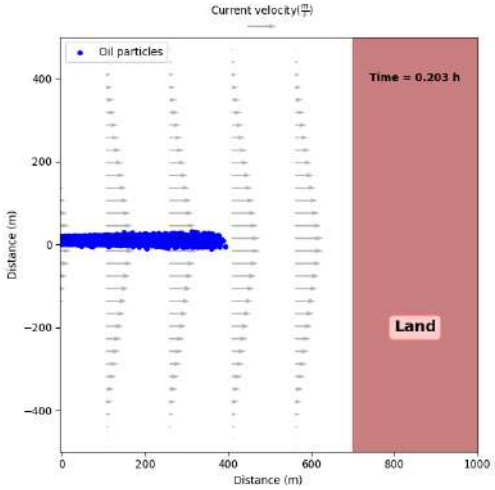

Propagation of an oil slick on a parallel current, continuous source. After 0.203 h.

Figure 4.26 - Propagation of an oil slick

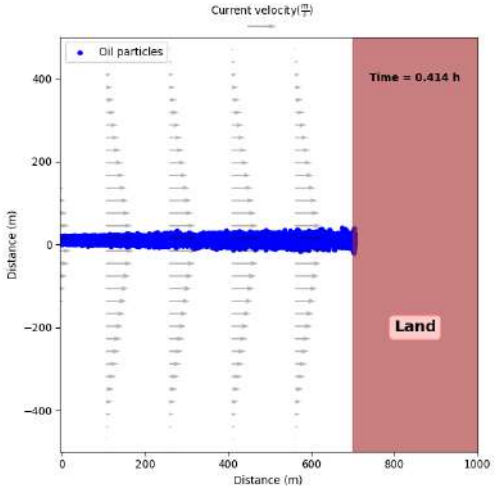

Propagation of an oil slick on a parallel current, continuous source. After 0.414 h.

Figure 4.27 - Propagation of an oil slick

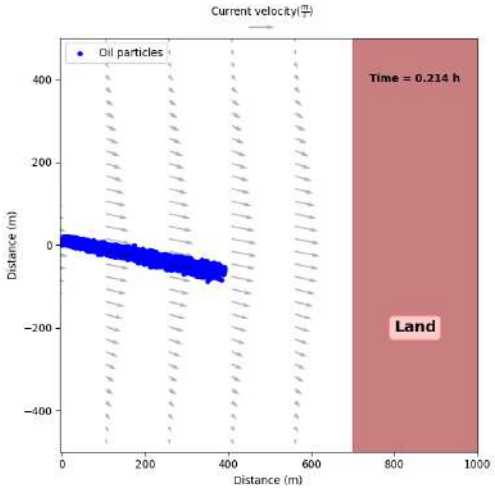

Propagation of an oil slick on a current rotated downwards, continuous source. After 0.214 h.

Figure 4.28 - Propagation of an oil slick

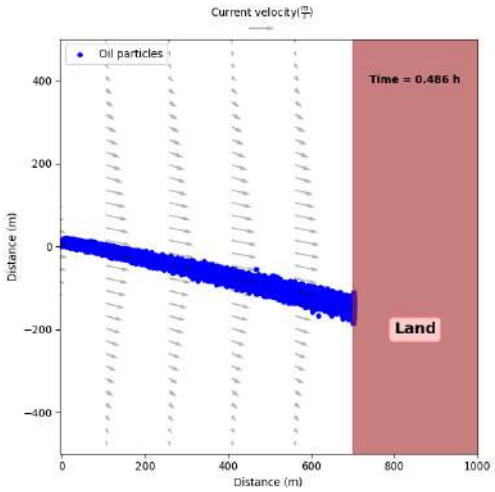

Propagation of an oil slick on a current rotated downwards, continuous source. After 0.486 h.

Figure 4.29 - Propagation of an oil slick

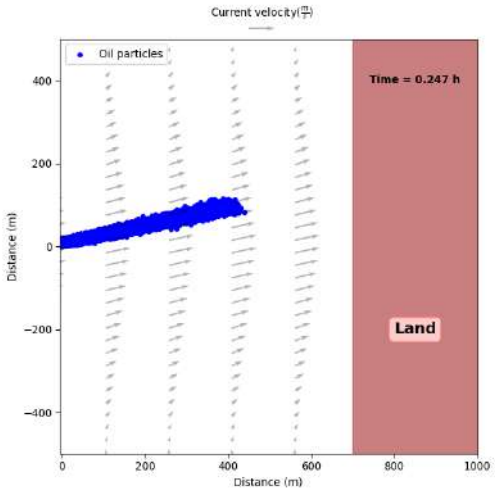

Propagation of an oil slick on a current rotated northwards, continuous source. After 0.247 h.

Figure 4.30 - Propagation of an oil slick

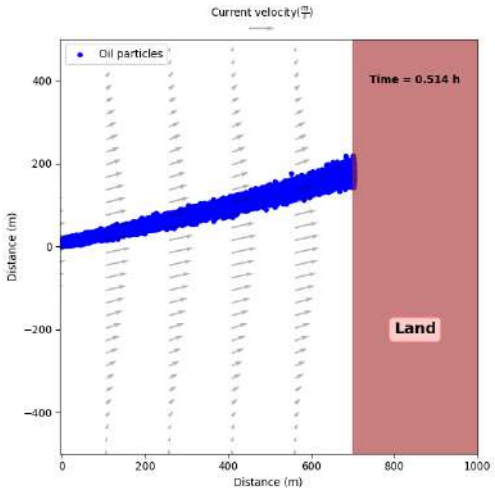

Propagation of an oil slick on a current rotated northwards, continuous source. After 0.514 h.

In all cases the oil particles advected following the direction of the current, and it is possible to observe, as in Figures 4.18 and 4.19, the shear of oil slick resulting from the velocity shear.

In the experiment with horizontal current the first particle took aproximatelly 0.3319 h to travel 600 m, in accordance with expected for a current velocity of 0.5 m/s (0.3333). The difference is related to the turbulent diffusion.

The expansion of the area occupied by the slick observed along the temporal evolution is explained by the turbulent diffusion.

At the final time it is possible to observe the stranding of the oil particles when reaching land.

These experiments show the correct implementation of the advection of the oil slick for both sources, instantaneous and continuous.

4.1.6 Vertical dispersion

Figure 4.31 shows the comparison of the observed and model predicted entrainment rate flux calculated with the formulations of Delvigne e Sweeney

(1988) and Li et al. (2017) as a function of oil viscosity. The observed data are based on recent experiments conducted in the Oil and Hazardous Material Simulated Environmental Test Tank (OHMSETT), and was calculated assuming either a constant initial oil thickness without additional spreading throughtout the entrainment experiment, and a mean thickness as a result of spreading .

Estimates of oil entrainment rates during the OHMSETT experiments show little sensitivity to oil viscosity. In addition, for the initial thickness it was found entrainment rates three orders of magnitude higher. According to Li et al. (2017) this highlights the importance of performing experiments where the majority of oil spreading has already occurred prior to making entrainment estimates, thus removing this as a variable from the experiments.

Regarding the modelled results, both Delvigne e Sweeney (1988) and Li et al. (2017) formulations presented values bounded by the two experiment results (at least for this viscosity range), as in Li et al. (2017). However, Li et al. (2017) formulation presented a weaker dependence to oil viscosity, as in the observed results, where it was not observed a dependency with viscosity.

These results show the difficulty in parameterizing the entrainment rate in oil models, which is related to the great number of variables influencing vertical dispersion. Great effort is currently being spent in this field, since the correct representation of the entrainment rate is paramount in oil spill fate and transport models. However, between the two entrainment formulations implemented in this model, Li et al. (2017) formulation should be chosen due to its better qualitative results and independence to droplet size classes.

Figure 4.31 - Entrainment rate of oil in kg/m^2-sec

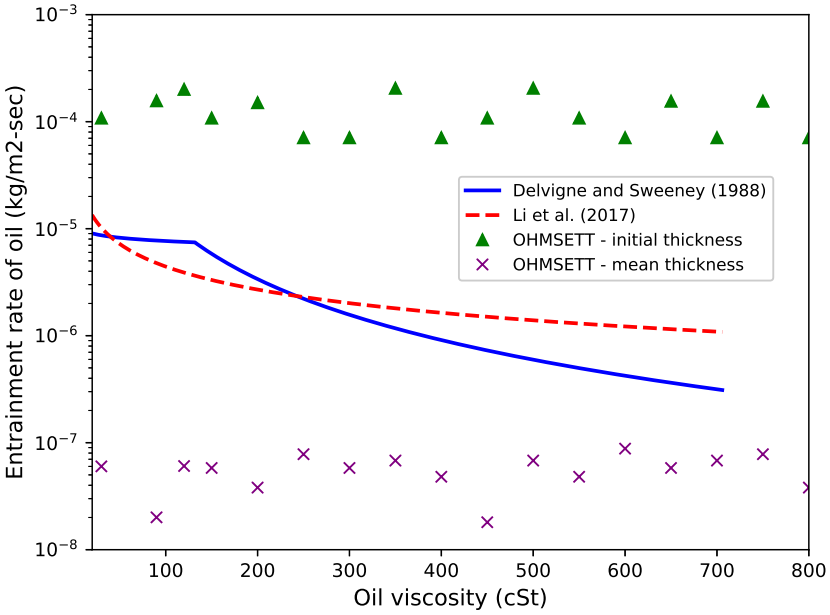

Estimated entrainment rate of oil (kg/m^2/s) as function of oil viscosity. Predictions from Delvigne e Sweeney (1988) and Li et al. (2017) are shown. Also shown are estimates from the OHMSETT experiments assuming the initial oil thickness (no spreading) and mean thickness (with spreading)

SOURCE: Produção do autor.

To understand the influence of the vertical dispersion in a water body, the droplets cloud resultant from an environment with a $H_{sig} = 0.1628\,m$ was plotted in three dimensional figures representing the water column, showing the dynamics of the entrained oil in the water column. The droplets are collored following their vertical positions, with lighter colors indicating more proximity with the water surface. Only one breaking event is considered in the plotting.

In order to better represent the droplets dispersion, it was not considered the advection by currents.

The droplets were plotted for three timesteps, at the beginning of the simulation (figure 4.32), after 15 minutes (figure 4.33), and after 30 minutes (figure 4.34).

Figure 4.32 - Floating oil droplets dispersion in the water column - Beginning of simulation

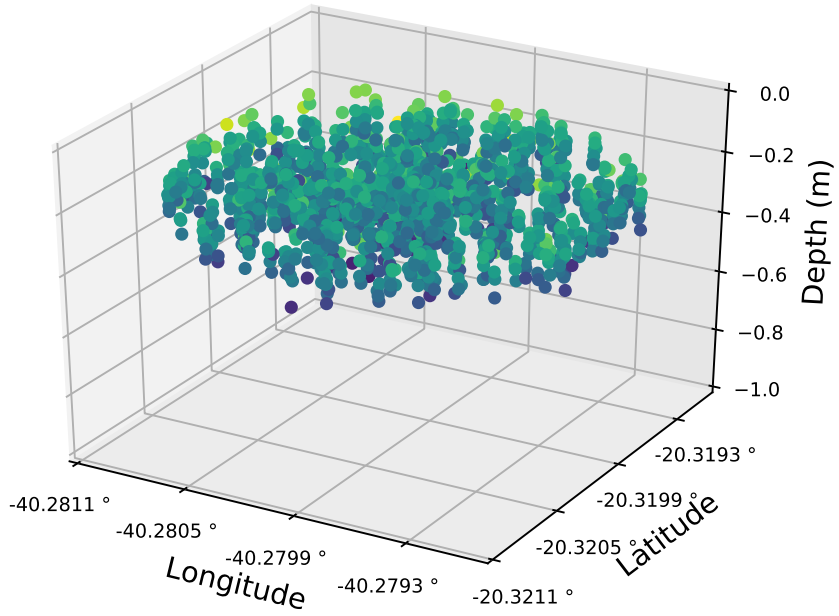

Oil droplets dispersion in the water column. The droplets are collored following their vertical positions, with the lighter colors indicating more proximity with the water surface. The oil slick is not represented in the figure.

Figure 4.33 - Floating oil droplets dispersion in the water column - After 15 minutes

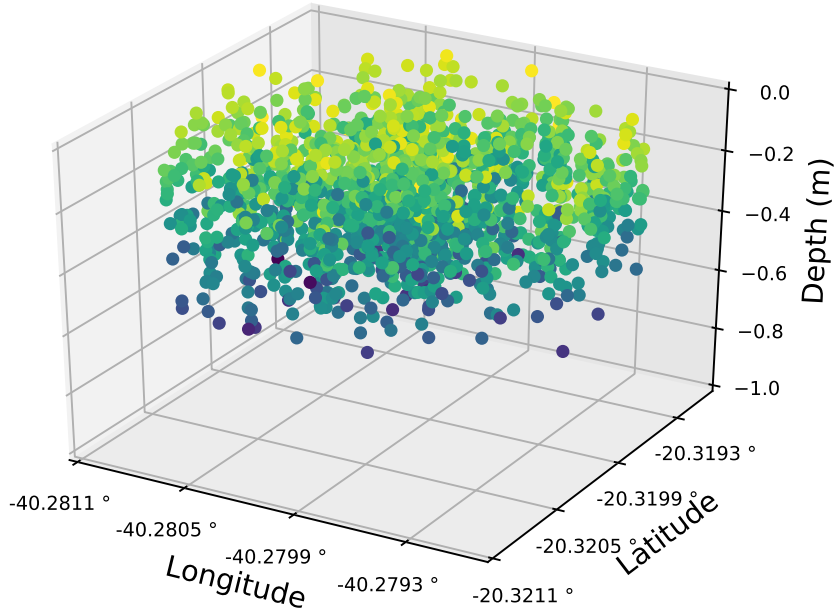

Oil droplets dispersion in the water column. The droplets are collored following their vertical positions, with the lighter colors indicating more proximity with the water surface. The oil slick is not represented in the figure.

Figure 4.34 - Floating oil droplets dispersion in the water column - After 30 minutes

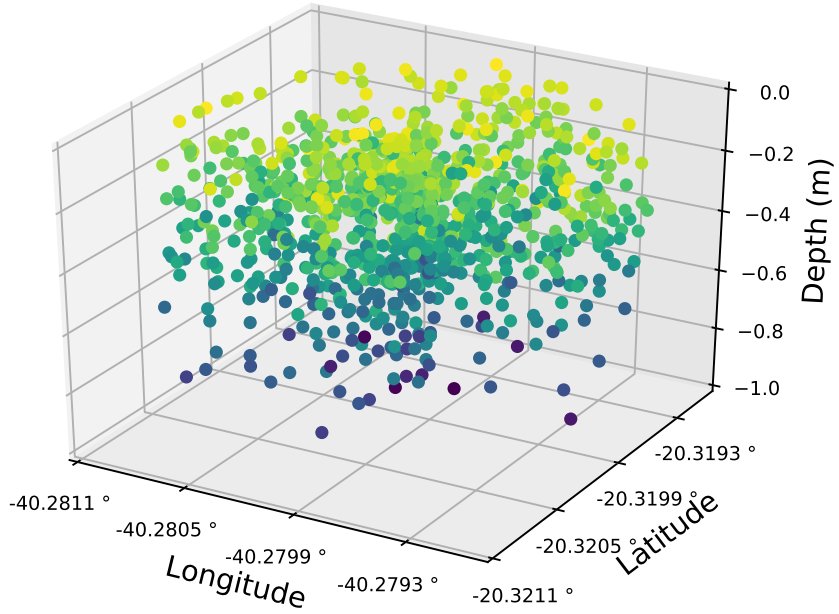

Oil droplets dispersion in the water column. The droplets are collored following their vertical positions, with the lighter colors indicating more proximity with the water surface. The oil slick is not represented in the figure.

The figures show that the model reproduced the cloud of droplets cited by Huang (1983), and photographed by Delvigne e Sweeney (1988) in their experiment (figure 2.1). After the wave breaking, oil entrains into the water column in the form of droplets (Figure 4.32). As time evolves the volume occupied by the cloud of droplets increases as a result of the turbulent diffusion.

In order to visualize the influence of the wave breaking on the vertical dispersion, it was calculated the depth to which the dispersed droplets mix (Z_{mix}) for two significant wave heights, 0.16 and 0.63 m (figure 4.35).

For the $H_{sig} = 0.16\ m$ the model calculated a Z_{mix} equal to $0.24\ m$, and for the $H_{sig} = 0.63\ m$ a Z_{mix} equal to $0.94\ m$, in accordance with the stated by equation 2.41.

Figure 4.35 - Depth of dispersed oil droplets after wave break

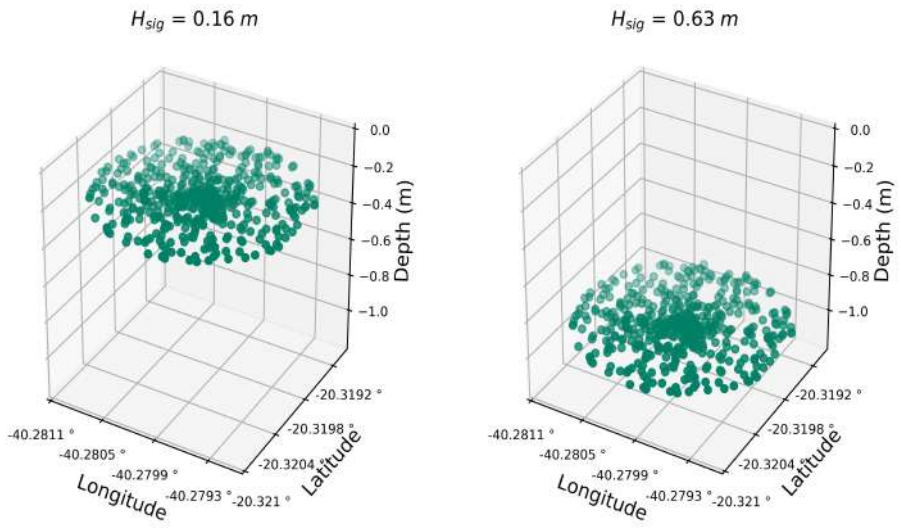

Depth to which the dispersed droplets mix (Z_{mix}) for two significant wave heights, 0.16 and 0.63 m.

4.1.7 Mass conservation

Before moving to the scenarios in the study area it was checked the oil mass conservation of the model. For that it was measured the oil mass loss percentage against initial oil mass due to each modelled weathering process, using stationary and uniform value of temperature, salinity and wind velocity. According to Spaulding (2017), rigorous attention must be paid to ensure that the oil mass balance is preserved in each algorithm and throughout the integrated model.

Figure 4.36 shows the time evolution in 175 hours, for the mass losses and the remaing mass. Since emulfication does not affect the mass of oil, it is not included in the plot. For this case it was used Ekofisk oil and the entrainment formulation of Li et al. (2017). These same configurations will used in the following scenarios.

The mass of the oil is conserved along the simulation, with the greatest loss due to evaporation, and lowest to dissolution. This pattern corroborates the findings of Reed et al. (1995), Reed et al. (1999) , Daae et al. (2011).

Regarding the rate of entrainment, it decreased as a result of emulsification, as shown in figure 4.31. To highligh the maintenance of the mass conservation in the model, in this case it was not considered the return movement of oil droplets to the slick.

It is important to mention that, since emulsification is acting along with the other processes, the decrease in the oil mass does not necessarily represents a decrease in the slick mass, due to the input of seawater and emulsion formation.

Figure 4.36 - Oil Mass loss percentage due to weathering processes

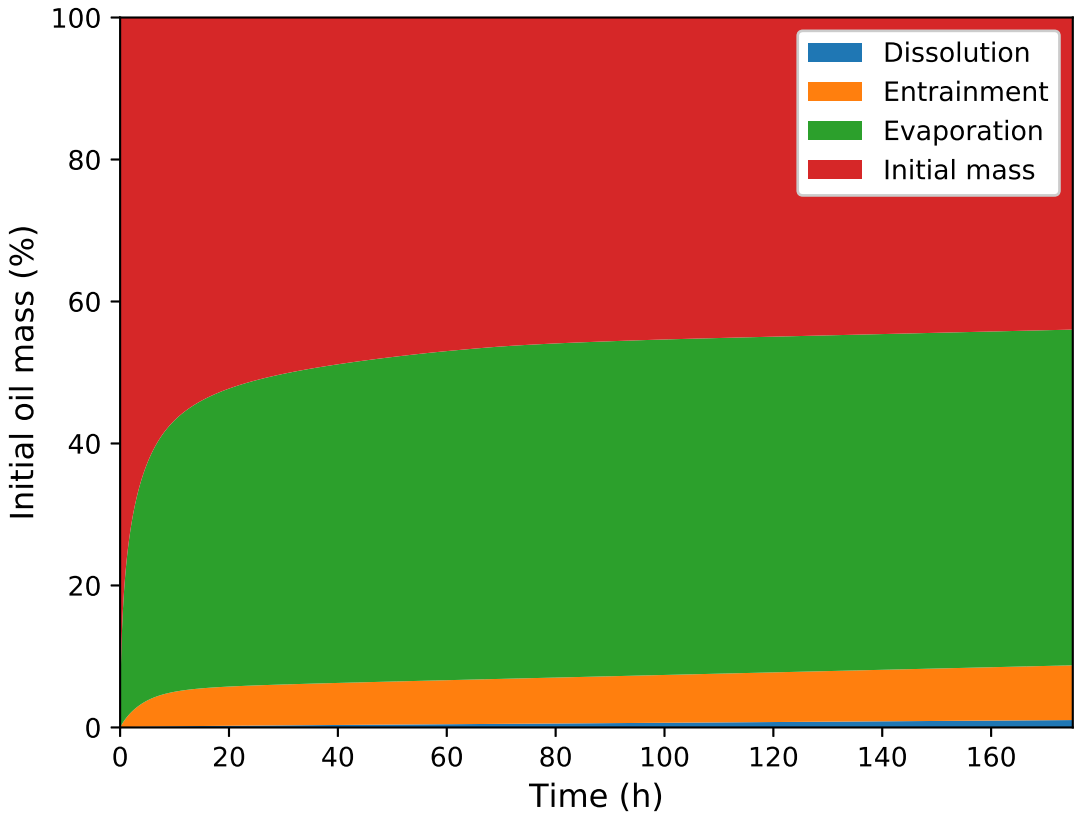

Time evolution of the oil mass loss percentage as a result of dissolution, evaporation and entrainment. Emulsification does not affect the mass of the oil.

4.2 Oil spill scenarios

4.2.1 Slick transport

The maps of the parameters analysed in the following sections does not contain the visual representation of the slick, presenting a statistical information over the many deterministic runs. To visualize the transport of the slick in the study region, were plotted the evolution of the position of surface particles along 12 hours of 10/01/2013, one semidiurnal tidal cycle, selected from the deterministic runs of the Vitória Bay Spill and the Tubarão port spill.

The Figure 4.37 shows the advection of the oil particles by the current field (represented by arrows) for the Vitória Bay Spill, with the slick being transport to inner parts of Vitória Bay channel and towards Espírito Santo bay as a result of flooding and ebbing dynamics of the tide.

In the first 6 hours the flooding is represented by the current arrows directed towards inner parts of the Vitória Bay, with the oil particles following the current direction. As the slick moves inwards, the beaching of particles is revealed in northern parts of the bay.

In the last 6 hours the current arrows reverse its direction as the ebbing movement starts in the domain. As a result, the slick is advected outwards Vitória Bay, following the direction of the current field. After the tidal cycle, oil particles are beached inside Vitória Bay on the nothern shoreline.

The results from Figure 4.37 show the control of the tidal dynamics on the slick transport, with the ebbing and flooding of the current field reflected on the movement of the oil particles along the 12 hours evolution.

For the Tubarão port spill (Figure 4.38), the transport of the oil slick along the tydal cycle is not as significant as in the Vitória Bay Spill, a result of weaker tidal currents associated with the Espírito Santo bay, as opposed to the Vitória Bay channel. It is observed a net transport towards Camburi beach, probably related to the wind-induced advection, and to wind-induced currents.

Figure 4.37 - Slick evolution under flood and ebb conditions

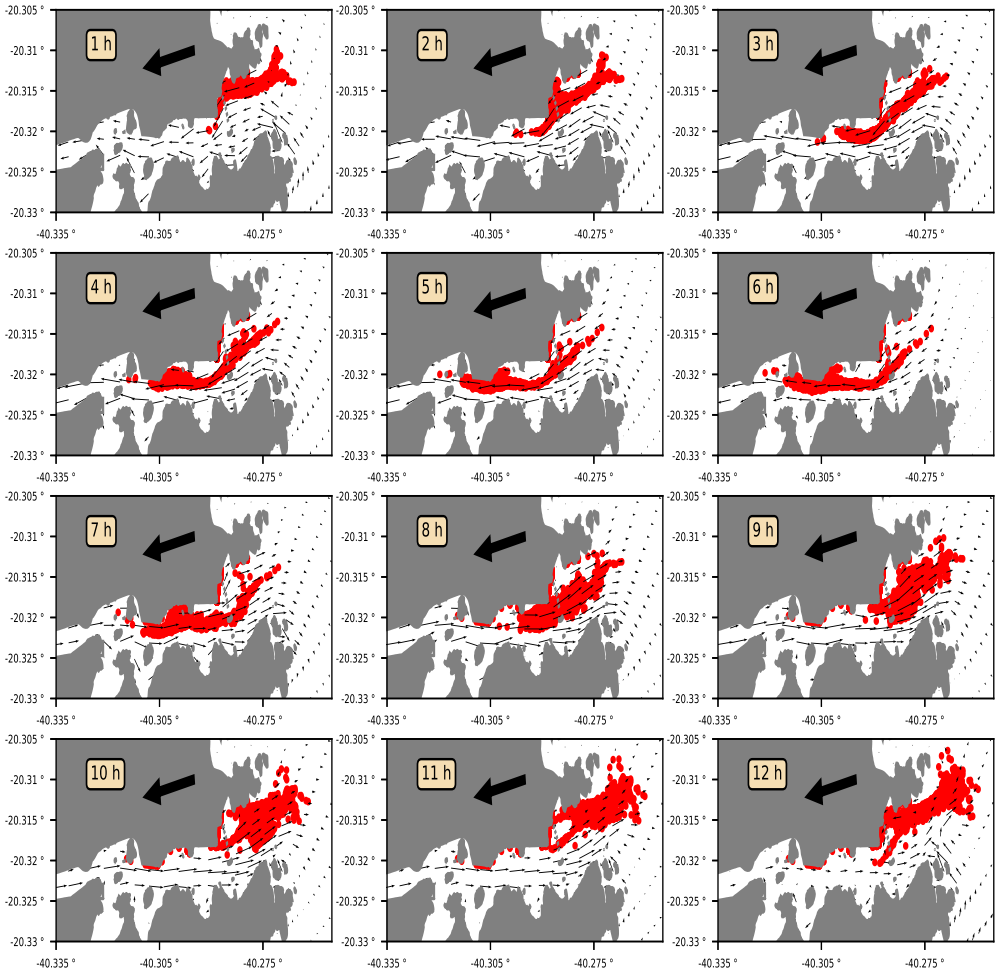

Hourly snapshots of the particles position along 1 tidal cycle for the Vitória Bay Spill. The black arrow represents the prevailing wind direction along the simulation.

Figure 4.38 - Slick evolution under flood and ebb conditions

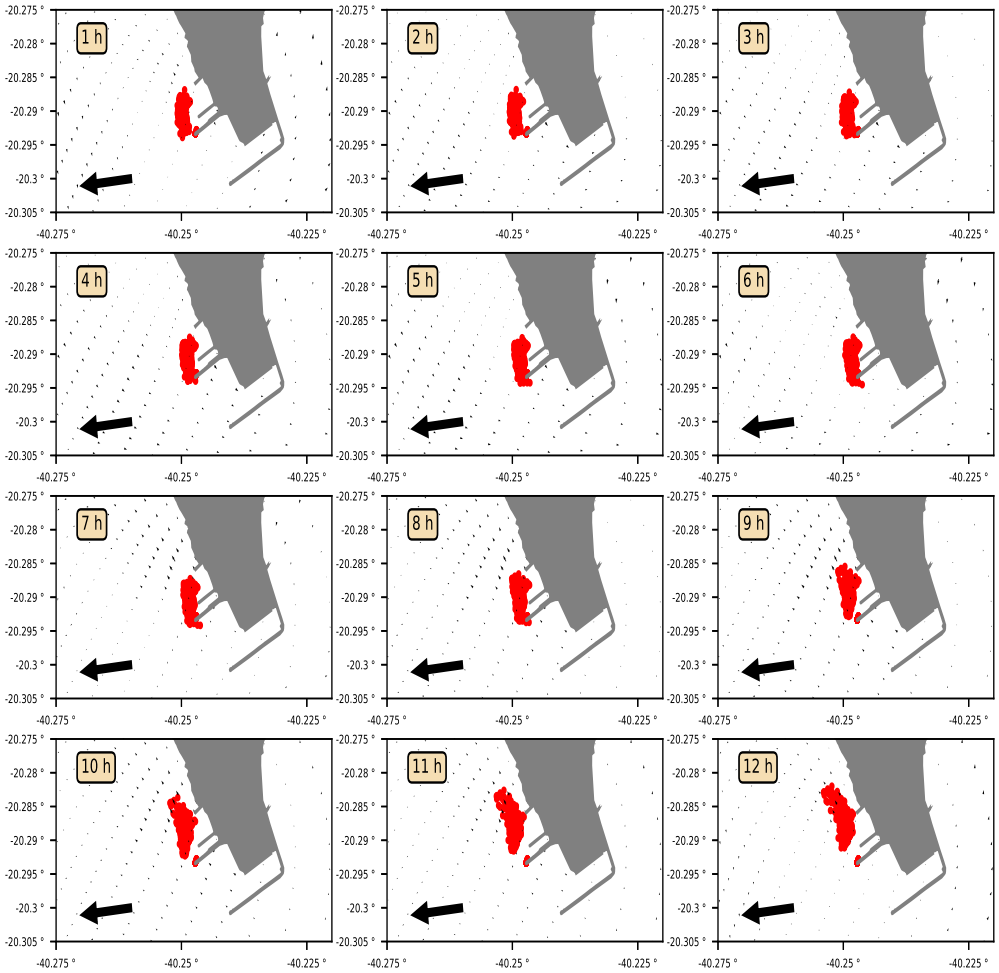

Hourly snapshots of the particles position along 1 tidal cycle for the Tubarão port spill. The black arrow represents the prevailing wind direction along the simulation.

4.2.2 Vitória Bay Spill

Following will be presented the discussion over the data analysis performed on the results provenient from probabilistic simulation.

In figures 4.39 and 4.40 are shown the distribution of the oil slick for the periods of summer and winter, respectivelly, with the region with higher percentage indicated by red circles. These maps show the shape of the oil slick by the end of 60 hours averaged over all deterministic runs, with the percentages reflecting the quantity of oil in each cell. This parameter is very important when planning strategies for contigency and cleaning, since it gives the final transport of the slick after some period of time.

The low values of the percentage (maximum values approximately 0.2%) indicate a great dispersion/advection undergone by the oil slick, occupying a great area of the Vitória and Espírito Santo bays. For both cases there was not a significant stranding of particles at the shoreline, with the most part of these found at the Espírito Santo bay (71% for winter and 59% for summer), which can be related to the ebb dominance of the current system in Vitória bay (as shown in section 4.1.1).

The largest difference between the two seasons is the significant transport observed in the winter case towards Tubarão port, occupying a greater area inside Espírito Santo bay than the summer case. In winter was also observed a significant transport towards inner parts of the Espírito Santo bay, highlighted by the red circle.

Figure 4.39 - Distribution of the oil slick - Summer

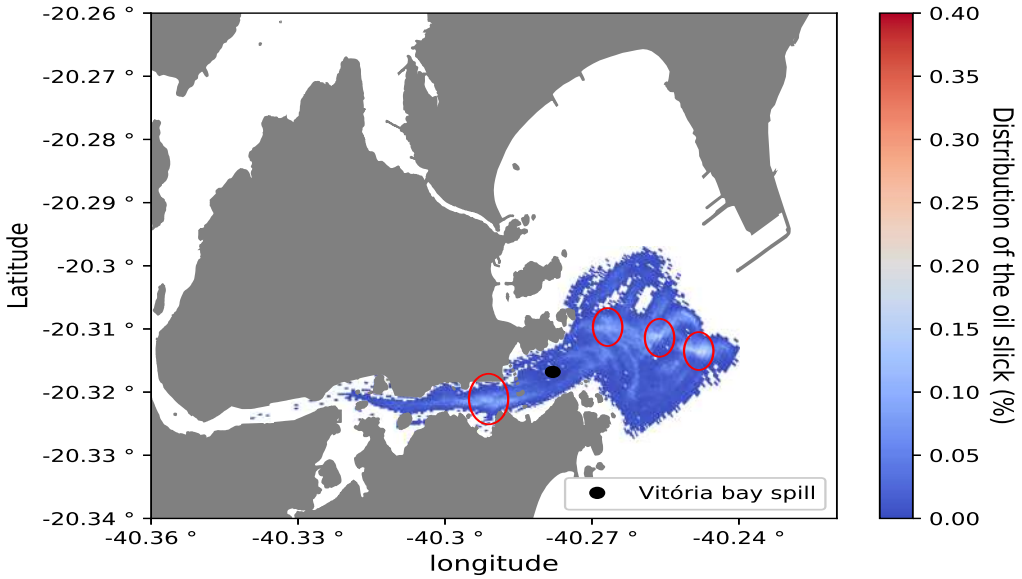

Percentage of the distribution of the oil slick for the probabilistic case. The red circles indicate the regions with the greatest percentages

Figure 4.40 - Distribution of the oil slick - Winter

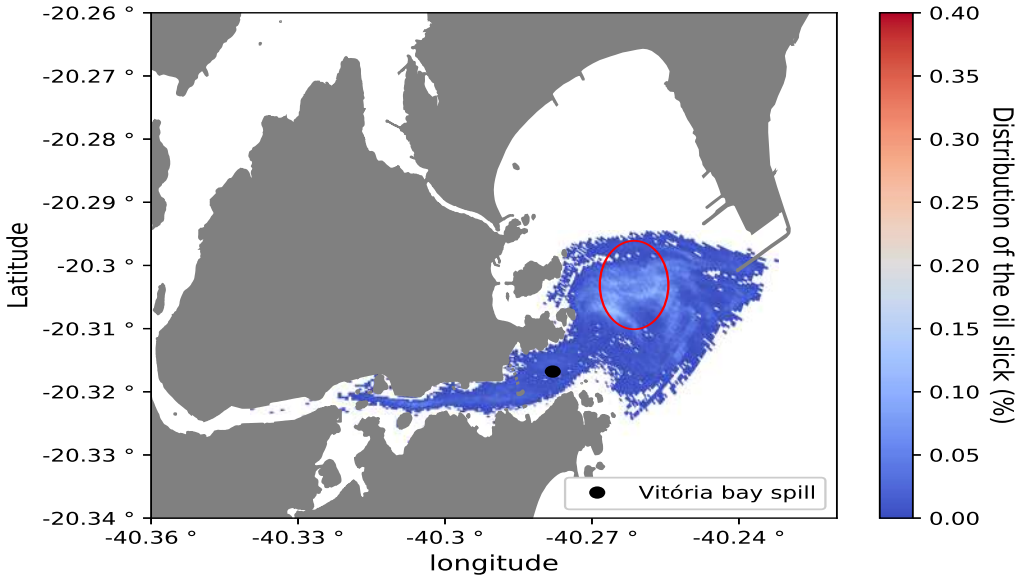

Percentage of the distribution of the oil slick for the probabilistic case. The red circles indicate the regions with the greatest percentages

In figures 4.41 and 4.42 are shown the maps for the probability of ocurrence of the slick for the periods of summer and winter, respectivelly. This parameter is one of the most important since it shows all the locations exposed to the oil slick along the determininistic runs, giving all polluted areas in the study region.

The mean difference between the probability of ocurrence and the previous parameter is that in the first the spatial location of the particles in all timesteps are accounted for, indicating the regions more prone to oil damages.

The figures show that the values of probability are greater near the spill site, since this region is affected by the slick in all spill events, decreasing outwards due to local dynamics of current and wind, responsible to disperse and advect the oil particles.

The dynamic of tides and the dominance for ebbing currents is very clear in these maps, for both seasons, with the greatest probabilities directed towards the Espŕito Santo bay, and lowest towards inner parts of Vitória bay. This result shows that a mitigation plan should initially concentrate its eforts in the nearby Espírito Santo bay region, since this region is recurrently affected by the oil slick.

For both seasons it was not reproduced the transport of oil to the Camburi beach, being the shoreline affected by the spill located almost entirely inside the Vitória bay. The largest difference between winter and summer is a greater probability in the ebbing direction for winter case.

Figure 4.41 - Probability of ocurrence of the oil slick - Summer

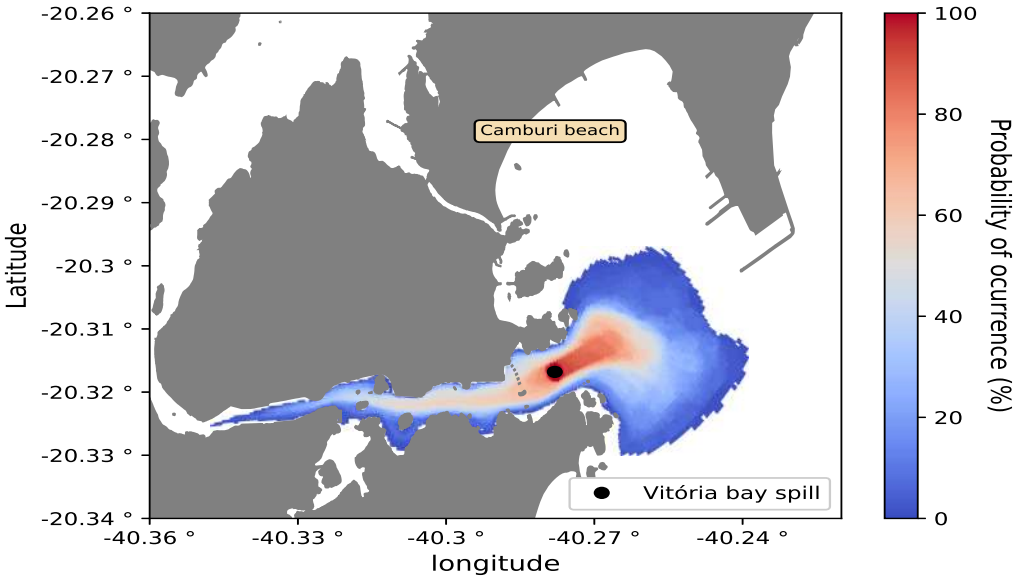

Probability of ocurrence of the oil slick for the probabilistic case

Figure 4.42 - Probability of ocurrence of the oil slick - Winter

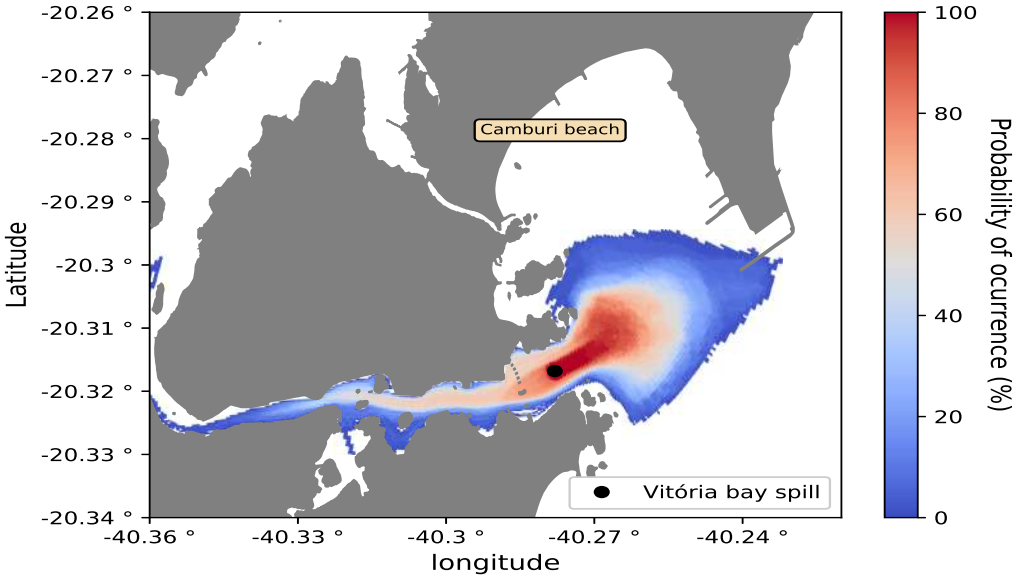

Probability of ocurrence of the oil slick for the probabilistic case

Ecological impact has been estimated to occur at $10\,g/m^2$ according to French et al. (1996) and French-McCay (2009), as this level of oil has been observed to mortally impact birds and other wildlife associated with the water surface.

In figure 4.43 and 4.44 are shown maps of area density (g/m^2) of oil per unit area for summer and winter, respectivelly, using as minimum limit the threshold of $10\,g/m^2$ as the zone of potential moderate exposure on the sea surface. These maps are important to optimize cleanup strategies, directing more resources in area with more potential to damage after some period of time.

As expected the maps for area density resemble the maps for the distribution of the oil slick, with the regions of greatest percentages presenting more oil per m^2. However, following the ecological criteria defined above, the area for potential biological impact is smaller than the area affected by the oil spill, for both summer and winter.

In spite of some spots of stranded oil inside Vitória bay with a area density aroung $300\,g/m^2$, regions of greatest area density of floating oil presented values approximately $100\,g/m^2$ (circled in red), classifying these locations as zones of high sea surface exposure, according to French-McCay (2009).

For winter, patches of oil with area density greater than $100\,g/m^2$ are located entirely inside Espírito Santo bay, while in summer the zones of high sea surface exposure are found in both bays. This result corroborates the found in the probability of ocurrence of the slick, with greater probability in the ebbing direction for winter case.

Figure 4.43 - Area density (g/m^2) - Summer

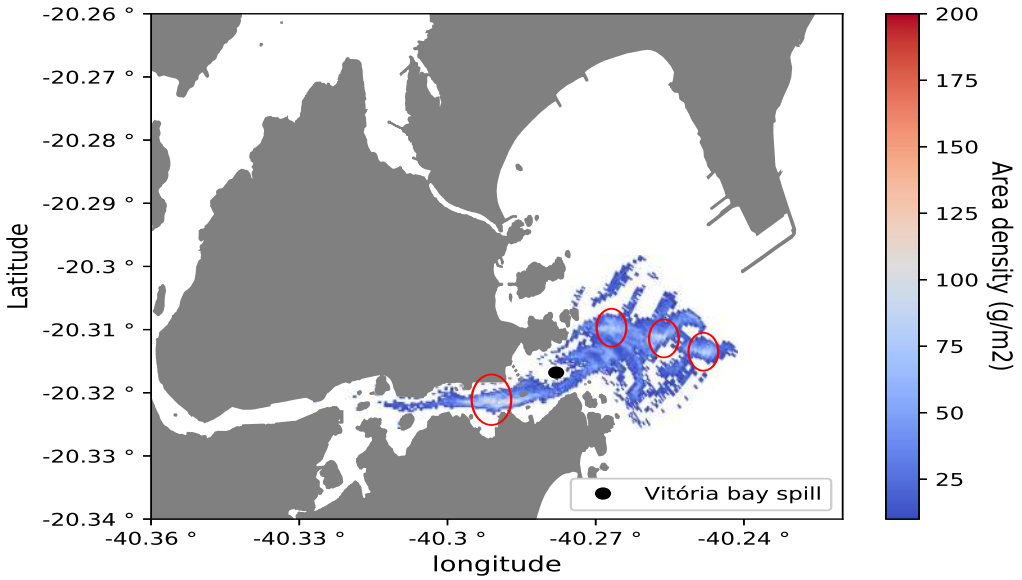

Area density showing the amount of oil (g) per unit area for the probabilistic case. Red circles indicate highlight zones of high sea surface exposure

Figure 4.44 - Area density (g/m^2) - Winter

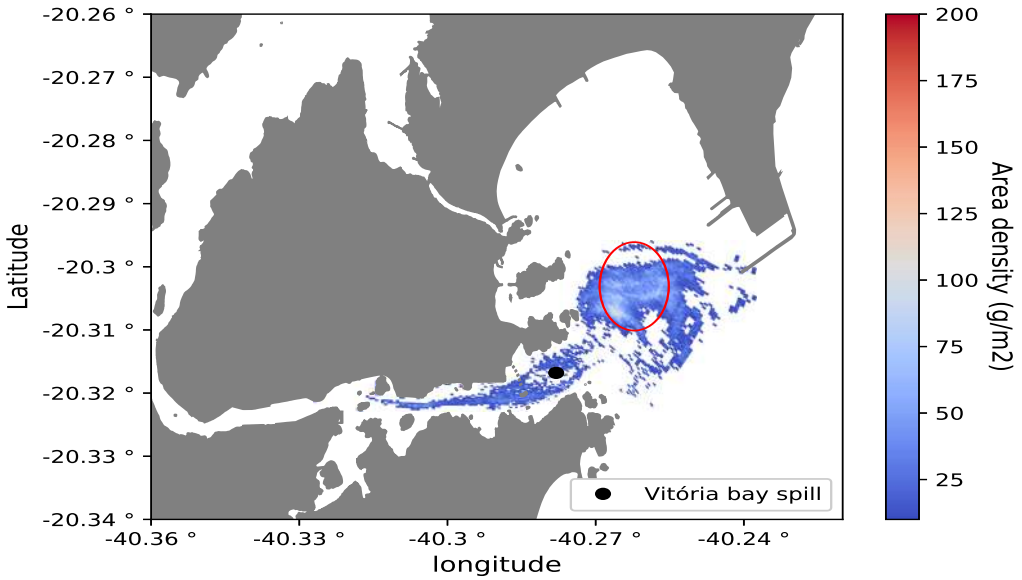

Area density showing the amount of oil (g) per unit area for the probabilistic case. Red circles indicate highlight zones of high sea surface exposure

In figure 4.45 and 4.46 are shown maps of the time percentage for summer and winter, respectivelly. This parameter reckons the duration each cell was exposed to the oil slick considering all deterministic runa. This is important since the longer a region stays in contact with the slick, more propense it is to affect the local biodiversity or any enginnering structure installed in the region.

For both seasons the regions with a persistent presence of the oil slick are situated along the mean axis of the Vitória bay and near Espírito Santo bay region, with a percentage above 10%, indicating the control of the tidal dynamics in the transport of the slick. The low value for time percentage (maximum value approximately 15%) is related to the high dispersion/advection undergone by the slick in this case.

Figure 4.45 - Time percentage - Summer

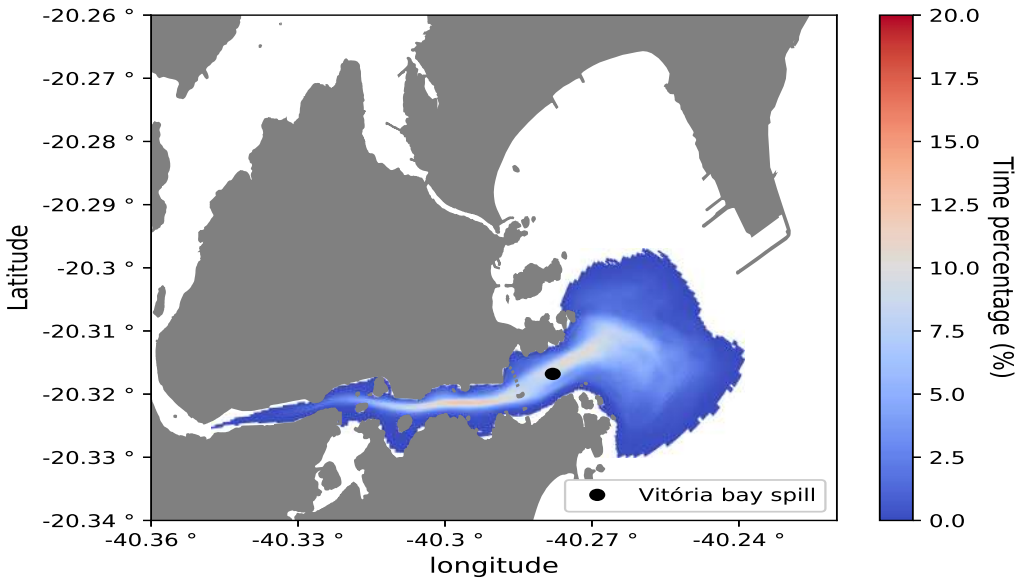

Map for the percentage of time (%) a grid point was in contact with oil in the simulation

Figure 4.46 - Time percentage - Winter

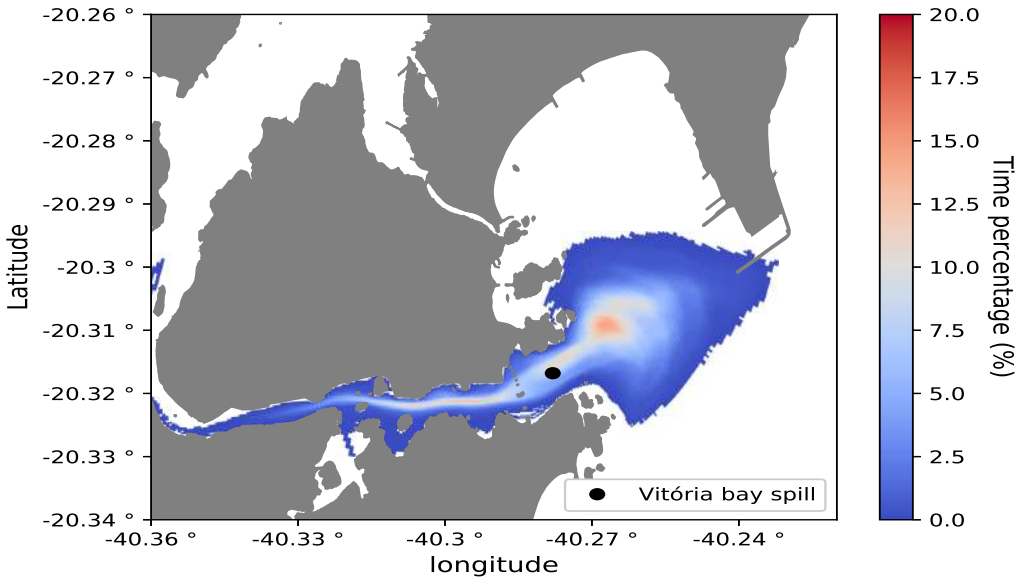

Map for the percentage of time (%) a grid point was in contact with oil in the simulation

The analysis of the results from the probabilistic simulations showed that, for the Vitória bay spill, the oil slick affected part of the Vitória bay region and of the adjacent Espírito Santo bay region, with no ocurrence of oil reaching the Camburi beach, within the period of 60 hours, for both summer and winter periods. The small values of the distribution of the oil slick and time percentage indicate a great dispersion/advention undergone by the slick, increasing the necessary effort for cleaning actions, since oil is expected to reach longer distance from the spill location. The weak difference between summer and winter for all parameters can be explained by the dominance of the tidal dynamics over the wind regime and the seasonal flow rate variation of the tributaries.

The results indicate that the same oil spill response plan can be applied for both summer and winter, and should initially involve the installation of contention barries in the Vitória bay main channel and in the nearby Espírito Santo bay region. The application of dispersants is not recomended in the region, since the growth in the entrainment rate resultant from this chemical would accelerate the dissolution process undergone by the oil, increasing the risk of contamination of the estuarine ecosystem, the camburi beach and nearby shelf region.

In figure 4.57 and 4.58 are show the affected area by the spill considering a

continuous spillage along 15 days, for summer and winter, respectivelly. In spite of the piers of Tubarão port being represented in the figures, they were not considered in the hydrodinamic simulation, and therefore, in the oil simulation.

Figure 4.47 - Continuous simulation - Summer

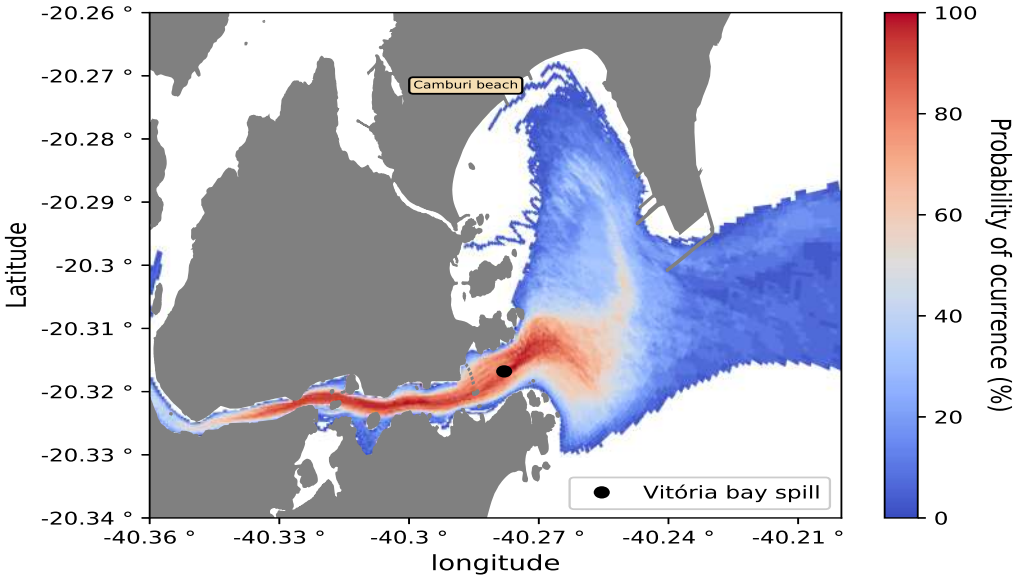

Map of the probability of ocurrence (%) for the continuous simulation.

Figure 4.48 - Continuous simulation - Winter

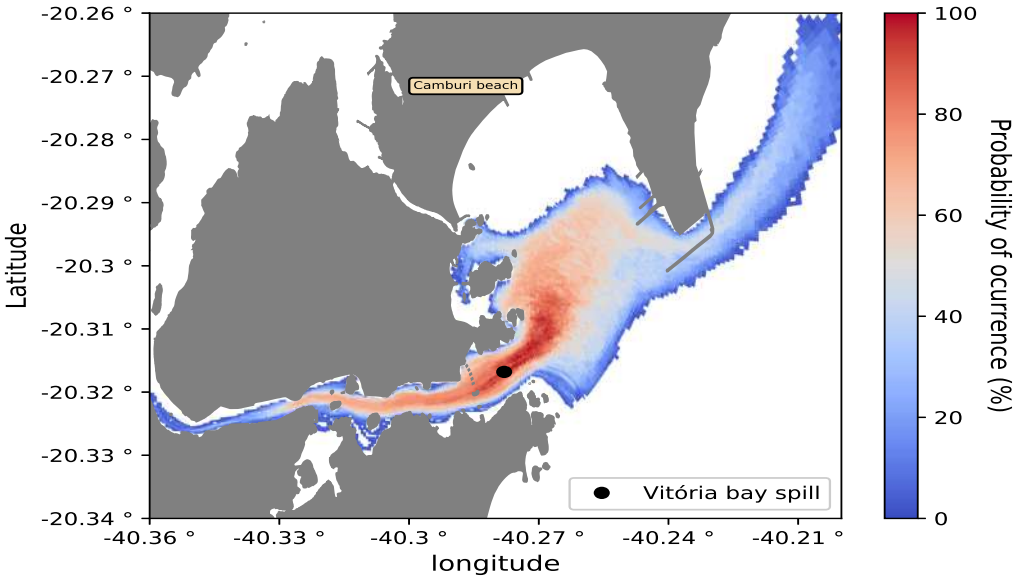

Map of the probability of ocurrence (%) for the continuous simulation.

For both simulations there was a clear transport of the oil out of the Espírito Santo bay, a process not observed in the 60 hours span deterministic simulations, confirming the need for the first contigency actions to be taken within the first days. In the summer case were found greater probabilities of occurence towards Cambury beach, indicating a greater impact in this location associated with summer months. On the contrary of the summer case, in the winter the oil slick did not reach Camburi Beach, what is probably related to particulaties in the flow dynamics in the period simulated.

4.2.3 Tubarão port Spill - without piers

In this section the piers for the mooring of vessels in the Tubarão port (inner and outer piers in figure 3.7) were not considered in the simulation. For this reason, they impose no influence in the propagation of the oil slick.

In figures 4.49 and 4.50 are shown the distribution of the oil slick for the periods of summer and winter, respectivelly, with the regions with higher percentage indicated by red circles. These maps indicate the distribution of the oil slick by the end of 60 hours averaged in all deterministic runs.

For the summer case it was observerd a tendency of the oil slick to propagate towards Camburi beach and outwards of Espírito Santo bay, forming a slick with an elongated shape. No significant fraction of the slick got stranded along the shoreline.

For the winter case all oil slick was transported outside of Espírito Santo bay, with no oil stranded along the shoreline, forming a slick with the classical drop shape.

For both cases no oil was transported towards the middle parts of the Espírito Santo bay.

Comparing with the Vitória bay spill, it is observed a weaker advection/diffusion process associated with the Tubarão port spill for the probabilistic simulation, with a smaller area occupied by the slick. This result is confirmed by the higher percentage for the distribution of the oil slick for the Tubarão port spill, indicating a greater aggregation of oil particles.

Figure 4.49 - Distribution of the oil slick - Summer

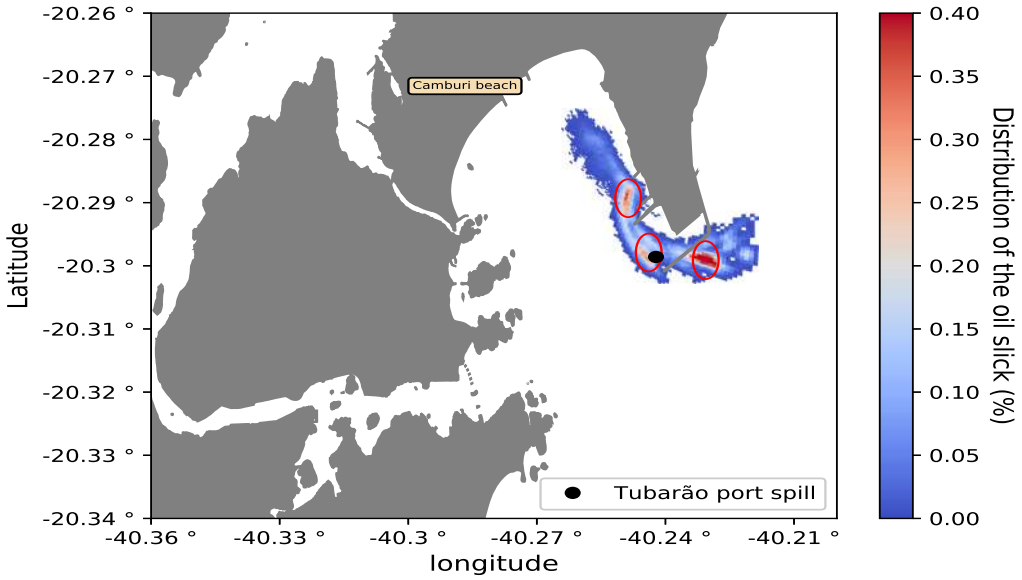

Percentage of the distribution of the oil slick for the probabilistic case. The red circles indicate the regions with the greatest percentages

Figure 4.50 - Distribution of the oil slick - Winter

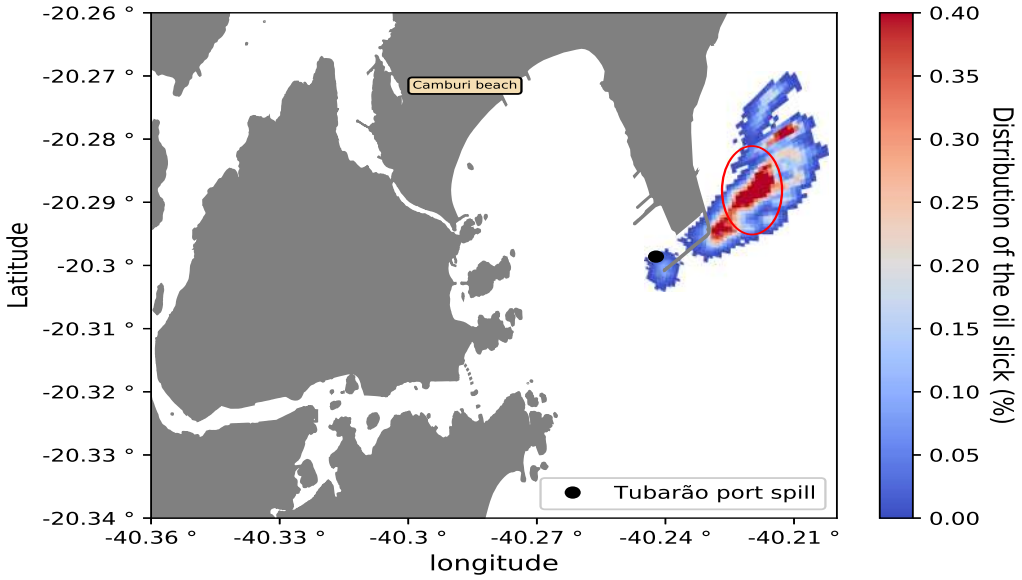

Percentage of the distribution of the oil slick for the probabilistic case. The red circles indicate the regions with the greatest percentages

In figures 4.51 and 4.52 are shown the maps for the probability of ocurrence of the slick for the periods of summer and winter, respectivelly.

For the summer case it is observed greater probabilities around the spill location and towards the Camburi beach. Smaller values of probability was found outwards the Espírito Santo bay, indicating a prevailing transport towards Camburi beach. This pattern was not clear in previous analysis, and is related to particularities of the frequency of measurement each parameter.

For the winter case it was observed greater probabilities around the spill location and outwards the Espírito Santo bay, forming a well defined plume to nothern parts of the shelf region.

Figure 4.51 - Probability of ocurrence of the oil slick - Summer

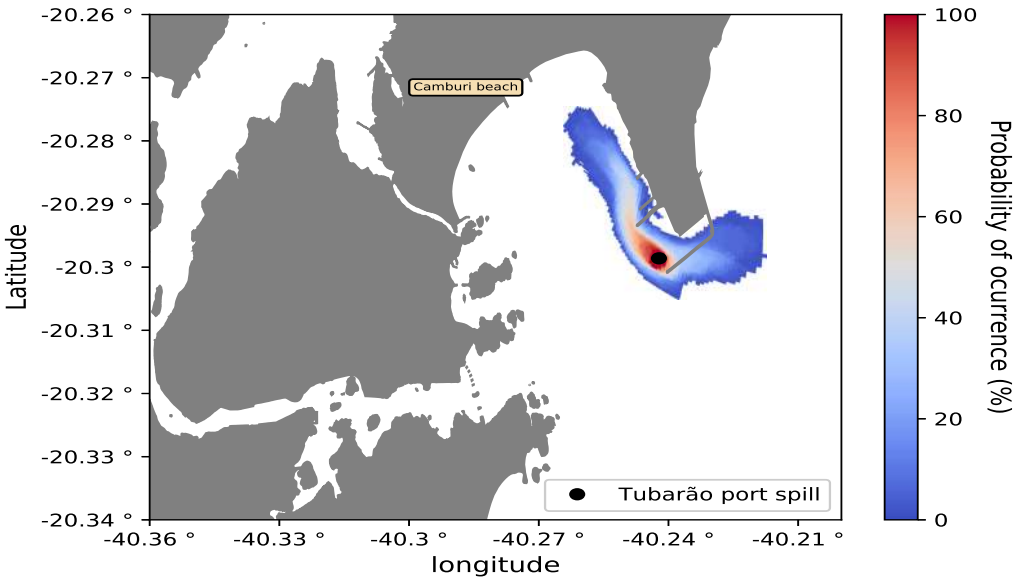

Probability of ocurrence of the oil slick for the probabilistic case

Figure 4.52 - Probability of ocurrence of the oil slick - Winter

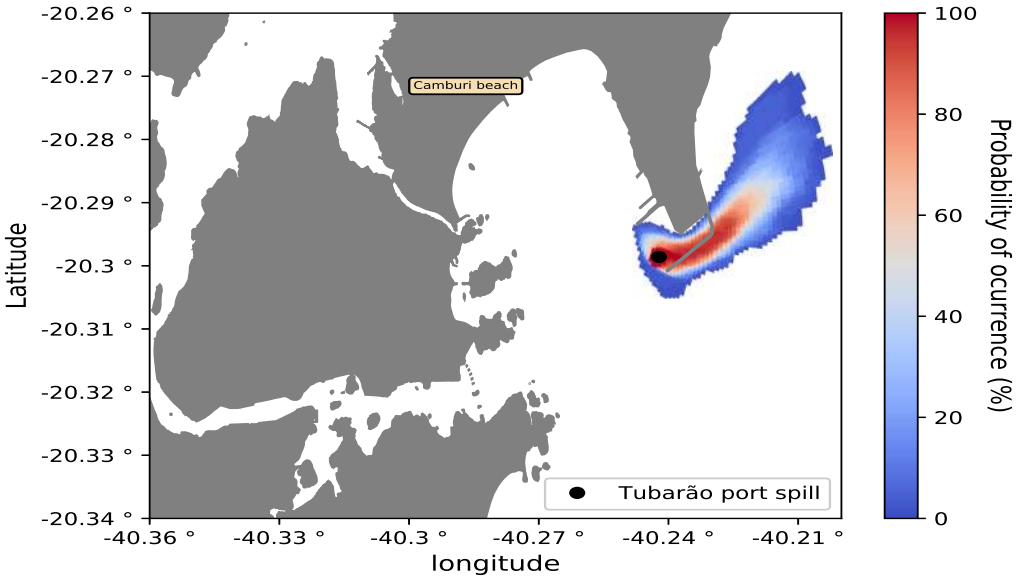

Probability of ocurrence of the oil slick for the probabilistic case

In figure 4.53 and 4.54 are shown maps of area density (g/m^2) of oil per unit area for summer and winter, respectivelly, using as minimum limit the threshold of $10\,g/m^2$ as the zone of potential moderate exposure on the sea surface.

The spatial distribution of the area density folllowed the distribution of the oil slick, as expected, for both cases. The greatest value found in summer was approximately $250\,g/m^2$, indicated by the red circle nearest to the Camburi beach, and for winter approximately $175\,g/m^2$. These values are higher than the simulated for the Vitória bay spill case, and is probably related to the weaker dispersion/advection undergone by the slick in the present case.

Figure 4.53 - Area density (g/m^2) - Summer

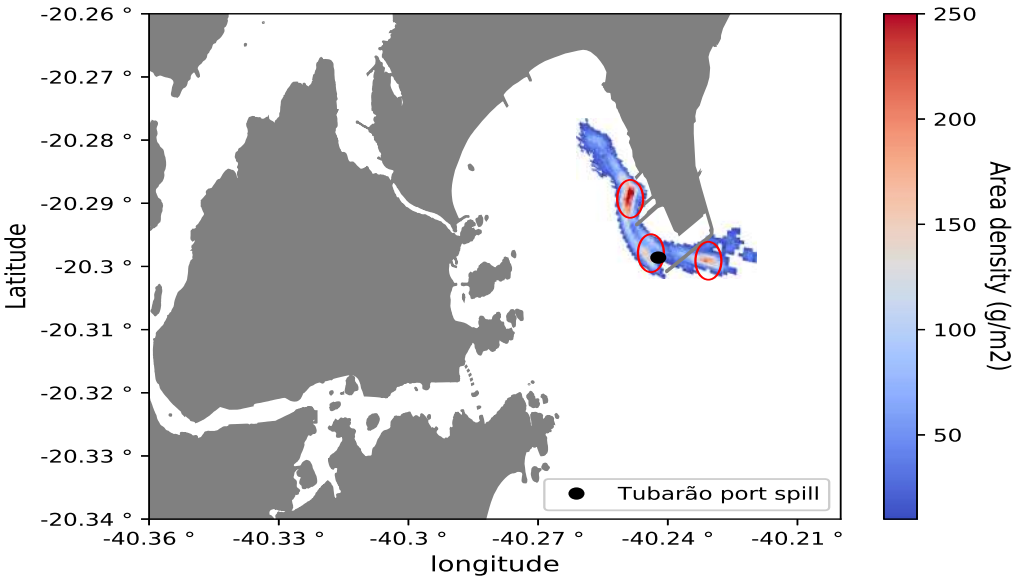

Area density showing the amount of oil (g) per unit area for the probabilistic case. Red circles indicate highlight zones of high sea surface exposure

Figure 4.54 - Area density (g/m^2) - Winter

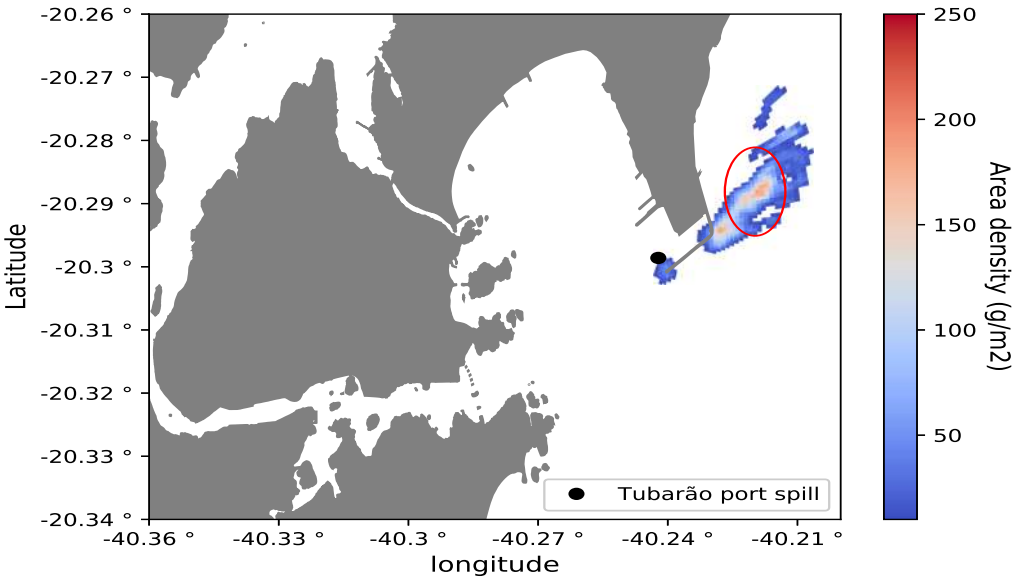

Area density showing the amount of oil (g) per unit area for the probabilistic case. Red circles indicate highlight zones of high sea surface exposure

In figure 4.55 and 4.56 are shown maps of the time percentage for summer and winter, respectivelly.

For the summer case it is observed higher values of time percentage towards the Camburi beach, and smaller outwards the Espírito Santo bay. The opposite occurred in the winter case, with the highest values towards the adjacent shelf region. The values of time percentage found in Tubãrao port Spill are also higher than in Vitória port spill, corroborating previous parameters.

Figure 4.55 - Time percentage - Summer

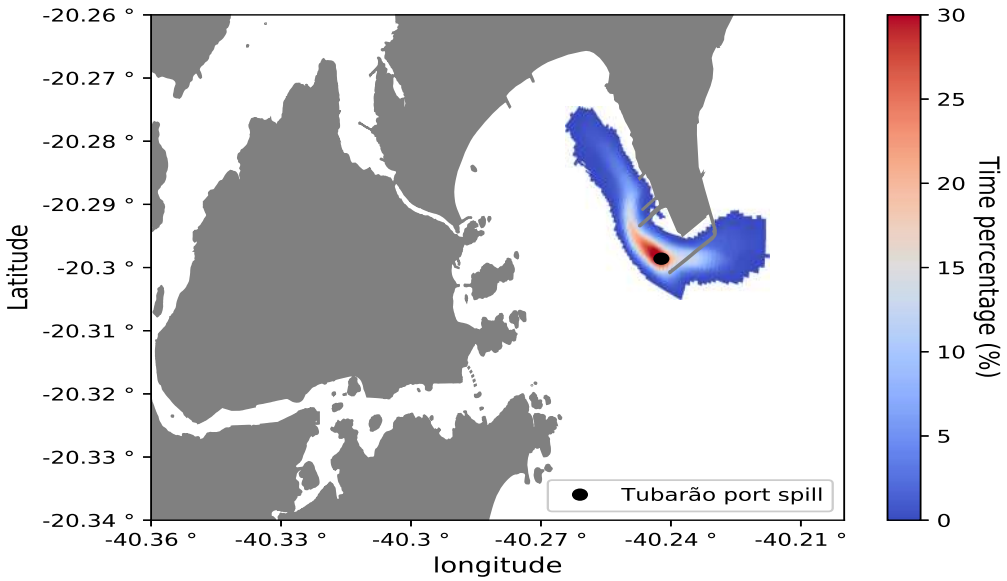

Map for the percentage of time (%) a grid point was in contact with oil in the simulation

Figure 4.56 - Time percentage - Winter

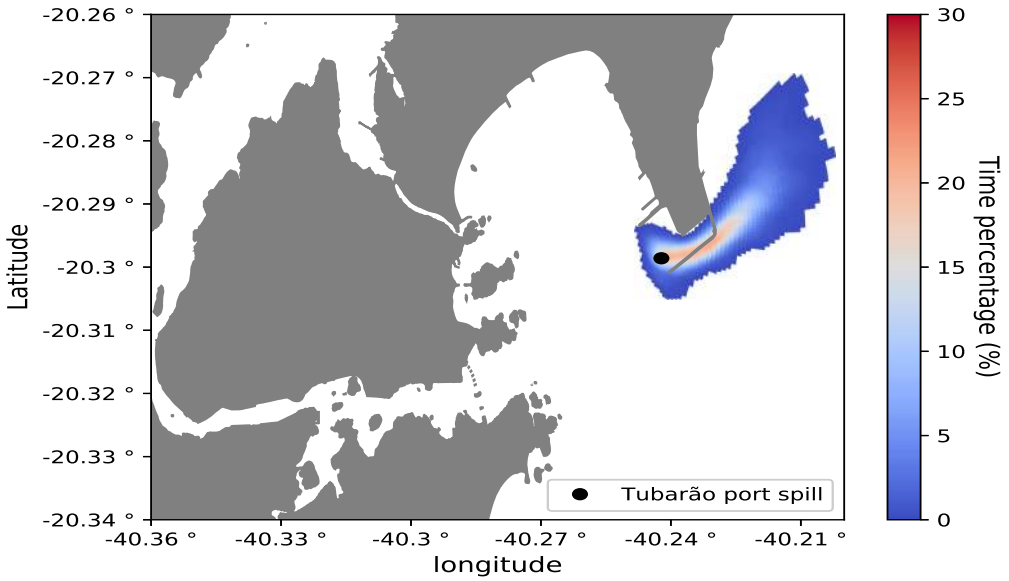

Map for the percentage of time (%) a grid point was in contact with oil in the simulation

The analysis of the results from the probabilistic simulation for the Tubarão port spill without piers showed a very distinct pattern between summer and winter, not observed for the Vitória bay spill, where similar patterns was observed for both seasons. While in summer there was a tendency of the slick to propagate towards Camburi beach, corroborated by the distributions of the probability of ocurrence and time percentage, for the winter case all deterministic runs showed a clear movement of the slick outwards of Espírito Santo bay. Moreover, the results show a weaker advection/diffusion associated with the Tubarão port spill, in comparison to Vitória bay spill, which is probably related to weaker tidal currents associated with the region, being controlled meanly by wind-induced currents.

The results indicate that distinct oil spill response plans must applied for summer and winter. For summer it should initially involve the installation of contention barries in the region towards Camburi beach, and for winter the installation of contention barries at the entrance of the Espírito Santo bay. The application of dispersants is not recomended in the region, since the growth in the entrainment rate resultant from this chemical would accelerate the dissolution process undergone by the oil, increasing the risk of contamination of the Camburi beach and nearby shelf region.

In figure 4.57 and 4.58 are show the affected area by the spill considering a continuous spillage along 15 days, for summer and winter, respectivelly.

Figure 4.57 - Continuous simulation - Summer

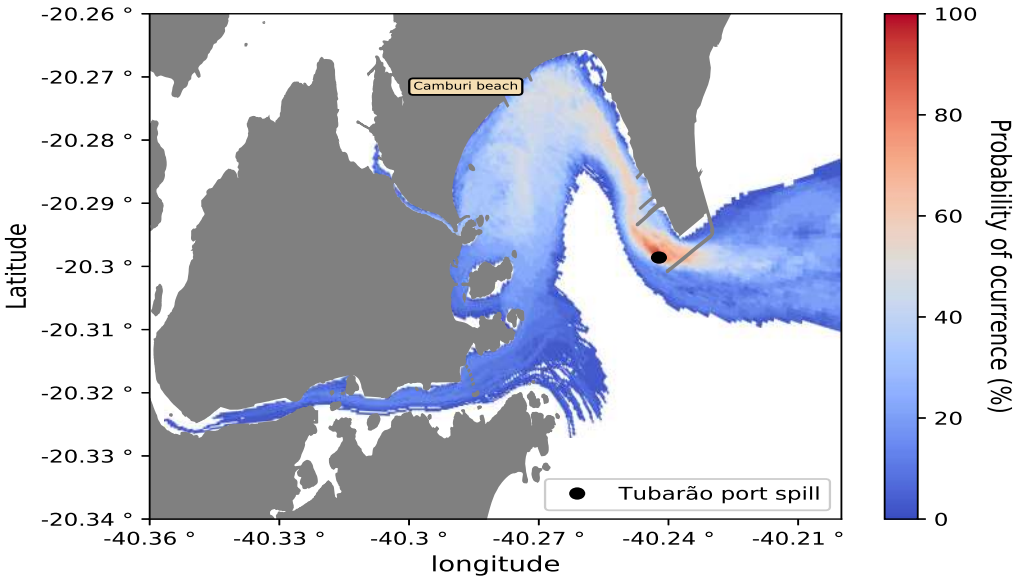

Map of the probability of ocurrence (%) for the continuous simulation.

Figure 4.58 - Continuous simulation - Winter

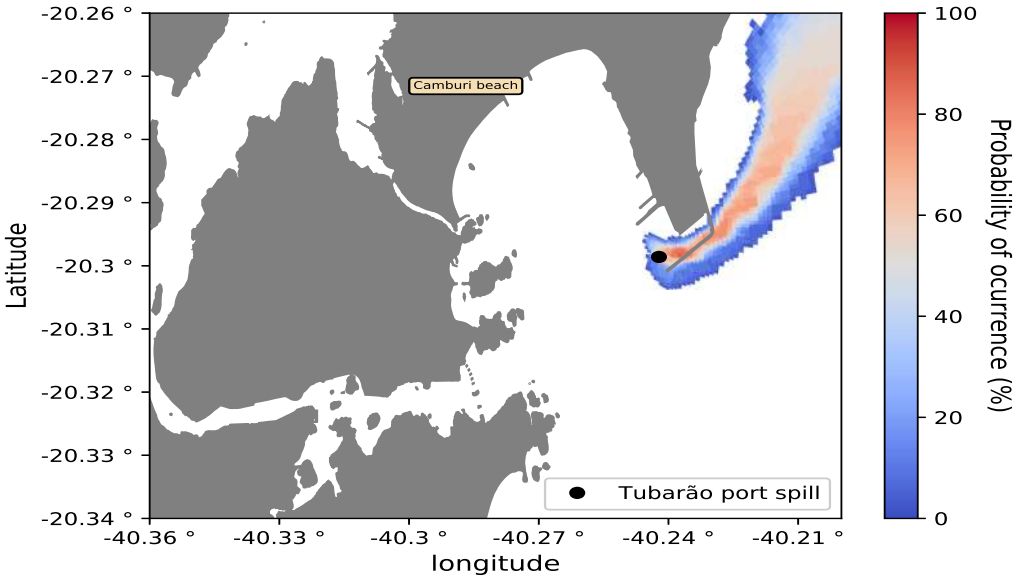

Map of the probability of ocurrence (%) for the continuous simulation.

In the summer continuous case, the affected areas included regions inside Espírito Santo bay, Vitória bay (including Canal da Passagem), and the adjacent shelf region. All the extent of Camburi beach was affected by the spill, something not observed in all other cases (including Vitória bay spill). Comparing to Vitória bay spill, we can infer that Tubarão spill presented more overall risk to SEIV system, since a greater area was affected by the slick, demanding more efforts for cleaning actions. In the winter continuous case, all slick was directed outside the Espírito Santo, to the adjacent shelf region to the north of Espírito Santo bay.

4.2.4 Tubarão port Spill - with piers

In this section, the piers for the mooring of vessels in the Tubarão port (inner and outer piers in figure 3.7) were considered in the simulation. As stated previously, the boundary condition implemented in the model imposes that all particles and droplets in contact with a hard surface have 100% probability of adhering to it. To reckon the varying probability of the stranding of oil particles, a complex study is required to compute the interaction between specific kinds of surfaces and oil, since oils with different chemical properties interact differently with the many types of hard surface, like sand, gravel, concrete, and absorbents.

Figures 4.59, 4.60, 4.61, and 4.62 depict the distribution of the oil slick and the maps for the probability of ocurrence of the slick for the periods of summer and winter, respectivelly, showing the great influence of the piers in the transport of the oil slick.

For both seasons the longer outer pier was responsible for the largest number of stranded parcels, shaping the area affected by the oil particles and the final distribution of the slick. The inner pier presented no significant influence in the winter case, affecting the landward border of the slick in summer.

As expected from previous section, the winter case was the most affected by the port structures, with the transport of the oil restrained inside of the Tubarão port, hampering the formation of the drop shape observed in the case without piers.

For summer, in both cases, with and without piers, was observed a similar advection of the slick towards Camburi beach. However, due to the stranding of oil in the port structures, smaller values for the distribution of oil slick and for the probability of ocurrence were found with the presence of piers, reflecting on a smaller area of the oil slick.

Figure 4.59 - Distribution of the oil slick - Summer

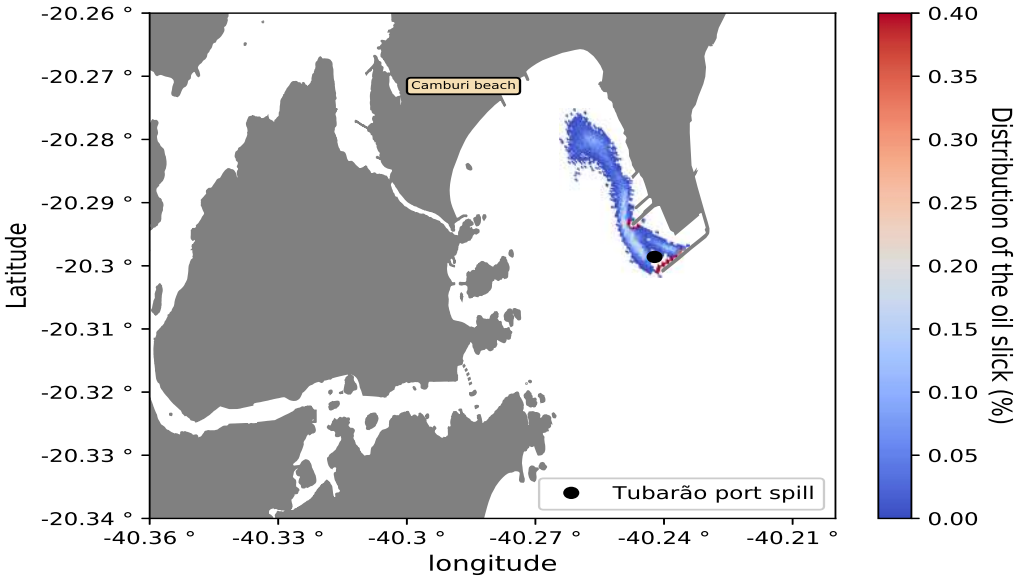

Percentage of the distribution of the oil slick for the probabilistic case.

Figure 4.60 - Distribution of the oil slick - Winter

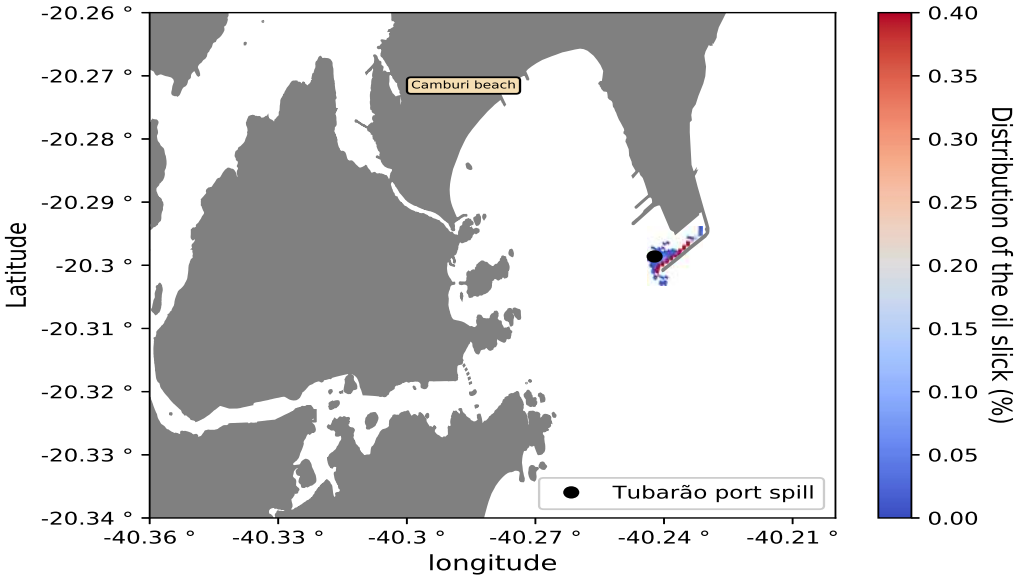

Percentage of the distribution of the oil slick for the probabilistic case

Figure 4.61 - Probability of ocurrence of the oil slick - Summer

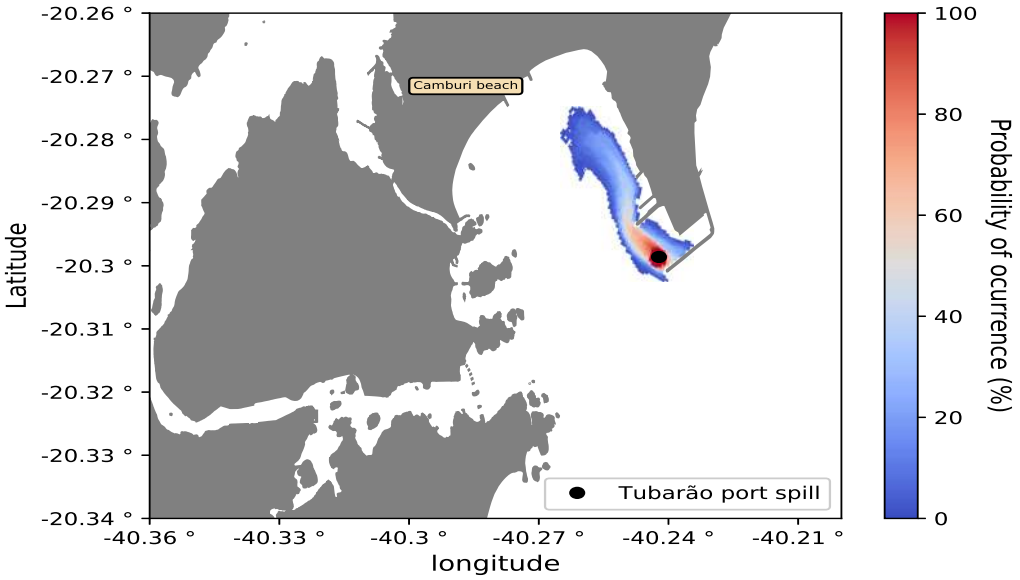

Probability of ocurrence of the oil slick for the probabilistic case

Figure 4.62 - Probability of ocurrence of the oil slick - Winter

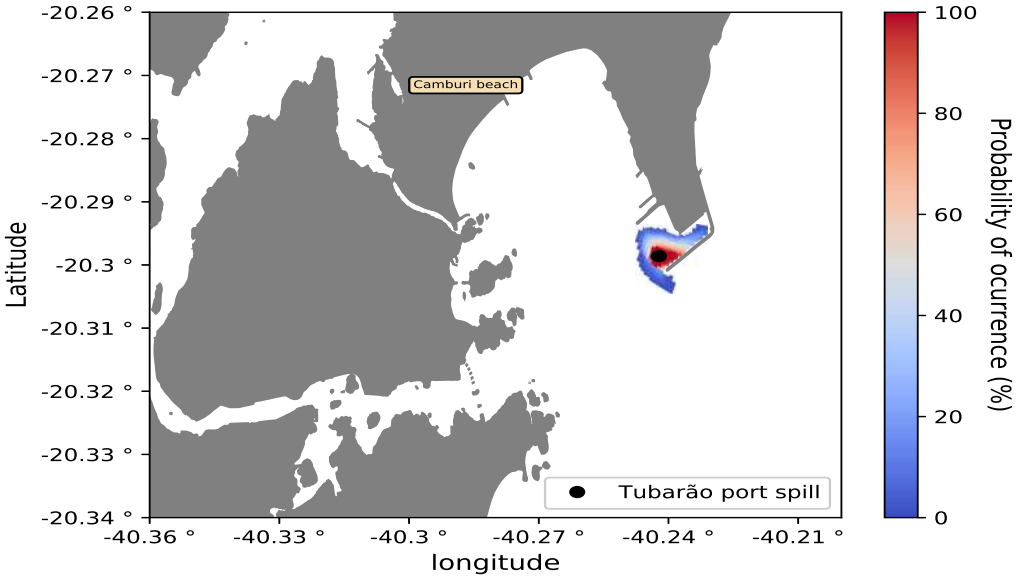

Probability of ocurrence of the oil slick for the probabilistic case

Figures 4.63, 4.64, 4.65, and 4.66 depict maps of area density (g/m^2) of oil per unit area and maps of time percentage for the summer and winter, respectivelly, confirming the great influence of the mooring structure on the physical caracteristics of the oil slick.

For both seasons the greatest values of area density and time percentage occured along the moorings, with smaller values for the floating fraction when compared to the case without piers. In summer was found a maximum area density of the floating oil approximately $125\,g/m^2$, against the $250\,g/m^2$ found without the mooring. The area delimited by the threshold of $10\,g/m^2$ was also significally smaller after the inclusion of the port structures. In winter, almost no concentrations above $10\,g/m^2$ were found in the floating fraction.

Figure 4.63 - Area density (g/m^2) - Summer

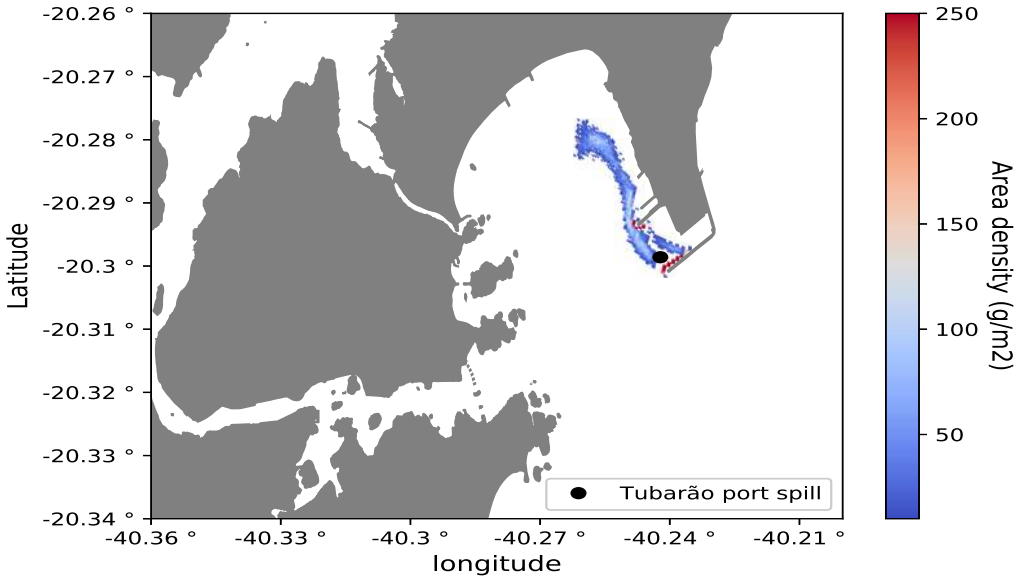

Area density showing the amount of oil (g) per unit area for the probabilistic case.

Figure 4.64 - Area density (g/m^2) - Winter

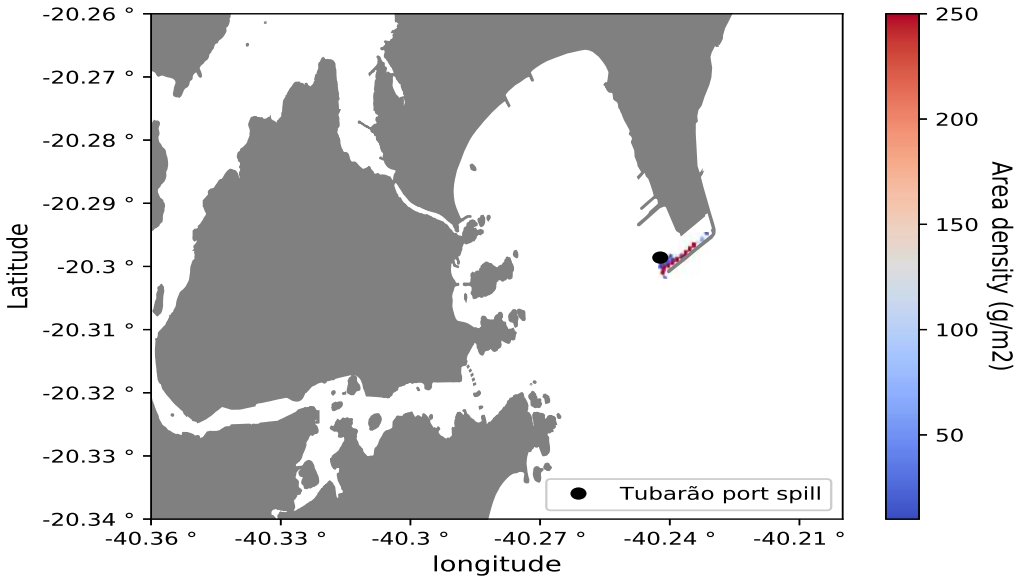

Area density showing the amount of oil (g) per unit area for the probabilistic case.

Figure 4.65 - Time percentage - Summer

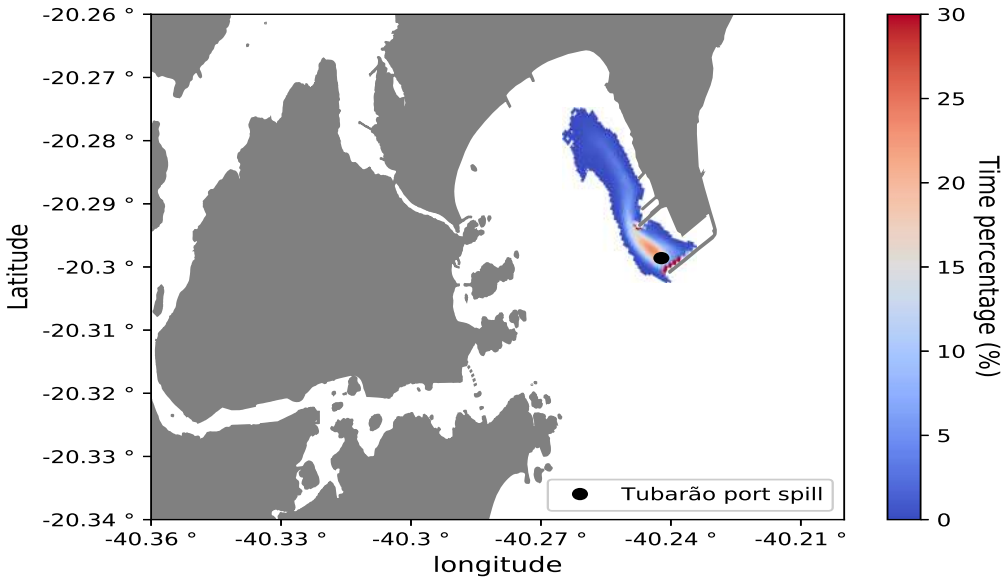

Map for the percentage of time (%) a grid point was in contact with oil in the simulation

Figure 4.66 - Time percentage - Winter

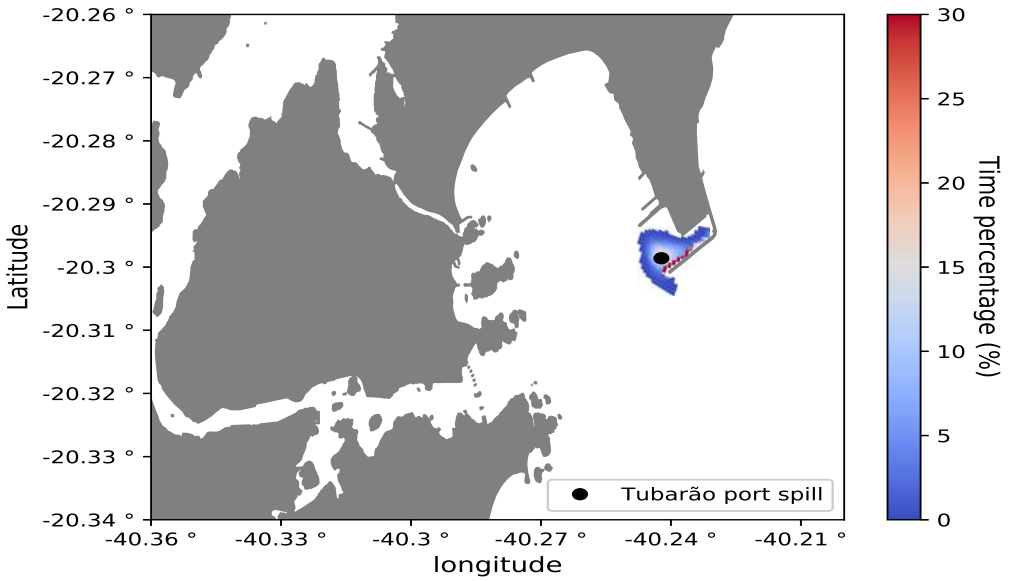

Map for the percentage of time (%) a grid point was in contact with oil in the simulation

In figure 4.67 and 4.68 are show the affected area by the spill considering a continuous spillage along 15 days, for summer and winter, respectivelly.

For the winter case the oil slick was completelly blocked by the longer outer pier, with the transport limited to the Tubãrao port.

For summer, the transport of the oil slick was similiar to the case without piers, affecting regions inside Espírito Santo bay, Vitória bay (including Canal da Passagem), and all the extent of Camburi beach. The main differences are the blocking of the oil slick towards offshore region (high values of probability of ocurrence along the outer pier), and smaller values of probability of ocurrence inside Espírito Santo bay, indicating a lower susceptibility to the spill in the SEIV.

The results in this section show the influence of the port structures on the impacts resultant from a spill in the region around Tubãrao port, behaving like a contention barrier in the study region. The inclusion of the piers in the oil simulation leaded to a decrease in the vulnerability of the study region, with a reduction in the final area of the slick, in the visitation frequency of oil particles, in the area density of the slick, and in the time by which a region was effected by the slick.

Figure 4.67 - Continuous simulation - Summer

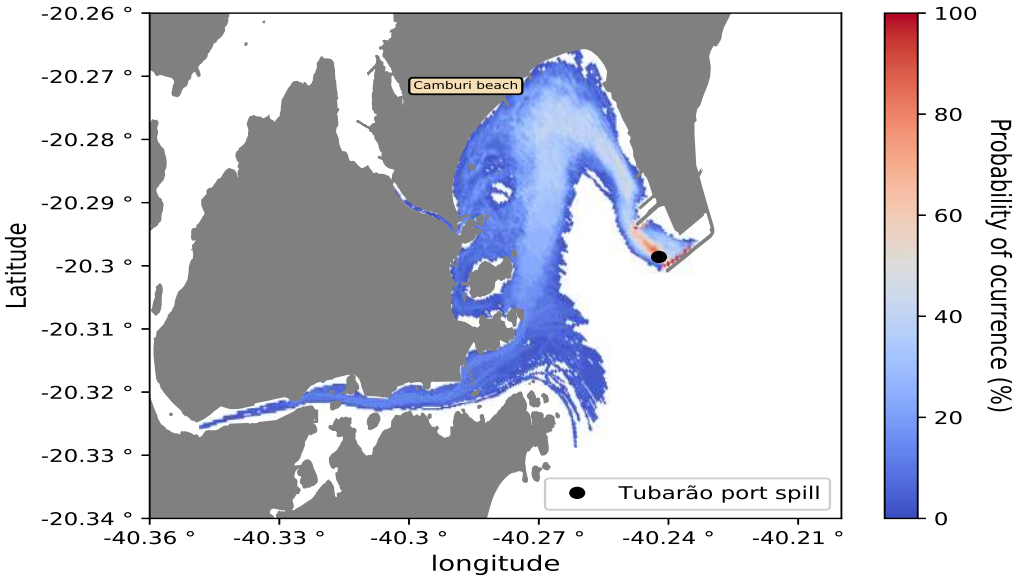

Map of the probability of ocurrence (%) for the continuous simulation.

Figure 4.68 - Continuous simulation - Winter

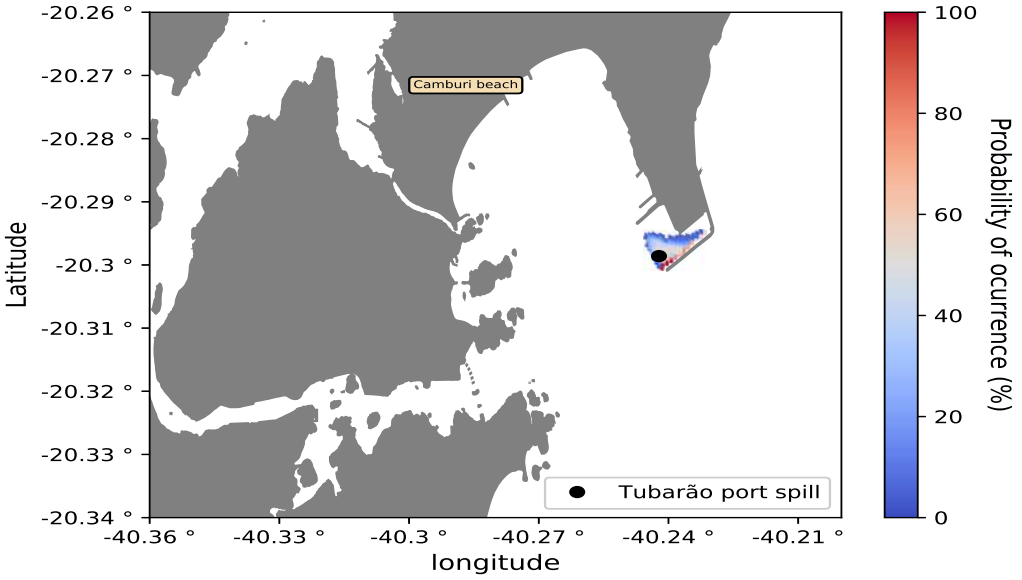

Map of the probability of ocurrence (%) for the continuous simulation.

5 CONCLUSIONS AND FUTURE WORK

The validation of the physical-chemical processes that comprise the oil model showed its ability to be employed as a tool for the assessment of impacts associated with oil spills. All parametrizations presented a good agreement against measured and theoretical data, reproducing the fate of the oil in an aqueous enviroment.

The curves of the volume fraction of evaporated oil matched the experimental data for the Ekofisk and the Kuwait oil. When varying the temperature and wind speed, the rate of evaporation was directly proportional to both variables, as expected from the equations.

The model presented a good agreement against experimental data for the diffusion coefficient, the mass transference, the evolution of droplet radius, and the volume fraction of dissolved oil, showing the proper simulation of dissolution.

For the emulsification, the model reproduced fairly well the measured data from the Large Scale Experimental oil spill citeaundunson1984, for the evolution of water content, viscosity and Density.

Regarding the vertical dispersion, the modelled entrainment rates were bounded by the experimental data, as in Li et al. (2017). The model also reproduced the cloud of droplets described by Huang (1983), and photographed by Delvigne e Sweeney (1988).

In the transport tests, the slick for both continuous and instanteneous sources followed the main direction of the current field. The time for the slick to travel across the flume was also in accordance with the velocity magnitude.

For the case study, the analysis of the data from the probabilistic simulation showed great differences in the pattern of the slick transport between Vitória bay and Tubarão port spills.

In the Vitória bay spill the slick dynamics was basically controled by the flooding/ebbing movement of the tide, reflecting the ebb dominance of the tidal regime, with the slick reaching inner parts of Vitória bay and central parts of Espírito Santo bay. For neither winter or summer the oil reached Camburi beach nor the adjacent shelf region. The results showed that for the Vitória bay spill the regions more vulnerable to damages are the mean channel and the shoreline associated with Vitória bay, and the central parts of Espírito Santo bay.

In the Tubarão port spill it was observed a smaller transport of the slick inside the Espiŕito Santo bay when compared to Vitória bay spill, generating regions with greater values of area density and time percentage for the cases without the mooring structure. For the summer case there was a clear tendency for the slick to propagate towards Camburi beach, with no oil transported to middle parts of the Espírito Santo bay. For the winter case, the transport of the oil slick was greatly controlled by the presence of the piers, due to the dominant transport of oil outwards Espiŕito Santo bay.

The piers greatly influenced the slick dynamics in the Tubarão port spill for both probabilistic and continuous simulation, decreasing the values of all statistical parameters in the study region.

While the results from Vitória bay spill presented a smaller dependence to seasonal variations, with all meanly affected areas located inside Vitória and Espírito Santo bays, the results from Tubarão port spill varied highly between the two seasons, with a dominance of the transport of oil to the nearby northern shelf region for the winter, and towards Camburi beach in summer.

Among the continuous cases, the Tubarão port spill in summer presented the most worrisome results for the SEIV, with the slick affecting the greatest area among all cases, including all the extented of the Camburi beach and the Canal da passagem.

Considering the 60 h period defined by CONAMA resolution №6 398/08, the impacts resultant from the spill are concentrated inside the Vitória and Espírito Santo bays system for all cases but the Tubarão port spill in winter. Meanwhile, for all continuous cases there was a tendency of oil to be advected/dispersed to the nearby shelf region, hampered by the presence of the port structures. Therefore, depending on the timespan and on the location of the spill inside the SEIV, a significant part of slick can be transported out of the bays system, refuting the hypothesis established in this thesis.

For future work we aim to implement additional physical-chemical processes and improvements for the numerical method in the oil spill modelling system, as the stokes drift to compute wave-induced advection, the dynamics of the dissolved fractions from particles and droplets, mass loss by sedimentation and biodegration, the runge-kutta 4th-order method for time integration (allowing greater values for TS), an oil droplet size distribution to improve the

parametrization of the vertical dispersion, the use of dispersants [1], and a coupling between the oil spill model and a blow-out model currently in development as part of a great project. In addition, it will be implemented a case with the ROMS ocean model to reproduce the outcrop of oil at Campo de Frade, in Campos Basis - Brasil, using remote sensing data to validate the propagation of the oil slick.

[1] dispersants primarily affect oil droplet size distribution

REFERENCES

AAMO, O. M.; REED, M.; DOWNING, K. Oil spill contingency and response (OSCAR) model system: sensitivity studies. **International Oil Spill Conference Proceedings**, n. 1, p. 429–438, 1997. 50

ABASCAL, A. J.; CASTANEDO, S.; MENDEZ, F. J.; MEDINA, R.; LOSADA, I. J. Calibration of a lagrangian transport model using drifting buoys deployed during the prestige oil spill. **Journal of Coastal Research**, v. 25, n. 1, p. 80–90, 2009. 14

Al Rabeh, A. H.; LARDNER, R. W.; GUNAY, N. Gulfspill version 2.0: a software package for oil spills in the arabian gulf. **Environmental Modelling and Software**, v. 15, n. 4, p. 425–442, 2000. 1

AMERICAN PETROLEUM INSTITUTE. **Technical report - petroleum refining**. Washington, D.C., 1997. Sinth edition. 18

AUNDUNSON, T.; CELIUS, H. K.; JOHANSEN, Ø.; STEIBAKKE, P.; SØORSTRØM, S. E. **The experimental oil spill on Haltenbanken 1982**: . Norway, 1984. v. 112. Technical Documentation. A Report by the Continental Shelf Institute. 68, 69, 70

AVEYARD, R. A surface tension approach to the salting-out of nonpolar nonelectrolytes. **Canadian Journal of Chemistry**, v. 60, n. 11, p. 1317–1326, 1982. 13

BARTH, A.; ALVERA-AZCARATE, A.; WEISBERG, R. H. Benefit of nesting a regional model into a large-scale ocean model instead of climatology. Application to the West Florida Shelf. **Continental shelf research**, v. 28, p. 561–573, 2008. 57

BEEGLE-KRAUSE, C. J. General noaa oil modeling environment (gnome): A new spill trajectory model. In: 2001 OIL SPILL CONFERENCE, 2001, Washington. **Proceedings...** [S.l.]: American Petroleum Institute, 2001. p. 865–871. 1, 7

BERRY, A.; DABROWSKI, T.; LYONS, K. The oil spill model oiltrans and its application to the celtic sea. **Marine Pollution Bulletin**, v. 64, n. 11, p. 2489–2501, 2012. 1, 10, 11, 25

BLUMBERG, A. F.; MELLOR, G. L. A description of a three-dimensional coastal ocean circulation model. In: **Coastal and Estuarine Sciences**. [S.l.]: Am. Geophys. Union, 1987. 9

BOBRA, M. A. Water-in-oil emulsification; a physicochemical study. In: AMERICAN PETROLEUM INSTITUTE, 1991. **Proceedings...** Washington, DC: International Oil Spill Conference, 1991. p. 483–488. 30

CABRAL, C. A. O.; TEIXEIRA, L. S. P. **Investigação do incidente de vazamento de petróleo no Campo de Frade**: relatório final. Rio de Janeiro, 2012. 71 p. Available from: <www.anp.gov.br/SITE/acao/download/?id=61108>. Access in: 11 out. 2017. 1

CAMILLI, R.; REDDY, C. M.; YOERGER, D. R.; MOOY, B. A. S. V.; JAKUBA, M. V.; KINSEY, J. C.; MCINTYRE, C. P.; SYLVA, S. P.; MALONEY, J. V. Tracking hydrocarbon plume transport and biodegradation at Deepwater Horizon. **Science**, v. 333, p. 201–204, 2010. 6

CERC. **Shore protection manual volume I.** Vicksburg, MS, USA, 1984. 25

CLIFT, R.; GRACE, J. R.; WEBER, M. E. **Bubbles, drops and particles**. Nova Iorque: Academic Press, Inc., 1978. 394 p. 15, 16

COMPANHIA AMBIENTAL DO ESTADO DE SãO PAULO (CETESB). **Principais acidentes no Brasil**. 2017. Emergências Químicas - Vazamento de Óleo. Available from: <http://emergenciasquimicas.cetesb.sp.gov.br/tipos-de-acidentes/vazamentos-de-oleo/panorama-geral/>. Access in: 05 jan. 2017. 1

CONCAWE. **Characteristics of petroleum and its behaviour at sea**. [S.l.], 1983. Report N. 8/83. 19

DAAE, R. L.; FAKSNESS, L.; DURGUT, I.; BRANDVIK, P. J.; LEIRVIK, F. **Modelling of oil in ice with OSCAR**. Norway, 2011. 22 p. SINTEF Report np. 35. 85

DALING, P. S.; AAMO, O. M.; LEWIS, A.; STROM-KRITIANSEN, T. Sintef/iku oil-weathering model: Prediction oil properties at sea. In: 1997 OIL SPILL CONFERENCE, 1997, Washingto. **Proceedings...** [S.l.]: API Publication, 1997. p. 297–307. 21

DELTARES. **Delft3D**: functional specifications. Delft, 2014. 48 p. Versão: 2.20.23866. Available from:

<http://www.deltaressystems.com/hydro/product/621497/delft3d-suite>. Access in: 24 mar. 2014. 34, 37

DELVIGNE, G. A. L.; HULSEN, L. J. M. Simplified laboratory measurements of oil dispersion coefficients - application in computations of natural oil dispersion. In: ARCTIC AND MARINE OIL SPILL PROGRAM (AMOP) TECHNICAL SEMINAR ON ENVIRONMENTAL CONTAMINATION AND RESPONSE, 1994. Ontario: Environment Canada, 1994. p. 173 – 187. 24, 25, 43

DELVIGNE, G. A. L.; SWEENEY, C. E. Natural dispersion of oil. **Oil and Chemical Pollution**, v. 4, n. 4, p. 281–310, 1988. 23, 24, 26, 28, 43, 80, 81, 84, 116

EGBERT, G. D.; EROFEEVA, S. Y. Efficient inverse modeling of barotropic ocean tide. **J. Atmospheric and Oceanic Technology**, p. 183–204, 2002. 37

EUROPEAN CENTRE FOR MEDIUM-RANGE WEATHER FORECASTS (ECMWF). **ERA5 data documentation**. 2019. Available from: <https://confluence.ecmwf.int/display/CKB/ERA5+data+documentation>. Access in: 2 jan. 2019. 40

FAY, J. A. The spread of oil slicks on a calm sea. In: HOULT, D. P. (Ed.). **Oil on the sea: proceedings of a symposium on the scientific and engineering aspects of oil pollution of the sea**. Nova Iorque: Plenum Press, 1969. p. 53–63. 10

____. Physical processes in the spread of oil on a water surface. In: JOINT CONFERENCE ON PREVENTION AND CONTROL OF OIL SPILLS, 1971, Washington, DC. **Proceedings...** Washington, DC.: American Petroleum Institute, 1971. p. 463–467. xii, 10

FERNENDES, R. Integration of an oil and inert spill model in a framework for risk management of spills at sea: A case study for the atlantic area. In: ARCTIC AND MARINE OIL SPILL PROGRAM (AMOP) TECHNICAL SEMINAR ON ENVIRONMENTAL CONTAMINATION AND RESPONSE, 36., 2013. **Proceedings...** Ottawa: Environment Canada, 2013. p. 326–353. 7

FINGAS, M. Water-in-oil emulsion formation: a review of physics and mathematical modelling. **Spill Science & Technology Bulletin**, v. 2, n. 1, p. 55–559, 1995. 17, 19, 70

____. **The basics of oil spill cleanup**. 2. ed. Flórida: CRC Press, 2001. 245 p. 20

____. **Oil spill science and technology**: prevention, response and cleanup. 1. ed. Oxford: Elsevier Inc., 2011. 1189 p. 3, 11

FINGAS, M.; FIELDHOUSE, B. Formation of water-in-oil emulsions and application to oil spill modelling. **Journal of hazardous materials**, v. 107, n. 0, p. 37–50, 2004. 30, 70

FINGAS, M. F.; FIELDHOUSE, B.; MULLIN, J. Studies of water-in-oil emulsions: stability studies. In: ARCTIC AND MARINE OIL SPILL PROGRAM (AMOP) TECHNICAL SEMINAR ON ENVIRONMENTAL CONTAMINATION AND RESPONSE, 1997. **Proceedings...** Ottawa: Environment Canada, 1997. 3, 20

FINGAS, M. F.; FIELDHOUSE, B.; NOONAN, J.; LAMBERT, P. Studies of water-in-oil emulsions: testing of emulsion formation in OHMSETT, year II: . In: ARCTIC AND MARINE OIL SPILL PROGRAM (AMOP) TECHNICAL SEMINAR ON ENVIRONMENTAL CONTAMINATION AND RESPONSE, 25., 2002. **Proceedings...** Ottawa: Environment Canada, 2002. 20

FRENCH, D.; REED, M.; JAYKO, K.; FENG, S.; RINES, H.; PAVIGNANO, S.; ISAJI, T.; PUCKETT, S.; KELLER, A.; FRENCH, F. W.; GIFFORD, D.; MCCUE, J.; BROWN, G.; MACDONALD, E.; QUIRK, J.; NATZKE, S.; BISHOP, R.; WELSH, M.; PHILLIPS, M.; INGRAM, B. S. **The CERCLA Type A natural resource damage assessment model for coastal and marine environments**: Technical Documentation. Washington DC, 1996. Volume I - Model Description. 94

FRENCH, D. P. Modeling the impacts of the north cape oil spill. In: ARCTIC AND MARINE OIL SPILL PROGRAM (AMOP) TECHNICAL SEMINAR, 21., 17, Alberta. **Proceedings...** Edmonton: Environment Canada, 1998. p. 387–430. 21

FRENCH-MCCAY, D.; HORN, M.; LI, Z.; CROWLEY, D.; SPAULDING, M.; MENDELSOHN, D.; JAYKO, K.; KIM, Y.; ISAJI, T.; FONTENAULT, J.; SHMOOKLER, R.; ROWE, J. **Simulation modeling of Ocean circulation and oil spill in the Gulf of Mexico - Appendix VI data collection, analysis and model validation**: . New Orleans, LA, 2016. 8, 9

FRENCH-MCCAY, D.; JAYKO, K.; LI, Z.; HORN, M.; KIM, Y.; ISAJI, T.; CROWLEY, D.; SPAULDING, M.; DECKER, L.; TURNER, C.; ZAMORSKI, S.; FONTENAULT, J.; SHMOOKLER, R.; ROWE, J. **Technical Reports for Deepwater Horizon Water Column Injury Assessment - WCTR14: Modeling Oil Fate and Exposure Concentrations in the Deepwater Plume and Cone**

of Rising Oil Resulting From the Deepwater Horizon Oil Spill: DWH NRDA Water Column Technical Working Group Report. South Kingstown, RI, 2015. 1, 7

FRENCH-MCCAY, D. P. Oil spill impact modelling: development and validation. **Environmental Toxicology and Chemistry**, v. 23, n. 10, p. 2441–2456, 2004. 24

____. State-of-the-art and research needs for oil spill impact assessment modelling: a chemical view. In: ARCTIC AND MARINE OIL SPILL PROGRAM (AMOP) TECHNICAL SEMINAR ON ENVIRONMENTAL CONTAMINATION AND RESPONSE, 32., 2013. **Proceedings...** Ottawa: Environment Canada, 2009. p. 601–653. 94

FRENCH-MCCAY, D. P.; PAYNE, J. R. Model of oil fate and water concentrations with and without application of dispersants: . In: ARCTIC AND MARINE OIL SPILL PROGRAM (AMOP) TECHNICAL SEMINAR ON ENVIRONMENTAL CONTAMINATION AND RESPONSE, 24., 2001. **Proceedings...** Ottawa: Environment Canada, 2001. p. 611–645. 30

GARNER, F. H.; FOORD, A.; TAYEBAN, M. Mass transfer from circulating liquid drops. **Journal of Applied Chemistry**, v. 9, n. 6, p. 315–323, 1959. 65, 66

GOLD, G.; RODRIGUEZ, S. The effect of temperature and salinity on the setschenow parameters of naphthalene in seawater. **Canadian Journal of Chemistry**, v. 67, n. 5, p. 822–826, 1989. 13

GOODSON, S. **API Gravity description**. 2009. Available from: <http://mycommittees.api.org/standards/copm/Shared%20Documents/Miscellaneous/>. Access in: 06 jan. 2017. 1

GRACE, J. R.; WAIREGI, T.; BROPHY, J. Break-up of drops and bubbles in stagnant media. **The Canadian Journal of Chemical Engineering**, v. 56, n. 1, p. 3–8, 1978. 27

HEERTJES, P. M.; HOLVE, W. A.; TALMAS, H. Mass transfer between isobutanol and water in a spray-column. **Chemical Engineering Science**, v. 3, n. 3, p. 122–142, 1954. 65, 66

HUANG, J. C. A review of the state-of-the-art of oil spill fate/behavior models. In: OIL SPILL CONFERENCE, 1983. [S.l.], 1983. p. 313 – 322. 22, 84, 116

HUNTER, J. R. Application of Lagrangian particle-tracking technique to modelling of dispersion in the sea. In: NOYE, J. (Ed.). **Numerical modelling:**

Applications for Marine Systems. North Holland, Amsterdam: [s.n.], 1987. p. 257–269. 15

HUNTLEY, H. S.; LIPPHARDT, B. L.; KIRWAN, A. D. Surface drift predictions of the Deepwater Horizon spill: The Lagrangian perspective, in Monitoring and Modeling of the Deepwater Horizon Oil Spill. In: LIU, Y. (Ed.). **A Record-Breaking Enterprise**. Washington, D.C: AGU, 2011. p. 179–195. 6

INTERNATIONAL TANKER OWNERS POLLUTION FEDERATION LIMITED (ITOPF). **Oil tanker spill statistics 2011**. Londres, 2011. 55 p. Available from: <http://www.itopf.com/knowledge-resources/documents-guides/document/itopf-handbook/>. Access in: 05 jan. 2017. 1

JOHANSEN, Ø. **Dissolution of oil components from dispersed oil droplets**. Noruega, 2003. 34 p. SINTEF Applied Chemistry, SINTEF Report STF66 F03048. 11, 43, 44, 45, 62, 64

JOHANSEN, Ø.; REED, M.; BODSBERG, N. R. Natural dispersion revisited. **Marine Pollution Bulletin**, v. 23, p. 20–26, 2015. 22, 70, 71

JONES, C. E.; DAGESTAD, K.; BREIVIK, Ø.; HOLT, B.; ROHRS, J.; CHRISTENSEN, K. H.; ESPESETH, M.; BREKKE, C.; SKRUNES, S. Measurement and Modeling of oil slick transport. **Journal of Geophysical Research**, p. 7759–7775, 2016. 6

KOROTENKO, K. A.; MAMEDOV, R. M.; MOOERS, C. N. K. Prediction of the dispersal of oil transport in the caspian sea resulting from a continuos release. **Spill Science and Technolohy Buletin**, n. 6, p. 323–339, 2001. 3

KUIPER, J.; BRINK, W. J. V. den. **Fate and effects of oil in marine ecosystems**: . Boston: Martinus Nijhoff Publishers, 1987. 6

LARGE, W. G.; POND, S. Open ocean momentum flux measurements in moderate to strong winds. **J. Phys. Ocean.**, v. 11, p. 324–481, 1981. 37

LEFEBVRE, A. H. **Atomization and Sprays**. New York: Hemisphere Publishing Corporation, 1989. 27

LEHR, W.; JONES, R.; EVANS, M.; SIMECEK-BEATTY, D.; OVERSTREET, R. Revisions of the ADIOS Oil Spill Model. **Environmental Modeling Software**, v. 17, p. 191–199, 2002. 1, 7

LEMOS, A. T.; SOARES, I. D.; GUISOLFI, R. D.; CIRANO, M. Oil spill modeling off the Brazilian eastern coast: the effect of tidal currents on oil fate. **Rev. Bras. Geof.**, v. 27, n. 4, p. 625–639, 2009. 9

LI, A.; REIDENBACH, M. A. Forecasting decadal changes in sea surface temperatures and coral bleaching within a Caribbean coral reef. **Coral reefs**, v. 33, n. 3, p. 847–861, 2014. 57

LI, Z.; SPAULDING, M. L.; FRENCH-MCCAY, D. An algorithm for modeling entrainment and naturally and chemially dispersed oil droplet size distribution under surface breaking wave conditions. **Marine Pollution Bulletin**, v. 119, p. 145–152, 2017. 26, 27, 29, 43, 80, 81, 85, 116

LI, Z.; SPAULDING, M. L.; FRENCH-MCCAY, D.; CROWLEY, D.; PAYNE, J. Development of a unified oil droplet size distribution model with application to surface breaking waves and subsurface blowout releases considering dispersant effect. **Marine Pollution Bulletin**, v. 114, p. 247–257, 2016. 28

LIUNGMAN, O.; MATTSSON, J. **Scientific documentation of SeatrackWeb; physical processes, algorithms and references**. [S.l.], 2011. 25

LONIN, S. A. Lagrangian Model for oil spill diffusion at sea. **Spill Science & Technology Bulletin**, v. 5, n. 5-6, p. 331–336, 1999. 15

MACKAY, D.; BUIST, I.; MASCARENHAS, R.; PETERSEN, S. **Oil spill processes and models**. Canada, 1980. Report n. EE-8. 20, 43

MACKAY, D.; MATSUGU, R. Evaporation rate of liquid hydrocarbon spills on land and water. **J. Chem. Eng.**, v. 51, n. 0, p. 434–439, 1973. xii, 17, 18

MACKAY, D.; MCAULIFFE, C. D. Fate of hydrocarbons discharged at sea. **Oil & Chemical Pollution**, v. 5, p. 1–20, 1988. 6

MACKAY, D.; ZAGORSKI, W. water-in-oil emulsions: a stability hypothesis: . In: **Proceedings...** Ottawa: Environment Canada, 1982. p. 61–74. 20

MCAULIFFE, C. D. The weathering of volatile hydrocarbons from crude oil slicks on water. In: **Proceedings of the 1989 Oil Spill Conference**. San Antonio, Texas: [s.n.], 1989. p. 357–364. 29

MCDONALD, I. R.; GARCIA-PINEDA, O.; BEET, A.; ASL, S. D.; FENG, L.; GRAETTINGER, G.; FRENCH-MCCAY, D.; HOLMES, J.; HU, C.; HUFFER, F.; LEIFER, I.; MULLER-KARGER, F.; SOLOW, A.; SILVA, M.; SWAYZE, G. Natural and unnatural oil slicks in the gulf of mexico. **J. Geophys. Res.**, v. 120, 2015. 9

NASCIMENTO, T. F. do; CHACALTANA, J. T. A.; PICOLLI, F. P. Análise da Influência do Alargamento de um Estreitamento na Hidrodinâmica do Canal da Passagem, Vitória-ES, Através de Modelagem Numérica. **Revista Brasileira de Recursos Hídricos**, v. 18, n. 3, 2013. 32, 57

NORTH, E. W.; SCHLAG, Z.; HOOD, R. R.; LI, M.; ZHONG, L.; GROSS, T.; KENNEDY, V. S. Vertical swimming behaviour influences the dispersal of simulated oyster larvae in a coupled particle-tracking and hydrodynamic model of Chesapeake Bay. **Mar. Ecol. Prog. Ser.**, v. 359, p. 99–115, 2008. 15

OHNESORGE, W. Formation of drops by nozzles and the breakup of liquid jets. **Journal of Applied Mathematics and Mechanics**, v. 16, p. 355–358, 1936. 27

PAYNE, J. R.; KIRSTEIN, B. E.; MCNABB, G. D.; LAMBACH, J. L.; REDDING, R.; JORDON, R. E.; HORN, W.; OLIVEIRA, C.; SMITH, G. S.; BAXTER, D. M.; GEAGEL, R. **Multivariate analysis of petroleum weathering in the marine environment-subarctic. Vol I and II**: Environmental Assessment of the Alaskan Continental Shelf. [S.l.], 1984. 17

PIEROTTI, R. A. A scaled particle theory of aqueous and nonaqueous solutions. **Chemical Reviews**, v. 76, n. 6, p. 717–726, 1976. 12

PROCTOR, R.; FLATHER, R. A.; ELLIOT, A. J. Modelling tides and surface drift in the Arabian Gulf - application to the Gulf oil spill. **Continental shelf research**, v. 14, n. 5, p. 531–545, 1994. 21

REED, M. The physical fates component of the natural resource damage assessment model system. **Oil Chem. Pollut.**, v. 5, n. 2, p. 99–123, 1989. 17, 18, 42

REED, M.; AAMO, O. M.; DALING, P. S. Quantitative analysis of alternate oil spill response strategies using OSCAR. **Spill Science & Technology Bulletin**, v. 2, n. 1, p. 67–74, 1995. 85

REED, M.; DALING, P. S.; BRAKSTD, O. G.; SINGSAAS, I.; FAKSNESS, L. G.; HETLAND, B.; EFROL, N. Oscar 2000: A multi-component 3-dimensional oil spill contigency and response model. In: ARCTIC AND MARINE OIL SPILL PROGRAM (AMOP) TECHNICAL SEMINAR, 23., 2000, Vancouver. **Proceedings...** Ottawa: Environment Canada, 2000. p. 663–952. 1, 7, 21

REED, M.; EKROL, N.; RYE, H.; TURNER, L. Oil spill contingency and response (OSCAR) analysis in support of environmental impact assessment offshore Namibia. **Spill Science & Technology Bulletin**, v. 5, n. 1, p. 29–38, 1999. 85

REED, M.; FRENCH, D.; RINES, H.; RYE, H. A three dimensional oil and chemical spill model for environmental impact assessment. In: 1995 OIL SPILL CONFERENCE, 1995. [S.l.]: American Petroleum Institute, 1995. p. 61–66. 14, 43

REED, M.; GUNDLACH, E. A coastal zone oil spill model: development and sensitivity studies. **Oil & Chemical Pollution**, v. 5, p. 411–449, 1989. 70

REED, M.; JOHANSEN, Ø.; BRANDVIK, P. J.; DARLING, P.; LEWIS, A.; FIOCCO, R.; MACKAY, D. **Revision of MMS offshore continental shelf oil weathering model: Evaluation**. Anchorage, 1998. 21

REED, M.; JOHANSEN, Ø.; LEIRVIK, F.; BROS, B. **Numerical Algorithm to compute the effects of breaking waves on surface oil spilled at sea**. NOAA/UNH, 2009. 65 p. 27

REID, R. C.; PRAUSNITZ, J. M.; POLING, B. E. **The properties of gases and liquids**: . 4. ed. México: McGraw-Hill Inc., 1987. 753 p. 12

RIAZI, M. R.; AL-ENEZI, G. A. Modelling of the rate of oil spill disappearance from seawater for Kuwaiti crude and its products. **Chemical engineering journal**, v. 73, p. 161–172, 1999. 7, 67

RIGO, D. **Levantamento Topo Batimétrico dos Manguezais e Canais da Baía de Vitória**: Relatório Final. Vitória, 2001. v. 45, n. 1, 21-25 p. 37

ROHRS, J.; DAGESTAD, K.; ASBJØRNSEN, H.; NORDAM, T.; SKANCKE, J.; JONES, C. E.; BREKKE, C. The effect of vertical mixing on the horizontal drift of oil spills. **Ocean Science**, p. 1581–1601, 2018. 22

ROSS, S.; BUIST, I. Preliminary laboratory study to determine the effect of emulsification on oil spill evaporation. In: ARCTIC AND MARINE OIL SPILL PROGRAM (AMOP) TECHNICAL SEMINAR ON ENVIRONMENTAL CONTAMINATION AND RESPONSE, 1995. **Proceedings...** Ottawa: Environment Canada, 1995. 3, 30

RYE, H. Model for calculation of underwater blowout plume. In: ARCTIC AND MARINE OIL SPILL PROGRAM (AMOP) TECHNICAL SEMINAR, 17., 1994, Vancouver. **Proceedings...** Ottawa: Environment Canada, 1994. p. 849–865. 11

SEBASTIAO, P.; SOARES, C. G. Modeling the fate of oil spills at sea. **Spill Science & Technology Bulletin**, v. 2, n. 2, p. 121–131, 1995. 17, 19, 44

SMITH, S. D.; BANKE, E. G. Variation of the sea surface drag coefficient with wind speed. **Q J R Meteorol. Soc**, v. 101, p. 655–673, 1975. 37

SPAULDING, M. L. State of the art review and future directions in oil spill modeling. **Marine Pollution Bulletin**, v. 115, p. 7–19, 2017. 8, 11, 14, 17, 30, 40, 85

SPAULDING, M. L.; HOWLETT, E.; ANDERSON, E.; JAYKO, K. Oilmap: a global approach to spill modeling. In: ARCTIC AND MARINE OIL SPILL PROGRAM (AMOP) TECHNICAL SEMINAR, 15., 1992, Alberta. **Proceedings...** Edmonton: Environment Canada, 1992. p. 15–21. 1, 7

SPAULDING, M. L.; MENDELSOHN, D.; CROWLEY, D.; LI, Z.; BIRD, A. **Draft technical reports for Deepwater Horizon water column injury assessment: Application of OILMAP DEEP to the Deepwater Horizon blowout**: . South Kingstown, RI, 2015. 8

STIVER, W.; MACKAY, D. Evaporation rate of spills of hydrocarbons and petroleum mixtures. **Environ. Sci. Technol**, v. 18, n. 11, p. 834–840, 1984. 18

SU, J. T.; NEEDHAM, D. Mass transfer in the dissolution of a multicomponent liquid droplet in an immiscible liquid environment. **Langmuir**, v. 29, n. 44, p. 13339–13345, 2013. 66

SUN, S.; HU, C.; FENG, L.; SWAYZE, G. A.; HOLMES, J.; GRAETTINGER, G.; MCDONALD, I.; GARCIA, O.; LEIFER, I. Oil slick morphology derived from AVIRIS measurements of the Deepwater Horizon oil spill: implications for spatial resolution requirements of remote sensor. **Mar. Pollut. Bull.**, v. 103, n. 1-2, p. 276–285, 2016. 9

VERBOOM, G. K.; SLOB, A. Weakly-reflective boundary conditions for two-dimensional shallow water flow problems. **Adv water Resources**, v. 7, 1984. 36

VERONEZ, P.; BASTOS, A.; QUARESMA, V. S. Morfologia e distribuição sedimentar em um sistema estuarino tropical: Baía de Vitória, ES. **Revista Brasileira de Geofísica**, v. 27, n. 4, p. 609–624, 2009. 32

WILKE, C. R.; CHANG, P. Correlation of diffusion coefficient in dilute solutions. **American Institute of Chemical Engineers Journal**, v. 1, n. 2, p. 264–270, 1955. 12

WITHERSPOON, P. A.; BONOLI, L. Correlation of diffusion coefficients for paraffin, aromatic, and cycloparaffin hydrocarbons in water. **Industrial & Engineering Chemistry Fundamentals**, v. 8, n. 3, p. 589–591, 1969. 65

XIE, H.; YAPA, P. D.; NAKATA, K. Modeling emulsification after an oil spill in the sea. **Journal of marine systems**, v. 68, p. 489–506, 2007. 19, 29, 30

XIE, W. H.; SHIU, W. Y.; MACKAY, D. A review of the effect of salts on the solubility of organic compounds in seawater. **Marine Environmental Research**, v. 44, n. 4, p. 429–444, 1997. 12

YANG, W. C.; WANG, H. Modeling of oil evaporation in aqueous environment. **Water research**, v. 11, p. 879–887, 1977. 30

YAPA, P. D. Modeling oil spills to mitigate coastal pollution. In: FERNANDO, H. J. S. (Ed.). **Handbook of environmental fluid dynamics**: systems, pollution, modeling, and measurements. 2. ed. Boca Raton, FL: CRC Press, Taylor & Francis Group, 2013. p. 243–256. 15

ZAFIRAKOU, A. Oil Spill Dispersion Forecasting Models. In: FOUZIA, H. B. (Ed.). **Monitoring of Marine Pollution**. [S.l.]: IntechOpen, 2018. p. 135–189. 2

ZHENG, L.; YAPA, P. D. Buoyant velocity of spherical and non-spherical bubbles/droplets. **Journal of Hydraulic Engineering**, v. 126, n. 11, p. 852–854, 2000. 17

ZHENG, L.; YAPA, P. D.; CHEN, F. A model for simulating deepwater oil and gas blowouts - Part I: theory and model formulation. **Journal of Hydraulic Research**, v. 41, n. 4, p. 339–351, 2002. 4